Impacts of freshwater flow regulation of Quebec's large rivers on the physical environment and krill transport in the Gulf of St. Lawrence and on the Scotian Shelf

Lavoie, D., G. Gilson, J. Chassé, N. Lambert, C. B.-Brunelle, M. Starr, S. Plourde, D. Brickman and F. Maps

Fisheries and Oceans Canada
Pelagic and Ecosystem Science Branch
Maurice Lamontagne Institute
C.P. 1000, 850 route de la mer
Mont-Joli (Québec)
G5H 3Z4

2017

Canadian Technical Report of
Hydrography and Ocean Sciences 318

Fisheries and Oceans Canada | Pêches et Océans Canada

Canada

Canadian Technical Report of Hydrography and Ocean Sciences

Technical reports contain scientific and technical information of a type that represents a contribution to existing knowledge but which is not normally found in the primary literature. The subject matter is generally related to programs and interests of the Oceans and Science sectors of Fisheries and Oceans Canada.

Technical reports may be cited as full publications. The correct citation appears above the abstract of each report. Each report is abstracted in the data base *Aquatic Sciences and Fisheries Abstracts.*

Technical reports are produced regionally but are numbered nationally. Requests for individual reports will be filled by the issuing establishment listed on the front cover and title page.

Regional and headquarters establishments of Ocean Science and Surveys ceased publication of their various report series as of December 1981. A complete listing of these publications and the last number issued under each title are published in the *Canadian Journal of Fisheries and Aquatic Sciences*, Volume 38: Index to Publications 1981. The current series began with Report Number 1 in January 1982.

Rapport technique canadien sur l'hydrographie et les sciences océaniques

Les rapports techniques contiennent des renseignements scientifiques et techniques qui constituent une contribution aux connaissances actuelles mais que l'on ne trouve pas normalement dans les revues scientifiques. Le sujet est généralement rattaché aux programmes et intérêts des secteurs des Océans et des Sciences de Pêches et Océans Canada.

Les rapports techniques peuvent être cités comme des publications à part entière. Le titre exact figure au-dessus du résumé de chaque rapport. Les rapports techniques sont résumés dans la base de données *Résumés des sciences aquatiques et halieutiques*.

Les rapports techniques sont produits à l'échelon régional, mais numérotés à l'échelon national. Les demandes de rapports seront satisfaites par l'établissement auteur dont le nom figure sur la couverture et la page de titre.

Les établissements de l’ancien secteur des Sciences et Levés océaniques dans les régions et à l'administration centrale ont cessé de publier leurs diverses séries de rapports en décembre 1981. Vous trouverez dans l'index des publications du volume 38 du *Journal canadien des sciences halieutiques et aquatiques*, la liste de ces publications ainsi que le dernier numéro paru dans chaque catégorie. La nouvelle série a commencé avec la publication du rapport numéro 1 en janvier 1982.

Canadian Technical Report of
Hydrography and Ocean Sciences 318

2016

IMPACTS OF FRESHWATER FLOW REGULATION OF QUEBEC'S LARGE RIVERS ON THE PHYSICAL ENVIRONMENT AND KRILL TRANSPORT IN THE GULF OF ST. LAWRENCE AND ON THE SCOTIAN SHELF

by

Diane Lavoie[1], Gaëlle Gilson[1], Joël Chassé[2], Nicolas Lambert[1], Corinne B.-Brunelle[1], Michel Starr[1], Stéphane Plourde[1], Dave Brickman[3] and Frédéric Maps[4]

[1]Institut Maurice-Lamontagne
Fisheries and Oceans Canada
850, Route de la Mer, C.P. 1000
Mont-Joli, Québec, G5H 3Z4

[2]Gulf Fisheries Centre
Fisheries and Oceans Canada
343 Université Avenue, PO Box 5030
Moncton, New Brunswick, E1C 9B6

[3]Bedford Institute of Oceanography
Fisheries and Oceans Canada
P. O. Box 1006
Dartmouth, Nova Scotia, B2Y 4A2

[4]Département de biologie
Université Laval
Québec, Québec, G1V 0A6

Cat. No. Fs97-18/318E-PDF ISBN 978-0-660-08480-0 ISNN 1488-5417

Correct citation for this publication:

Lavoie, D., Gilson, G., Chassé, J., Lambert, N., B.-Brunelle, C., Starr, M., Plourde, S., Brickman, D., and Maps, F. 2017. Impacts of freshwater flow regulation of Quebec's large rivers on the physical environment and krill transport in the Gulf of St. Lawrence and on the Scotian Shelf. Can. Tech. Rep. Hydrogr. Ocean Sci. 318: xii + 101 p.

TABLE OF CONTENTS

LIST OF TABLES

LIST OF FIGURES

ABSTRACT

Lavoie, D., Gilson, G., Chassé, J., Lambert, N., B.-Brunelle, C., Starr, M., Plourde, S., Brickman, D., and Maps, F. 2017. Impacts of freshwater flow regulation of Quebec's large rivers on the physical environment and krill transport in the Gulf of St. Lawrence and on the Scotian Shelf. Can. Tech. Rep. Hydrogr. Ocean Sci. 318: xii + 101 p.

We use a three-dimensional numerical circulation model and river runoff from a hydrological model to assess the large-scale impacts of harnessing Quebec's large rivers on the dynamics of the Gulf of St. Lawrence and Scotian Shelf. We first look at the impact of harnessing a single river (St. Lawrence River, Romaine River) or a subgroup of rivers (Saguenay, Manicouagan, Betsiamites, and Outardes rivers; Romaine and Little Mecatina rivers), and finally at the cumulative impact of harnessing all these rivers. Most of the rivers are already harnessed, dams are currently under construction on the Romaine River, and harnessing of the Little Mecatina River is at the planning stage. We analyzed the changes brought to the top 50 m of the water column in terms of salinity, temperature, and circulation. Transport at different cross sections was also analyzed as well as the sea-ice conditions. Lastly, we looked at the impact of changes in circulation and turbidity on krill transport and mean density in specific regions of the Gulf of St. Lawrence. The greatest changes in runoff were brought by harnessing of the Saguenay, Manicouagan, Betsiamites, and Outardes river subgroup. However, significant changes at Cabot Strait (circulation, transport) were simulated with the modifications of all river flows. The response varied depending on the location of the river mouth. Some changes were found to be significant when compared to the simulated interannual variability. However, the significance of the changes will vary depending on the process or marine species considered.

RÉSUMÉ

Lavoie, D., Gilson, G., Chassé, J., Lambert, N., B.-Brunelle, C., Starr, M., Plourde, S., Brickman, D., and Maps, F. 2017. Impacts of freshwater flow regulation of Quebec's large rivers on the physical environment and krill transport in the Gulf of St. Lawrence and on the Scotian Shelf. Can. Tech. Rep. Hydrogr. Ocean Sci. 318: xii + 101 p.

Nous utilisons un modèle numérique tridimensionnel de la circulation ainsi que les débits de rivières obtenus à l'aide d'un modèle hydrologique pour évaluer l'impact du harnachement des grandes rivières du Québec sur la dynamique du Golfe du Saint-Laurent et du plateau Néo-Écossais. Nous regardons en premier lieu l'impact du harnachement d'une seule rivière (i.e., le Saint-Laurent ou la Romaine), pour ensuite regarder l'impact du harnachement d'un sous-groupe de rivières (i.e., les rivières Saguenay, Manicouagan, Betsiamites et Outardes, ou les rivières Romaine et Petit-Mécatina), et finalement l'impact cumulé du harnachement de toutes ces rivières. La plupart des rivières sont déjà harnachées, alors que des barrages hydro-électriques sont en construction sur la rivière Romaine. Le harnachement de la rivière Petit-Mécatina est quant à lui au stade de la planification. Nous avons analysé les changements causés par la modification des débits d'eau douce sur les 50 premiers mètres de la colonne d'eau pour la température, la salinité et la circulation. Les changements dans le transport à différentes sections ont aussi été analysés ainsi que les changements dans la glace de mer. Finalement, l'impact des changements de circulation et de turbidité sur le transport et la densité de krill dans différentes régions du Golfe du Saint-Laurent a été évalué. Les plus importants changements résultent du harnachement du sous-groupe composé des rivières Saguenay, Manicouagan, Betsiamites et Outardes. Toutefois, des changements significatifs dans la circulation et le transport au détroit de Cabot ont été simulés avec tous les scénarios. La réponse du système varie en fonction de l'emplacement de l'embouchure des rivières en raison de leurs impacts sur différents processus océanographiques. Certains changements ont été estimés significatifs lorsque comparés avec la variabilité interannuelle simulée. Toutefois, l'importance de certains changements va ultimement dépendre du processus ou de l'espèce marine à l'étude.

1 INTRODUCTION

Large dams are regularly built on rivers for different purposes, such as irrigation, flood control, improved navigation, and generation of hydroelectricity. Flow alterations caused by the presence of dams vary between relatively small to major, and, at a global scale, can modify the freshwater inputs to oceans (Biemans et al., 2011). The presence of large dams, either through the changes in land-use surrounding the dams or through the development of the large reservoir meant to retain the water for gradual release over the year, can affect the local meteorological conditions in some regions (Hossain et al., 2009; Degu et al., 2011). The presence of reservoirs can also reduce the delivery of sediment (Syvitski et al., 2005) and dissolved silica by rivers to coastal areas (Humborg et al., 2000; Ittekkot et al., 2000; Harrison et al., 2012; Maavara et al., 2014), modifying their geomorphology, productivity, and composition of the phytoplankton community. Reservoirs also have an impact on the emission of carbon gas to the atmosphere (Mendonça et al., 2012; Teodoru et al., 2012). All these changes have impacts on the ecosystem of the water body into which these rivers flow, on both the physical and biochemical environment. Some of the environmental impacts will be felt in the immediate area surrounding the river mouth while others will be felt on a much larger scale (Rosenberg et al., 1997; Rosenberg et al., 2000; Gillanders and Kingsford, 2002). Changes in the seasonality of the river flow modify the salinity and stratification, and thereafter mixing, upwelling, temperature, and circulation in the marine environment. In turn, changes in these physical properties can affect the abundance and distribution of certain marine species, such as euphausiids (Kaartvedt and Svendsen, 1990).

The St. Lawrence hydrographic system, including the Great Lakes, is one of the largest in the world and the third largest in North America, after the Mississippi and Mackenzie rivers (https://www.ec.gc.ca/stl/). Many of Quebec province's large rivers are located on the north shore of the Gulf of St. Lawrence (GSL, Figure 1). The rivers flowing directly into the Lower St. Lawrence Estuary (LSLE) represent about 80% of the total discharge to the GSL (Koutitonsky and Bugden, 1991; this study). This high freshwater runoff is the main driver of the estuarine circulation in the Estuary and Gulf of St. Lawrence. Combined with the wind forcing and inflow of water from the Strait of Belle Isle and Cabot Strait, it contributes to the formation and maintenance of two important circulation features of the St. Lawrence system: the Anticosti cyclonic gyre and the Gaspé Current (Ingram and El-Sabh, 1990; Koutitonsky and Bugden, 1991; Sheng, 2001; Lavoie et al., 2016). Freshwater runoff from the GSL also contributes to the coastal Nova Scotian Current (NSC) and the southward-flowing shelf break current (e.g., Hannah et al., 2001; Ohashi and Sheng, 2013; Urrego-Blanco and Sheng, 2014b). Tidal mixing at the head of the Laurentian Channel, which brings cold nutrient-rich water close to the surface (Therriault and Lacroix, 1976; Greisman and Ingram, 1977; Cyr et al., 2015) and modulates in part the strength of estuarine circulation, is also influenced by the quantity of freshwater that enters the system (Neu, 1970; Reid, 1977; Saucier et al., 2009).

Most of Quebec's large rivers are dammed for hydroelectric production (see Figure 2 of Neu, 1976 and Table 1). Dams are also under construction on the Romaine River, and the construction of hydroelectric installations is planned for the Little Mecatina River. In Quebec, the highest energy demand occurs in winter, thus large quantities of water from the spring runoff are retained in reservoirs until their release during the next fall and winter when the electricity demand increases. The two main freshwater sources of the St. Lawrence River (the Great Lakes and the Ottawa River) are also regulated for various purposes (water level control, navigation, flood control).

Despite its obvious potential for large-scale impact, studies looking at the impacts of river flow regulation in the GSL have only been made at local scales (Cataliotti-Valdina and Long, 1984; Hart and Long, 1990; MPO, 2008). A few authors have tried to infer the potential large-scale impacts of the regulation of the GSL's north shore rivers on the marine environment (Hassan, 1975; Neu, 1976;

Bugden et al., 1982; Neu, 1982). Neu (1976; 1982) inferred that the large modifications to the seasonal runoff cycle resulted in a reduction of saltwater and nutrient entrainment in the deep layers of the GSL in spring and summer, accompanied by an increase in surface salinity. Neu (1976), Hassan (1975), and Bugden et al. (1982) also inferred changes to the seasonal heat budget over the year and modifications to the formation, melting, and transport of sea ice, both through warmer surface temperature and an increase in the freezing point resulting from fresher surface waters. However, Bugden et al. (1982) assumed the impact of a change in freezing point would be negligible compared to the effect of reduced vertical mixing. Hassan (1975) and Neu (1982) also estimated the likely changes in transport at Cabot Strait; the estimates of Hassan (1975) were revisited by V.G. Koutitonsky in Appendix D of Drapeau (1980).

A few numerical modelling studies have looked at the impact of changes in freshwater runoff on the circulation and hydrography of the GSL. Ohashi and Sheng (2013) evaluated the impact of a long-term mean decrease and increase of the freshwater flux near Quebec City. However, sea ice was not included in their model, the inflow at the Strait of Belle Isle was constant, and the runoff of the Saguenay, Manicouagan, Betsiamites, and Outardes rivers, which is about one third of the St. Lawrence River flow (see Table 1), were all added at the same location (near Quebec City, labelled "St. Lawrence" on Figure 2). All of these set-ups could have a relatively strong impact on their results. The model results of Saucier et al. (2009), which also used a uniform runoff change over the years, are in agreement with Neu (1976; 1982), suggesting that an increase in freshwater runoff would lead to an increase in the estuarine circulation in spring and summer, but to a decrease of the deep layer advection towards the head of the Laurentian Channel in winter.

Zooplankton composition and distribution in the LSLE and GSL are affected by the deep layer advection towards the head of the Laurentian Channel and surface runoff (Runge and Simard, 1990; Lavoie et al., 2000; Plourde et al., 2001; Simard, 2009; Maps et al., 2011; Plourde et al., 2013; Lavoie et al., 2016). Changes in surface water turbidity also have an impact on the distribution of the different krill species (Maps et al., 2013; Plourde et al., 2013). Changes in zooplankton abundance and distribution, including krill, could in turn affect the distribution and abundance of their predators (e.g., herring, capelin, mackerel, flat fishes, cod, redfish, pollock, birds, and baleen whales; Runge et al., 1999; Simard and Harvey, 2010; Savenkoff et al., 2013). A relation between runoff variability and fisheries production was also demonstrated, although the direct mechanisms involved are not clear (e.g. Bugden et al., 1982 and references therein; Sinclair et al., 1986). Changes in sea-ice conditions could also have an impact on seal breeding (Bajzak et al., 2011). However, despite its suggested importance, the impacts of runoff alterations on the St. Lawrence system and downstream regions (Scotian Shelf and Gulf of Maine) are still essentially unknown.

Runoff modifications caused by the dams that have been built over the last decades are not reversible. We will nevertheless attempt to evaluate some of the past changes that occurred in the marine ecosystem. We will also evaluate the potential large-scale impacts of the Romaine River dam, which is under construction, and of the planned Little Mecatina dam. In this report, we used a 3D ocean circulation model forced with dammed or natural river runoff to investigate the cumulative impacts of runoff alterations of the major rivers flowing into the St. Lawrence system on the hydrodynamics of the GSL, Scotian Shelf, and Gulf of Maine. All the other forcings are kept constant. Here we use "cumulative impacts" to mean the impacts of harnessing multiple rivers over a large area. The impacts of changes in circulation and water turbidity (which affects the vertical position of krill during daytime) on the transport of krill in the GSL are also evaluated.

2 MATERIAL AND METHODS

2.1 OCEAN CIRCULATION MODEL

The ocean circulation model used in this study is based on the NEMO modelling system and is described in detail in Brickman and Drozdowski (2012). Additional model validation can be found in Lavoie et al. (2016). The ocean dynamics module of NEMO is based on the ocean code OPA version 9.0 (Madec, 2012). A thermodynamic-dynamic module of sea-ice (LIM2; Madec et al., 1998; Goosse and Fichefet, 1999) is coupled to the ocean circulation model. The grid of the model covers the GSL, the Scotian Shelf, and the Gulf of Maine (Figure 2). The grid has a resolution of 1/12° of latitude and longitude on the horizontal and 46 layers of variable thickness on the vertical (from 6 m below the surface to 250 m at depth in the ocean). The first 19 layers cover all depths of the GSL (maximum depth of 540 m with a 75 m-thick bottom layer).

It is a prognostic model, meaning that the temperature and salinity fields are free to evolve with time and are only constrained through open boundary conditions, freshwater runoff, and surface forcing. Monthly climatologies for temperature and salinity are used as initial and boundary conditions in the model. The code contains a simple restoring scheme towards the climatology for temperature and salinity but with a long enough restoring timescale (900 days) as to not affect our results which are based on monthly anomalies of surface salinity.

An annual cycle of the barotropic transport is prescribed at the Strait of Belle Isle in addition to the baroclinic transport calculated from the monthly temperature and salinity fields. Five tidal components (M_2, S_2, N_2, O_1, K_1) are included in the model through surface elevation and barotropic current at the open boundaries. Freshwater enters the domain through precipitation and monthly runoff from the 78 main rivers of the domain. Surface forcing, updated every three hours (air temperature, relative humidity, temperature, winds, cloud cover, and precipitation) were obtained from the Canadian Meteorological Centre Global Environmental Multiscale (CMC-GEM) atmospheric model (Pellerin et al., 2003).

2.2 DESCRIPTION OF PARTICLE TRACKING MODELS

2.2.1 LD model

To investigate the potential impacts of freshwater regulation on the transport of krill in the GSL, we first used the offline particle tracking module described in Lavoie et al. (2016), hereafter called LD (for Lavoie et al. vertical distribution). There is no growth or predation on krill in this model. The particles, representing krill, were released uniformly over the GSL domain (300 particles per grid cell) with boundaries at Cabot Strait and at the Strait of Belle Isle. Each trajectory was calculated using the common Runge-Kutta method with a predictor–corrector scheme. On the vertical, the particles were distributed according to the nighttime and daytime vertical distribution determined from the backscatter of two Acoustic Doppler Current Profilers (ADCP) located at the M4 mooring (Figure 3; see Figure 2 for the location of M4). Although designed for measuring currents, information on zooplankton can also be extracted from the ADCP data. A more thorough description of the method and presentation of the ADCP data are given in section 3.4.1 of Gagné et al. (2013). To move between the nighttime and the daytime distribution, the particles were randomly redistributed from one vertical distribution to the other one hour before sunrise or sunset. The vertical distribution is compressed as the particles move into areas shallower than 226 m and as long as the bottom depth is deeper than 100 m. When the bottom depth becomes shallower than 100 m, we used the compressed shape of the 0–175 m daytime distribution to reproduce the accumulation of krill close to the bottom (Figure 3). In our simulations, the particles are transported by horizontal currents and are not affected by vertical currents (i.e., we

made the assumption that krill can overcome any vertical current in the GSL). At the Strait of Belle Isle and Cabot Strait, particles were allowed to leave the domain with outflowing currents while new particles were generated and transported into the GSL with inflowing currents. The number of particles created varied in order to maintain an amount equal to half the initial conditions (150 particles per grid cell) in cells with inflowing currents (see Lavoie et al., 2016).

2.2.2 MD model

The diel vertical migration of krill in the second set-up was modified according to Maps et al. (2013), hereafter called MD (for Maps et al. vertical distribution). As in the LD model, growth and predation on krill are not included. In the LD model, the vertical distribution of krill accounts for the two main species, *T. raschii* and *M. norvegica*; different distributions are specified for each species in the MD model. Rivers carry particulate and dissolved matter that affect the surface water clarity (or turbidity) in the marine environment. Le Fouest et al. (2006) established a relationship between light attenuation and surface salinity that can be used to estimate the light level experienced by zooplankton in deeper waters. The weighted mean depth (Z_{day}) of each species is determined by the surface salinity, with:

$$Z_{day} = 11.4 \times S_0 - 201 \qquad \text{for } T.\ raschii$$
$$Z_{day} = 7.5 \times S_0 - 64 \qquad \text{for } M.\ norvegica$$

where S_0 is the salinity of the surface layer (Maps et al., 2013; Plourde et al., 2013). The vertical position of each particle is set randomly with a normal distribution around the weighted mean depth. To maintain a distribution that is close to our LD distribution, we used a 30 m standard deviation around the daytime mean, which is wider than the 15 m used by Maps et al. (2013). In the regions where the bottom is shallower than Z_{day}, the distribution of krill was vertically compressed as shown in Figure 3 (case with a bathymetry of 100 m). During the night, the vertical distribution of the two species is set around 15 m with a standard deviation of 12.5 m (Maps et al. (2013) used a standard deviation of 10 m). It should be noted that the simulations start with a uniform distribution of 150 particles per species per grid cell. The results for each krill species are then summed for comparison with the results obtained with the LD model (section 2.2.1).

2.3 RIVER RUNOFF AND SIMULATIONS

The runoff of the St. Lawrence River is estimated from sea-level measurements at Lauzon (Lévis), Québec, using the relation of Bourgault and Koutitonsky (1999) and obtained from the St. Lawrence Global Observatory (http://ogsl.ca/en.html). This runoff represents current dammed conditions. Runoff for all other rivers is obtained from a hydrological model described in Lambert et al. (2013). The modification by human alterations of the annual runoff cycle of rivers from different regions (St. Lawrence River, rivers from the north shore of the lower estuary, rivers from the north shore of the GSL) can have different impacts on the circulation of the whole system and on physical mechanisms like nutrient pumping at the head of the Laurentian Channel. To isolate the particular impacts of runoff regulation from these different regions, we need to proceed by steps. We first performed a six-year reference simulation (2006–2011) with all the rivers displaying natural runoff (NATURAL), i.e., without human alterations. The hydrological model is based on precipitation and evaporation and thus reproduces the natural runoff distribution of the rivers. To obtain a natural runoff curve for the St. Lawrence River, we calculated the proportion of the natural yearly runoff that was “released” every month based on the calculations of S. Senneville (Institut des Sciences de la Mer, UQAR, Rimouski, QC; pers. comm.), in a report submitted to the Center of expertise on Hydropower Impacts on Fish and fish habitat (CHIF) in 2010 (see Figure 4). For each month, the calculated proportion was applied to the total runoff of the previous 11 months to account for water retention in lakes and/or reservoirs. We

applied the same method to the harnessed rivers, but this time to convert from natural conditions to harnessed conditions. For this conversion, we used runoff observations from the Saguenay, Manicouagan, Outardes, and Betsiamites rivers (hereafter called SMOB) for the 1970 to 2000 period to calculate the proportion of the runoff released each month (Figure 4). We then redistributed the runoff obtained with the hydrological model (total from previous 11 months) according to these proportions (Figure 5). The observed runoff for the Saguenay River was obtained from Alcan, while Hydro-Québec provided the runoff for Manicouagan, Outardes, and Betsiamites rivers (personal communications). The runoff cycle of the Romaine River was modified according to the planned discharge by Hydro-Québec (Table F6 of Hydro-Québec, 2007). There are no data available yet on the planned discharge for the projected management on the Little Mecatina River. We thus decided to use the same proportions as for the Romaine River (Figure 4).

Although alterations to the runoff cycle of the St. Lawrence River in winter and spring are not as large as for the large rivers harnessed for hydroelectric production (SMOB; Figure 6), the St. Lawrence River is the main source of freshwater in the GSL (Table 1) and we want to isolate its effect. We thus produced a simulation (SL) over the same six-year period using the observed (with its main freshwater sources, the Great Lakes and the Ottawa River, dammed) runoff for the St. Lawrence River, while maintaining the natural cycle for the other rivers. The SMOB rivers flow directly into the LSLE, and their runoff cycle is strongly modified by the presence of hydroelectric dams. We produced another simulation (SMOB) using dammed conditions for these rivers while maintaining the natural cycle for all other rivers. The same thing was done with the Romaine River (ROM) and with a combination of the Romaine and Little Mecatina rivers (ROMLM). Finally, to investigate the cumulative effect of harnessing all these rivers (St. Lawrence, Saguenay, Manicouagan, Outardes, Betsiamites, Romaine, Little Mecatina), we made a final simulation with all these rivers harnessed (ALL) (see Figure 2 for locations).

2.4 DATA ANALYSIS

Simulated oceanographic variables included in the analysis are the monthly mean salinity, temperature, and horizontal currents for the 0–50 m layer currents; sea-ice concentration, thickness, and duration; and krill density at each grid cell (integrated number of particles from the surface to the bottom) obtained with the LD and MD vertical distributions (Figure 3). The 0–50 m layer was chosen as it encompass the spring–summer mixed layer where primary production occurs (which will be analyzed in a second report) and where many fish and plankton larvae and young stages reside. The transports through four cross sections (Pointe-des-Monts, Honguedo Strait, Cabot Strait, and Nova Scotian Current) are also presented (see Figure 2 for locations). Monthly means obtained over the six-year period with the base simulation (NATURAL) are presented along with the differences between each of the simulation with harnessed rivers (SL, SMOB, ROM, ROMLM, ALL) and the base simulation. Results are presented for the GSL, the Scotian Shelf, and the Gulf of Maine. The Gulf Stream area was masked due to its inherent instability, which was generating random changes. The areal averages over distinct areas (Figure 7) are also presented for the 0–50 m temperature and salinity, and for krill density to assess the significance of the observed changes. Vertical averages of the transport at the different cross sections are also displayed. The standard deviation was calculated based on the monthly mean of the six-year simulation with the natural conditions to represent natural variability. We show the half of one standard deviation envelope (0.5 SD) to try to assess if the observed changes are of some significance to different physical or biological processes. Here we arbitrarily define a change as significant if the difference between natural and harnessed conditions is higher than 0.5 SD of natural conditions.

Many maps are presented in this report because although the areal and temporal means for the regions presented in Figure 7 are useful, higher resolution details are lost (e.g. for smaller areas such as the American Bank at the tip of the Gaspé Peninsula). We thus decided to keep both the spatial average information as well as the synthesis figures. The impacts of harnessing a particular river (or group of rivers) are regrouped in different sections to facilitate the search of information for the different stakeholders. The rivers under study are also plotted on the different maps to help the reader locate the exact location where the change was applied.

In the initial conditions for the krill simulations, particles are spread uniformly over the domain of the model and the model is run continuously from December 2005 to December 2011. To remove any bias generated by the initial conditions on the mean krill distribution, we only use the years 2007 through 2011 for the analysis. This should be kept in mind when comparing with the other variables that are averaged over the 2006 to 2011 period.

3 RESULTS

3.1 NATURAL CONDITIONS

The results of the simulation with natural conditions are first shown. This simulation will be used as basis of comparison between the different harnessing scenarios examined.

For the natural conditions, the monthly mean temperatures for the 0–50 m layer are shown in Figures 8 and 9. A direct comparison with observed 0–50 m temperature is not presented here, but the reader can refer to Lavoie et al. (2016) for a comparison of the mean seasonal sea-surface temperature (SST) obtained from satellite data and a simulation with realistic conditions (including runoff). The root mean square error was also calculated for temperature and salinity data, which were available over the whole water column in 2009 (see Table 1 of Lavoie et al. 2016). Monthly mean salinities for the 0–50 m layer are shown in Figures 10 and 11.

Under this scenario, the mean 0–50 m circulation displays the known circulation features over the model domain, such as the Anticosti Gyre in the northwest GSL (NWGSL), the Gaspé Current, the southeastward flow along the Magdalen Shallows (e.g., Koutitonsky and Bugden, 1991; Urrego-Blanco and Sheng, 2014b; Lavoie et al., 2016), the coastal Nova Scotian Current (NSC) and the southward flowing shelf break current (e.g., Hannah et al., 2001; Urrego-Blanco and Sheng, 2014b), and finally, the cyclonic circulation around the Gulf of Maine (Figures 12 and 13). The transports at selected cross sections (see Figure 1 for locations) are also shown in Figures 14 and 15. The simulated transport in the NSC at the Halifax line (see last panel of Figure 15) is in good agreement with the transport calculated by Loder et al. (2003) and Anderson and Smith (1989). A comparison of the simulated and estimated transport at Cabot Strait can also be found in Lavoie et al. (2016). The two seasonal circulation modes described by Lavoie et al. (2016) are also discernable in the mean 0–50 m circulation and at the different cross sections. In general, in Mode 1 (winter and spring), the circulation inside the GSL is more intense and many gyres are present, while in Mode 2 (summer and fall), the circulation is more open, with the main currents following the coasts.

Except in a few areas, there is no sea-ice formation in the Gulf of Maine or on the Scotian Shelf. In the GSL, sea-ice formation is initiated in the LSLE in mid-December and progresses towards the east, to reach Cabot Strait in February (Figure 16). Sea-ice extent in the GSL reaches a maximum in March, when it starts to melt. Sea ice can be advected toward the Scotian Shelf in February and March, pushed by northwesterly winds and ocean currents (Petrie et al., 2008; Urrego-Blanco and Sheng, 2014a; Galbraith et al., 2016). Sea ice disappears relatively rapidly in April. The mean sea-ice concentration

and thickness simulated for the six-year period are shown in Figures 17 and 18. The model has a tendency to overestimate sea ice along the Gaspé Peninsula, but overall sea ice is well reproduced by the model (see Figure 9 of Lavoie et al., 2016).

The monthly mean krill densities for the base simulation for the LD vertical distribution set-up are shown in Figures 19 and 20. Although there is no growth or predation on krill in this model, particle aggregations do occur in areas where high krill biomass are generally observed (Berkes, 1976; Simard and Lavoie, 1999; Harvey et al., 2009; Maps et al., 2015; McQuinn et al., 2015). However, in the LSLE and at the entrance of Chaleur Bay, the accumulation of krill, although present, is less dense in our simulation than observed (relative to other areas). Nevertheless, the aim in this report is to look at the impact of changes in circulation on the distribution of krill, and this can be achieved regardless of the size of the patches, which are realistically located. The monthly mean krill densities for the base simulation for the MD vertical distribution were very similar to those obtained with the LD distribution and we chose not to include them. However, the mean krill densities for the natural and harnessed scenarios over selected regions (Figure 7) are shown for both vertical distribution (Figures 21 and 22). A smaller number of regions are presented for krill than for the other variables since the boundary conditions for krill were set at Cabot Strait. Thus, Scotian Shelf (SS) and Gulf of Maine (GoM) are not included, and the reader should note that the Cabot Strait (CS) region is not entirely represented. The Upper Estuary (UE) and Northumberland Strait (NS) regions were also omitted.

There are fewer krill particles in the GSL with the MD distribution compared to the LD distribution (last panel of Figures 21 and 22). The spatial distributions are relatively similar with the two vertical distributions, but some differences can be noticed. There are comparatively more krill in the NWGSL and in the CGSL in early winter with the MD distribution than with the LD distribution, while there are fewer krill in the Anticosti Channel (AC) region in winter with the MD distribution. This indicates that the differences in vertical distribution led to a greater amount of krill being transferred from the AC region towards the NWGSL and CGSL with the MD distribution (Figure 22). The krill found in the LSLE are advected farther up the estuary with the MD distribution during summertime (not shown), which resulted in a later mean density decline in the LSLE with the MD distribution compared to the LD distribution.

3.2 HARNESSING OF THE ST. LAWRENCE RIVER (SL SCENARIO)

3.2.1 Salinity

The simulation with the regulated St. Lawrence River runoff shows saltier water in the 0–50 m layer in the LSLE starting in April (corresponding to the negative runoff anomaly in Figure 6). The “salty” pulse can be observed in the Gaspé Current in May, in Chaleur Bay in June, and on the Magdalen Shallows in July, and it reaches Cabot Strait in August (Figures 23 and 24). Saltier waters can be seen in the Nova Scotian Current in September and October (Figure 24). The salty pulse is followed by a freshwater pulse in the LSLE starting in October (corresponding to the positive runoff anomaly in Figure 6) and in the NWGSL starting in November (Figure 24). The freshwater pulse moves down to Chaleur Bay and the Magdalen Shallows in December and reaches the Scotian Shelf in January (Figure 23). In the Gulf of Maine, conditions are either fresher or near normal. The 0–50 m salinity changes with this scenario are significant (i.e., greater than 0.5 SD) only in the LSLE (November and December) and NWGSL (November; Figure 25).

3.2.2 Temperature

The changes in the mean 0–50 m temperature between the SL and natural simulations are small in general (Figures 26 and 27) and not significant (Figure 28). However, we notice warmer temperatures in winter (particularly in January and February) in the LSLE and in the NWGSL, while it is colder on the Scotian Shelf and in the Gulf of Maine (Figures 26 and 27). Another notable feature is the patchy distribution of the temperature anomalies from July to October and the stronger anomalies in the northeast GSL (NEGSL; which roughly corresponds to the combined AC, EC, and MT regions in Figure 7) in September and October (Figure 27).

3.2.3 Circulation

The most noticeable changes in the mean 0–50 m circulation between the natural and SL scenarios occur in the NWGSL, at Honguedo Strait, in the NEGSL, in the Laurentian Channel outside of Cabot Strait, and in the shelf break current along the Scotian Shelf, with variable intensity depending on the time of the year (Figures 29 and 30). In winter (December to March), the mean 0–50 m circulation changes are generally small. In the NWGSL and Honguedo Strait, the largest changes occur from April to June (Figures 29 and 31), when the runoff is reduced compared to the natural conditions (Figures 5 and 6). These runoff changes lead to a significant decrease in the depth-integrated (0-bottom) transport at Pointe-des-Monts in April and May (Figure 31, pink line). Changes in the NWGSL gyre and in the circulation between the tip of Anticosti Island and the Gaspé Peninsula are also simulated during this period. At Honguedo Strait, the currents flowing westward along the southern shore of Anticosti Island are diverted southward by the currents flowing eastward and out of the NWGSL. This feature, which we call Honguedo Strait blocking, is displaced towards the NWGSL in April and towards the central GSL in May. In June, the southward currents at Honguedo Strait get stronger. The resulting changes east of Anticosti Island (stronger gyre at the junction of the deep channels) lead to weaker inflow at Cabot-E (Figures 15, 29, and 32). The inflowing current just outside Cabot Strait is deviated towards the western side of the strait, which leads to a narrower outflow at Cabot-W, to a greater recirculation in the Laurentian Channel outside of Cabot Strait, and to a stronger shelf break current along the Scotian Shelf (especially in June; Figure 29). The reduced inflow/outflow at Cabot-E and Cabot-W are significant in May (all layers; Figure 32). However, there is no significant change in the transport when averaged across the whole cross section since the changes in inflow and outflow more or less cancel out.

Noticeable changes are observed in the NEGSL from August to October, although no clear pattern emerges (Figure 30). This period corresponds to Mode 2 circulation described by Lavoie et al. (2016) and to the period when the “salty pulse” exits the GSL at Cabot-W (Figure 24). Changes are not apparent in the 0–50 m layer, but there is a stronger outflow at Cabot-W during this period in the deeper layers, that is accompanied by a slightly stronger inflow at Cabot-E in September (Figures 15 and 32). A stronger outflow is also simulated in the fall at Cabot Strait (significant changes in September and October) when averaged over the whole transect (laterally and 0–bottom; Figure 32).

3.2.4 Sea ice

In the SL scenario, there is a greater sea-ice concentration around the Gaspé Peninsula in January that extends to the Magdalen Shallows in February (Figure 33). Conversely, the LSLE sea-ice concentration decreased. The sea ice is generally thicker over the whole season, except in the LSLE, especially in March (Figure 34). These changes in sea ice correspond to the fresher and warmer conditions observed in winter (Figures 23 and 26). The warmer conditions result partly from the increase in the freezing point of seawater linked to the surface freshening. So even though the conditions are warmer, more sea

ice can form due to the higher freezing point. Indeed, in the Gaspé Current, ice formation occurs a few days earlier in the SL simulation than under natural conditions (3–4 days) with a corresponding extension of sea-ice duration (Figure 35). Changes in sea-ice concentration and thickness are small (less than 8% and 3 cm) compared to the mean conditions (see Figures 17 and 18), while the interannual variability is very high (e.g., see ice volumes in the GSL from one year to the next in Figures 36 and 37 of Galbraith et al., 2016). In this context, the changes resulting from the St. Lawrence River runoff regulation are not significant.

3.2.5 Krill distribution

Although the anomalies are very patchy—even for a given region—due to the patchy nature of krill distribution, some changes between the SL and natural scenarios stand out. There are fewer krill in the LSLE and more krill at the mouth of Chaleur Bay in winter with SL (Figures 36 and 38) due to increased circulation out of the estuary (see PdM in Figures 14 and 31). There is also an increase in the amount of krill in the NWGSL in spring and summer (Figures 36, 37, and 38). The changes obtained with the MD vertical distribution are similar to those just described with the LD distribution (Figure 39). The only noticeable difference is an increase in the amount of krill along the north shore in August in the NWGSL and AC regions with MD (not shown), which result from differences in krill daytime depth that led to changes in the westward advection along the GSL's north shore. The patchy nature of the krill distribution led to small mean differences over a given region and to small mean changes between the scenarios. The significance of the changes is thus difficult to assess for krill distribution, and we will focus on the larger and most likely changes (based on our knowledge of the system's dynamics).

3.3 HARNESSING OF THE SAGUENAY, MANICOUAGAN, OUTARDES, AND BETSIAMITES RIVERS (SMOB SCENARIO)

3.3.1 Salinity

Runoff from the SMOB rivers is about one third of the St. Lawrence River runoff. However, modifications in the seasonal cycle in natural runoff by the construction of large hydroelectric dams are much greater than those experienced in the St. Lawrence River and its tributaries, where regulation to the waterways are mainly for navigation and flood control (Figure 5, Figure 6, and Table 1). Of all scenarios, modifications in SMOB runoff had the largest simulated impact on the 0–50 m salinity of the system (Figures 40 and 41). Freshening can be observed in the LSLE and Gaspé Current in December. The salinity anomaly propagates to the NWGSL and Chaleur Bay in January and covers the whole Magdalen Shallows in March. Finally, it reaches Cabot Strait and the eastern Scotian Shelf in April. The anomaly progressively becomes positive (higher salinity water) in May in the LSLE, and this positive anomaly is propagated to the Gaspé Current, NWGSL, and Magdalen Shallows. The same propagation occurs as with the winter negative anomaly in the following months. The salty anomaly reaches Cabot Strait in August. It then propagates to the Scotian Shelf, along the coast of Nova Scotia, and towards the Gulf of Maine from September to February. With the SL simulation, the salinity anomaly in the LSLE was greater along the south shore; however, the salinity anomaly is also strong along the north shore with the SMOB simulation. Significant changes in the 0–50 m layer salinity (Figure 25) are observed in the LSLE (December to April, June, and July), NWGSL (January to April,

July), Chaleur Bay (October and November), Magdalen Shallows (May, September, and October), and Scotian Shelf (July and August).

3.3.2 Temperature

Changes with the SMOB scenario are somewhat similar to those obtained with the SL scenario (section 3.2.2) but with larger anomalies (Figures 42 and 43), although still not significant (Figure 28). The LSLE and NWGSL warming and the Scotian Shelf cooling in winter are more important and last longer. The LSLE gets warmer during the summer as well (Figures 42 and 43).

3.3.3 Circulation

Circulation changes in the LSLE are noticeable from December to July, with the greatest changes between January and April (Figures 44 and 45). The latter period corresponds to the period of sustained higher runoff with the SMOB simulation compared to the natural conditions (see Figures 5 and 6) and to Mode 1 circulation of Lavoie et al. (2016). The higher runoff led to an increased outflow in the 0–50 m layer at PdM-S and to a reduced inflow/outflow in the 50–150 m layer at PdM-N and PdM-S, respectively (Figures 14 and 31). These changes are significant in April only for PdM-N and PdM-S, and in March and April when averaging across the whole transect (PdM; Figure 31). A significant transport increase in the 0–50 m layer is also simulated in February (Figures 14 and 31). There is a major runoff reduction from May to July, with a maximum reduction in June (Figures 5 and 6). The impact on the transport at PdM is clearly seen in Figures 14 and 31, with a reduction of the 0–50 m and 0–bottom outflow, and a reduction of the 50–150 m inflow at PdM-S in June. These changes are significant in June for the 0–50 m layer and from May to July for the 0–bottom layer (Figure 31). Changes in the 0–50 m layer circulation are also clearly seen in the NWGSL and at Honguedo Strait during that period, and especially from April to June (Figure 44). In April and May, the Anticosti Gyre intensifies, the Gaspé Current at the tip of the Gaspé Peninsula decelerates, and the transverse current from the western side of Anticosti Island towards the tip of the Gaspé Peninsula accelerates (Figures 12 and 44).

Circulation changes are also apparent at Cabot Strait between April and July. There is a stronger outflow at Cabot-W and a stronger inflow at Cabot-E in all layers in April and again in June and July (Figures 15 and 32). This period (April to July), corresponds to the passage of the freshwater anomaly (generated during the winter months) at Cabot-W. In June and July, there is a decrease in the transverse currents in the Laurentian Channel, between Cabot Strait and its mouth, and an intensification of the currents along both sides of the channel, which leads to an increase of the southward shelf break current along the Scotian Shelf in June (Figures 44 and 45). The transport changes at Cabot Strait are significant, especially in the 50–150 m layer and in June, for both sides of the transect and for the whole transect (Figure 32). There are no significant changes in transport at NSC.

As for the SL simulation (section 3.2.3), circulation changes appear in the NEGSL in fall (between August and November; Figure 45), during the passage of the “salty” anomaly at Cabot-W. A reduced outflow at Cabot-W and a reduced inflow at Cabot-E are observed during this period (Figures 15 and 32). The changes are significant in August only (Cabot-W and Cabot-E, 50–150 m; Cabot and Cabot-W, 0–bottom).

3.3.4 Sea ice

As mentioned in section 3.2.4, the high interannual variability in sea-ice conditions leads to non-significant changes with regard to the 0.5 SD level. However, we find it noteworthy to describe the main changes. The sea-ice concentration in January is greater around the Gaspé Peninsula (Figure 46), but less so than with SL. In February and March, there is a greater sea-ice concentration in the LSLE (contrary to SL), Chaleur Bay, and Magdalen Shallows, but a lower sea-ice concentration around the Pointe-des-Monts area. The sea ice is generally thicker throughout the season, except in April when it is thinner and less concentrated around the Gaspé Peninsula (Figure 47). These changes in sea ice correspond to the much fresher and warmer conditions observed in winter (Figures 40 and 42). Changes in sea-ice occurrence are different than those simulated with SL (section 3.2.4). Sea ice appears a few days later and disappears a few days earlier in the NWGSL, while it disappears later in the LSLE (Figure 48). The sea-ice duration is thus almost a week longer in the LSLE while it is shorter in the NWGSL.

3.3.5 Krill distribution

The sign of changes in krill concentration obtained with the LD distribution (although not necessarily their magnitude) is mostly similar to those simulated with SL, except in the NWGSL in spring and summer (Figure 38). There is a decrease in the amount of krill in the LSLE and in the Gaspé Current, with an increase in Chaleur Bay in winter (especially in February and March; Figures 38 and 49), due to increased circulation out of the estuary (see PdM 0–50m and 0–bottom, and Honguedo 0–50 m in Figures 14 and 31). The decrease in the amount of krill in the LSLE is significant in April only, while the increase in Chaleur Bay is significant in March only (Figure 38). Other significant changes include decreases in Chaleur Bay (June), Cabot Strait (July), and Esquiman Channel (most of the summer, although only a small change; Figure 38). However, as discussed in section 3.2.5, the significance of krill changes is difficult to assess and the changes should be considered as qualitative rather than a quantitative. In the NWGSL, the krill densities simulated with the different scenarios fall within the range of natural variability. However, due to changes in transport in the deep and surface layers, there are fewer krill in the NWGSL in spring and summer. More krill are concentrated in the CGSL at this time, but there also appears to be fewer krill in the GSL in general.

Between September and December, there is a significant decrease in krill density in the western part of the NEGSL (part of the AC region), including south of Anticosti Island (Figures 38 and 50), as well as an increase in the eastern part of the NEGSL (EC region). In the CGSL, the decrease in krill density is significant in November and December.

The changes obtained with the MD distribution (Figure 39), are similar to those just described from the LD distribution. However, from July to September there are more krill along the north shore, in the Anticosti Channel and NWGSL regions when using the MD distribution (not shown). The same difference was noted with SL in August (section 3.2.5).

3.4 HARNESSING OF THE ROMAINE AND LITTLE MECATINA RIVERS (ROM AND ROMLM SCENARIOS)

3.4.1 Salinity

Hydro-Québec plans to increase the Romaine River runoff in winter (December to April) and to reduce it between May and July, with a maximum reduction in June (Figures 4, 5, and 6). We applied the same changes to the Little Mecatina River. The June reduction is similar to the runoff reduction for the St. Lawrence River during that month (Figure 6) while the average runoff remains relatively unchanged in the fall. From the location of the Romaine River mouth (Figure 2) and the monthly mean circulation in the 0–50 m layer (Figures 12 and 13), we can see that the freshwater flowing out of the Romaine River will mainly travel westward along the north shore of the GSL and into the Anticosti Gyre or the Gaspé Current. In winter, this freshwater journey led to a freshening of the NWGSL (Figures 25 and 51). In June and July, the Anticosti Gyre is smaller and there is a southward circulation at the western tip of Anticosti Island (Figures 12 and 13). This circulation and the runoff reduction of the Romaine River led to a freshening in the western side of the NWGSL and to an increase in salinity along the north shore of the NWGSL and at Honguedo Strait (Figures 51 and 52). Although there is not a clear salinity anomaly propagation at Cabot-W as was the case for SL and SMOB, we nevertheless see a decrease in salinity at Cabot Strait in October and an increase in salinity on the Scotian Shelf in the fall (October to December; Figures 25 and 52).

The response is different when both the Little Mecatina River and the Romaine River (ROMLM) are harnessed. From the location of the Little Mecatina River's mouth (Figure 2) and the monthly mean circulation in the 0–50 m layer (Figures 12 and 13), we can see that the Little Mecatina River runoff has a greater chance of recirculating east along the north shore of the Anticosti Island, especially in winter and spring. The anomalies in winter and spring are somewhat similar to those with ROM alone (Figures 51 to 54), although the amplitude of the mean change is greater in the Anticosti Channel (Figures 7 and 25). There is a noticeable change in winter with ROMLM compared to ROM: with ROMLM, there is a freshening of the western Scotian Shelf and Georges Bank, which were saltier with ROM (Figures 51 to 54). However, the mean salinity changes obtained with ROM and ROMLM are not significant in any of the subregions when compared to the natural variability (0.5 SD; Figure 25).

3.4.2 Temperature

Harnessing of the Romaine and Little Mecatina rivers does not bring much change to the 0–50 m temperature and overall temperature changes are not significant (Figures 28 and 55 to 58). As observed with the previous simulations (SL and SMOB), the changes observed in the fall in the NEGSL and Cabot Strait regions are very patchy.

3.4.3 Circulation

Harnessing of the Romaine and Little Mecatina rivers had an impact on the circulation over the whole model domain (Figures 59 to 62), with magnitudes that are comparable to those of the two previous simulations (SL and SMOB), except at Pointe-des-Monts and upstream (Figures 31 and 32). The main features at Honguedo Strait are an increased inflow in the 50–150 m layer (in March–April with ROM, and April–May with ROMLM), and a decreased outflow in the 0–50 m layer (in May–June with ROM, and from March to July with ROMLM; Figures 14 and 31). These changes are an average across the whole transect and most likely result from a slight increase in the circulation around the eastern tip of Anticosti Island (Figures 59 and 61). While these changes are not significant, significant changes do appear at Cabot Strait in June (ROM) and June–July (ROMLM) in all layers when looking at either

side of the transect (W and E). There is a stronger outflow at Cabot-W accompanied by a stronger inflow at Cabot-E (Figures 15 and 32). As was the case with SL (section 3.2.3), these differences cancel out when averaging across the whole transect. However, the stronger outflow led to a stronger shelf break current along the Scotian Shelf in June (Figures 59 and 61), which translated into significant transport changes at NSC (in June) with ROMLM (all layers; Figure 32).

Changes are less uniform with the two simulations in the fall. There is a reduced outflow/inflow at Cabot-W/Cabot-E with ROM in October–November, while the changes are more variable with ROMLM (Figure 32). When looking at the average transport across the whole Cabot Strait cross section, we observe an increased outflow in the 50–150 m layer (stronger with ROM). In the 0–bottom layer, there is a significant increase (October) in the outflow with ROM as well as with ROMLM (October and December), although a significant reduction in the outflow (August and September) precedes the increase with the ROMLM simulation (Figure 32). This increased outflow at Cabot Strait in October is accompanied by a significant reduction in transport at NSC in the 50–150 m layer with ROMLM (Figure 32).

3.4.4 Sea ice

Changes in sea ice (concentration, thickness, duration) are somewhat similar with both simulations (although slightly greater with ROM than with ROMLM). Changes in sea ice are greater in Jacques-Cartier Strait, where the Romaine River flows, and around the western tip of Anticosti Island (Figures 63 to 68). The LSLE and southern GSL are not affected by runoff alterations of the Romaine and Little Mecatina rivers. Sea-ice duration along the north shore west of the river mouth is extended by almost a week in the ROM simulation (Figure 67). However, all these changes are not significant when averaged over the different regions (Figure 7).

3.4.5 Krill distribution

With the ROM and ROMLM simulations, some similar patterns emerge, although sometimes stronger with ROMLM or ROM depending on the region. There is an increase in the amount of krill in the NEGSL from November to January; an increase in the NWGSL in spring and summer, accompanied by a decrease in Chaleur Bay (especially with ROMLM); and a decrease around the eastern part of Anticosti Island from October to December (Figures 38 and 69 to 72). However, one feature present with ROMLM but not with ROM is the increase in the amount of krill south of Anticosti Island (CGSL region) from July to September (Figures 38 and 72). When looking at the regional subdivisions (Figure 7), significant changes (with either or both simulations) are: the June decrease in Chaleur Bay, the July–August decrease at Cabot Strait, the fall (September to November) decrease in Anticosti Channel, and the August–September increase in CGSL (Figure 38).

The changes in krill density with the MD vertical distribution were mostly similar to those just described with the LD vertical distribution (Figure 39). However, with the ROM simulation, there is more krill along the north shore of the GSL, in the Anticosti Channel and NWGSL regions, from July to October with the MD distribution (not shown). A similar difference was noted with the SL simulation in August (section 3.2.5) and with the SMOB simulation from July to September (section 3.3.5). With ROMLM, there are also differences between the LD and MD distribution in the fall, but they are located in the Honguedo Strait region, with a greater accumulation of krill observed in that area with the MD distribution (not shown).

3.5 HARNESSING OF ALL RIVERS (ALL SCENARIO)

3.5.1 Salinity

The largest freshwater changes in the 0–50 m layer are obtained when all the rivers under study are harnessed (Figures 73 and 74). For the most part, the impact of the runoff changes on the salinity cumulates, but not always and not everywhere due to the impact of density changes on the circulation. In the LSLE, NWGSL, Magdalen Shallows, Chaleur Bay, and Northumberland Strait, the cumulative impact of harnessing all the rivers (ALL) on the salinity is to amplify the strong anomaly detected with the SMOB simulation (e.g., in Figure 25 the red line [ALL] is mostly the sum of SL and SMOB). In CGSL, Esquiman Channel, and Cabot Strait, the cumulative impact is similar to the SMOB impact, except at Cabot Strait in the fall (Figure 25). Note that at this time the salinity changes with SMOB and SL are of opposite signs. In Anticosti Channel, the changes in ALL follow those in ROMLM, while on the Scotian Shelf and in the Gulf of Maine there is no clear pattern.

The biggest significant cumulative salinity changes are observed in the LSLE and NWGSL regions in winter and in summer (Figure 25). Significant changes are also observed in Chaleur Bay (April, May, August to October), Magdalen Shallows (April to June, August to October), and Northumberland Strait (August to November). These regions are strongly influenced by the runoff originating in or transiting through the LSLE. Although no significant changes are observed at Cabot Strait, there is a significant change on the Scotian Shelf during the summer period (Figure 25). In addition to Cabot Strait, no significant changes are found in the 0–50 m layer in Anticosti and Esquiman channels, or in the Gulf of Maine. However, the freshening in CGSL in February is significant.

3.5.2 Temperature

When all the rivers are harnessed (ALL), the LSLE and NWGSL display warmer conditions in the 0–50 m layer in winter and summer with greater changes in January–February and July–August (Figures 75 and 76). Conversely, colder conditions are simulated for the Scotian Shelf in winter, in Chaleur Bay in June–July, and in Northumberland Strait in July–August. In the NEGSL, greater patchy, changes are observed from August to October. There are no strong or obvious changes for the Gulf of Maine. These temperature changes are not significant except in February in the LSLE (warming of about 0.25°C) and in July in Chaleur Bay (cooling of about 0.35°C; Figure 25).

3.5.3 Circulation

The cumulative impact on circulation of harnessing all the rivers is presented in Figures 31, 32, 77, and 78. Overall, the changes are similar to those obtained with SMOB but with additional features resulting from SL. However, the cumulative impact on the dynamics sometimes leads to changes opposite to those obtained when changing a single or a subgroup of rivers (e.g., transport at Cabot-W and Cabot-E in October; Figure 32).

The increased runoff in SMOB in winter led to an increased outflow at PdM and Honguedo Strait in the surface layer (significant transport changes in January and March at PdM and in February at Honguedo Strait; Figure 31). The response with ALL is more complex in the 50–150 m layer and is attenuated in winter compared to SMOB only, especially in February when the influence of ROM is strong (Figures 14 and 31). The decreased runoff in spring led to a reduced outflow at PdM (significant in June–July) and Honguedo Strait, and to a reduced inflow in the 50–150 m layer (significant in June; Figure 31). A

reduction in the strength of the Gaspé Current is also apparent in May and June in the ALL scenario (Figure 77).

At Cabot Strait, the circulation and transport changes obtained with the ALL simulation are complex. The different scenarios (SL, SMOB, ROM, and ROMLM) sometimes led to changes of opposite signs at Cabot Strait. For example, the transport changes at Cabot-W and Cabot-E in the 50–150 m layer and in the 0–bottom layer are of opposite signs between April and December for the SL and SMOB scenarios, although the origin of the freshwater anomaly is located in the LSLE (Figure 32). While the response with the ALL scenario is more or less an average of the SL and SMOB response during the spring and summer, the sign of the change can be different than with all the other scenarios, as in October for example. Interestingly, when considering the whole Cabot Strait cross section from the surface to the bottom, we find a significant increase in transport during that month (October; Figure 32). The circulation in this region is complex, with gyres just inside and just outside Cabot Strait. Since no changes in forcing other than the river runoff was made, it appears that changes in the dynamics at Pointe-des-Monts, Jacques-Cartier, and Honguedo Straits have an impact on the outflow/inflow at Cabot Strait. In other words, changes in the dynamics of the whole GSL are important, not only the local density changes generated on the western side of Cabot Strait by the passage of the salinity anomalies. The hydrodynamics is affected by changes in the stratification of the ocean that modify the vertical eddy viscosities and diffusivities that affect entrainment and mixing. There are no significant changes in transport at NSC with ALL.

3.5.4 Sea ice

The impact of the SMOB and ROM perturbations dominate the sea-ice changes obtained with the ALL simulation (Figures 79, 80 and 81). The sea-ice concentration is greater in the Betsiamites, Manicouagan, and Outardes river plumes in the LSLE, in the Romaine river plume, and in the NWGSL in general in January (Figure 79). In February and March, the concentration is greater just west of the Betsiamites and Outardes river mouths and smaller just east of them. The higher concentration near the Romaine River persists, and there is a greater sea-ice concentration in Chaleur Bay and Magdalen Shallows. The sea ice is thicker in general, except in the Gaspé Current in April (Figure 80). The sea ice starts to grow a few days earlier in the LSLE, NWGSL, CGSL, and Magdalen Shallows due to the lower salinities and disappears later, especially in the LSLE and near the Romaine River (Figure 81). Overall, the sea ice lasts a few days longer (Figure 81). However, as mentioned in the previous sections, these changes are not significant when compared to the high natural interannual variability in sea-ice conditions.

3.5.5 Krill distribution

The main changes in krill concentration with the ALL simulation are similar to those obtained with the SMOB simulation (Figures 38, 82, and 83). However, the response is amplified in the LSLE, NWGSL, and Chaleur Bay in winter, while it is reduced in Anticosti and Esquiman channels and in CGSL in fall (Figure 38). There is an important decrease in the amount of krill in the LSLE and in the Gaspé Current in winter and in spring (Figures 38 and 82). In the LSLE, the mean changes are significant in March and April (Figure 38). There is also an increase in Chaleur Bay in the first part of the year (significant in March), followed by a decrease in the second part (significant in September; Figures 38, 82, and 83). A significant decrease is also simulated in Esquiman Channel and Cabot Strait in summer and in Anticosti Channel in fall (Figure 38).

As with the other scenarios, the changes are similar with the MD and LD distributions except for a greater amount of krill along the north shore of the GSL in the AC and NWGSL regions in July and August (not shown).

4 SUMMARY AND DISCUSSION

4.1 SALINITY CHANGES

Significant changes to the mean 0–50 m salinity were obtained with the SL, SMOB, and ALL scenarios. The salinity anomalies propagated from the LSLE to the southern GSL regions (including Chaleurs Bay) and Scotian Shelf with propagation times that are similar to those reported in the literature (three to four months to reach Cabot Strait, e.g., Sutcliffe et al., 1976; Ohashi and Sheng, 2013). SMOB had the strongest impact on surface salinity and stratification because the runoff alterations are greater than with SL and the water is released directly into the surface layer of the LSLE. In the SL scenario, the freshwater anomaly is smaller and mixing taking place in the upper estuary is generally high, which increases the surface salinity. Increasing or decreasing the stratification by the addition or removal of freshwater influences the vertical mixing and entrainment between the different layers of the systems and thus the response will vary depending on the season.

4.2 TEMPERATURE CHANGES

Different studies suggest that runoff is not the principal factor controlling the thermal variability in surface waters. In the LSLE, the temperature anomalies are mostly determined by tidally induced upwelling at the head of the Laurentian Channel (Gratton et al., 1988). In the GSL, it is the coupling between air and sea-surface temperatures on seasonal time scales that seems to be determinant for surface water temperature (Galbraith et al., 2012). Sutcliffe et al. (1976) suggested that the St. Lawrence River discharge could have an impact on the sea-surface temperature in the Gulf of Maine, although not necessarily directly. We observed some temperature changes in the Gulf of Maine in the different scenarios. Bugden et al. (1982) estimated a potential upper layer temperature decrease of 0.5°C during spring in the GSL due to freshwater regulation of the St. Lawrence, Ottawa, and Saguenay rivers. The simulated temperature anomalies we obtained with the different scenarios are smaller than those inferred by Bugden et al. (1982). In winter, part of the surface warming results from freshening of the surface layer, which increased the freezing point of seawater (in the GSL). The remaining temperature changes in the different regions result from differences in entrainment and advection. Except for the LSLE in February and Chaleur Bay in July with the ALL scenario, none of the simulated temperature changes were significant.

4.3 CIRCULATION CHANGES

The response of the circulation to the runoff anomalies is strongly influenced by the location of the river mouth. For example, increasing the runoff of the SMOB rivers in winter had an impact on the inflow and outflow along the northern and southern sides of the Pointe-des-Monts transect in the 50–150 m layer. This could either result from a change in estuarine circulation due to reduced pumping at the head of the Laurentian Channel by tidal upwelling or from a deceleration of the inflowing current at Pointe-des-Monts resulting from a greater outflow along the north shore in the LSLE (described by Lavoie et al., 2016). Similarly, the Romaine River flows directly into the Jacques-Cartier Strait, where upwelling and current diversion also occur. Modifying the runoff of this river led to changes in the NWGSL circulation and in the circulation around Anticosti Island. Finally, outflow of Little Mecatina River has an impact on the coastal current in the NEGSL, which can be more or less close to the shore

depending on its strength. It thus has an impact on the circulation around the Anticosti Island, as does the ROM scenario, but also on the circulation in the NEGSL.

It is noteworthy that significant changes to the Nova Scotian Current were observed with the ROMLM scenario only. With the SL and SMOB scenarios, a salinity anomaly (positive or negative) propagates from the LSLE to the Cabot Strait, affecting the dynamics of different regions as it travels down. Past Cabot Strait, flow changes are observed along the shelf break and in the central Scotian Shelf (Emerald Basin) or closer to the coast (NSC). It thus appears that ROMLM, which had a greater influence on the circulation in the eastern GSL, had a greater impact in the near-shore region of the Scotian Shelf than the other scenarios.

It is also noteworthy that SL and SMOB generated changes of opposite signs at Cabot Strait in the 50–150 m and 0–bottom layers (see section 3.5.3, Figures 31 and 32) even though both displayed the passage of a salinity anomaly at Cabot-W. These differences most likely result from the different response in circulation and entrainment of the deeper layers that was observed at PdM. The response to SMOB is much more important at PdM-N and PdM-S than with SL (Figure 31). Lavoie et al. (2016) showed that the inflow at Cabot Strait contributed to the strength of the Anticosti Gyre. Our results here demonstrate that the opposite is also true, i.e., the dynamics inside the GSL—and not only near the strait—also have an impact on the flow at Cabot Strait, reinforcing the concept that the GSL behaves somewhat like a large estuarine system.

The circulation modes in which the anomalies occur also have an impact on the response of the system. For example, when the salinity anomaly reaches Cabot Strait in June (near the transition from Mode 1 to Mode 2), the inflow at Cabot-E and the outflow at Cabot-W reach their minimums, changes occur on both sides but cancel out when averaged across the transect. However, in fall (Mode 2), the outflow at Cabot-W is accelerating and is stronger than the inflow at Cabot-E (Figure 15). The passage of the salinity anomaly at Cabot-W predominates and generates instabilities in the NEGSL.

4.4 SEA-ICE CONDITIONS

Runoff regulations of the St. Lawrence, Saguenay, Manicouagan, Outardes, and Betsiamites rivers led to an increased flux of freshwater in winter that reduced the surface salinity in the GSL, therefore leading to an increase in the freezing point of seawater. The latter led to earlier sea-ice formation in general and to greater sea-ice concentration, at least in the southern GSL, due to increased transport in the surface layer. Because of these changes, the sea ice lasted longer. The very high interannual variability in sea-ice conditions over the 2006 to 2010 period prevents us from assessing the significance of these changes based on the standard deviation obtained with the base simulation. However, the harnessing of these rivers, which occurred between the 1920s and the 1970s (see Table 1), could have favoured seal populations that whelp on sea ice in the GSL, especially in the last decade when sea-ice conditions for the seals were poorer (Bajzak et al., 2011). A similar response is expected to occur with the damming of the Romaine and Little Mecatina rivers, although the impacted region is much smaller (Jacques-Cartier Strait and eastern part of the NWGSL). Sea ice is also thinner in this area than in the southern GSL.

4.5 KRILL

In general, the runoff alterations led to a greater transport of krill out of the LSLE in winter during their nighttime presence in the surface layer (except for ROM and ROMLM), and to a greater accumulation near the entrance of Chaleur Bay. The cumulative impact with all the rivers harnessed mostly followed the response of the SMOB scenarios. So although we simulate an increase in krill in the NWGSL in

spring and summer with SL, ROM, and ROMLM, we simulate a decrease with the SMOB and ALL scenarios. With the SMOB and ALL scenarios, flushing was greater and krill accumulated in the downstream region (CGSL) rather than in the NWGSL. There were also fewer krill in general in the GSL. So although harnessing ROM and ROMLM brought a greater transport of krill from the NEGSL towards the NWGSL (from north of Anticosti Island and south of Anticosti Island respectively), the greater flushing cancelled the impact the flow alterations would have had if the SMOB rivers still had a natural flow. The importance of the winter and spring changes in krill distribution is difficult to assess. Blue whales feed in the LSLE mainly in summer, and the quantity of krill at this time in the LSLE and NWGSL is relatively unchanged with the ALL scenario (see July and August in Figure 21 and 22). Whales are abundant in LSLE, and dams have been present for a few decades. Changes in whale distribution thus appear to be more influenced by natural variability. Adjustment of the krill daytime depth in relation to freshwater runoff could potentially have an impact in summer and fall. The differences obtained between each scenario were qualitatively similar with the LD and MD distributions, except that there were more krill along the north shore of the GSL at the end of the summer with MD. Krill also travelled further up the estuary in summertime with MD.

5 CONCLUSION

Harnessing of SL and SMOB rivers occurred between the 1920s and the 1970s. SMOB had the greatest impact on the surface salinity, sea ice, and circulation from the LSLE down to Cabot Strait. It potentially led to reductions of krill aggregations in the LSLE in winter and spring. Nevertheless, for these periods of the year, the LSLE is less frequented by marine mammals, including blue whales that feed mainly on krill. The greater sea-ice thickness and duration in the southern GSL could have been favourable to the seals that whelp on sea ice in that region.

The present construction of the Romaine River dams may have an impact on krill transport between the NEGSL (where it accumulates in winter) towards the NWGSL, from where it can then be advected towards the head of the Laurentian Channel in the LSLE. It also has the potential to have a significant impact on transport at Cabot Strait when the latter is weak. However, the mean changes brought by alterations of the Romaine River runoff generally remain below the natural variability simulated by the model.

It was shown that building a hydroelectric dam on the Little Mecatina River in addition of that on the Romaine River could affect the circulation around Anticosti Island, with a greater accumulation of krill in the CGSL and a significant impact on the Nova Scotian Current, both in the fall. Significant changes to this current were simulated with the ROMLM scenario only. However, when adding the transport changes at Cabot Strait generated by the SL and SMOB scenarios (which appear to have an effect on the shelf break current rather than the NSC), the changes remain below the natural variability. It thus appears that ROMLM could affect the NSC in the fall when the outflow at Cabot-W is weaker than normal.

Finally, it is difficult to assess the overall significance of the simulated changes for the different components of the ecosystem because responses differ depending on the time of the year and on the region. A second modelling study including the biogeochemical components (nutrient supply, primary production, hypoxia, and the inorganic carbon system) is underway. The results will be presented in a second report and will help to evaluate the importance of river harnessing on the ecosystems of the GSL and on the Scotian Shelf.

ACKNOWLEDGMENTS

We thank Daniel Bourgault from the Institut des Sciences de la Mer (ISMER) and Peter Galbraith from the Maurice-Lamontagne Institute (MLI) for their careful review of the report. We thank Salman Hafeez for the calculation of the river proportions used for runoff redistributions. We thank Gilles Fortin (MLI) for providing the river shapefiles used in the different figures. We also thank Simon Trépanier (MLI) for providing information on Hydro-Québec's plans for the Romaine River. This study was financed by the Center of expertise on Hydropower Impacts on Fish and fish habitat (CHIF) and by the Strategic Program for Ecosystem-based Research and Advice (SPERA).

REFERENCES

Anderson, C., and Smith, P.C. 1989. Oceanographic observations on the Scotian Shelf during CASP. Atmos.-Ocean 27(1): 130–156.

Bajzak, C.E., Hammill, M.O., Stenson, G.B., and Prinsenberg, S. 2011. Drifting away: implications of changes in ice conditions for a pack-ice-breeding phocid, the harp seal (Pagophilus groenlandicus). Can. J. Zool. 89(11): 1050–1062.

BAPE 2001. Projets de dérivation partielle des rivières Portneuf et du Sault aux Cochons. Bureau d'audiences publiques sur l'environnement (BAPE), Rapport 145, 168 pp. http://www.bape.gouv.qc.ca/sections/rapports/publications/bape145.pdf.

Berkes, F. 1976. Ecology of euphausiids in the Gulf of St. Lawrence. J. Fish. Res. Board Can. 33(9): 1894–1905.

Biemans, H., Haddeland, I., Kabat, P., Ludwig, F., Hutjes, R.W.A., Heinke, J., von Bloh, W., and Gerten, D. 2011. Impact of reservoirs on river discharge and irrigation water supply during the 20th century. Water Resour. Res. 47: W03509, doi: 10.1029/2009wr008929.

Bourgault, D., and Koutitonsky, V.G. 1999. Real-time monitoring of the freshwater discharge at the head of the St. Lawrence Estuary. Atmos.-Ocean 37(2): 203–220.

Brickman, D., and Drozdowski, A. 2012. Development and validation of a regional shelf model for Maritime Canada based on the NEMO-OPA circulation model. Can. Tech. Rep. Hydrogr. Ocean Sci. 278: vii+257 pp.

Bugden, G.L., Hargrave, B.T., Sinclair, M.M., Tang, C.L., Therriault, J.C., and Yeats, P.A. 1982. Freshwater runoff effects in the marine environment: The Gulf of St. Lawrence example. Can. Tech. Rep. Fish. Aquat. Sci. 1078: 1089 pp.

Cataliotti-Valdina, D., and Long, B.F. 1984. Évolution estuarienne d'une rivière régularisée en climat sub-boréal: la rivière aux Outardes (côte nord du golfe du St-Laurent, Québec). Can. J. Earth Sci. 21: 25–34.

Cyr, F., Bourgault, D., Galbraith, P.S., and Gosselin, M. 2015. Turbulent nitrate fluxes in the Lower St. Lawrence Estuary, Canada. J. Geophys. Res. 120(3): 2308–2330.

Degu, A.M., Hossain, F., Niyogi, D., Pielke, R., Sr., Shepherd, J.M., Voisin, N., and Chronis, T. 2011. The influence of large dams on surrounding climate and precipitation patterns. Geophys. Res. Lett. 38(4): L04405, doi: 10.1029/2010gl046482.

Drapeau, G. 1980. Appréciation préliminaire de l'estuaire et du golfe du Saint-Laurent dans le contexte des aménagements de bassins des principales rivières de la Côte Nord. INRS-Océanologie, Rimouski, 46 pp.

Fortin, G.R., and Pelletier, M. 1995. Synthèse des connaissances sur les aspects physiques et chimiques de l'eau et des sédiments du Saguenay: Rapport technique, zones d'intervention prioritaire 22 et 23. Centre Saint-Laurent, Environnement Canada, 192 pp.

Gagné, J.A., Ouellet, P., Savenkoff, C., Galbraith, P.S., Bui, A.O.V., and Bourassa, M.-N. 2013. Rapport intégré de l'initiative de recherche écosystémique (IRÉ) de la région du Québec pour le projet : les espèces fourragères responsables de la présence des rorquals dans l'estuaire maritime du Saint-Laurent. DFO Can. Sci. Advis. Sec. Res. Doc. 2013/086. vi + 181 pp.

Galbraith, P.S., Larouche, P., Chasse, J., and Petrie, B. 2012. Sea-surface temperature in relation to air temperature in the Gulf of St. Lawrence: Interdecadal variability and long term trends. Deep-Sea Res. II 77–80: 10–20.

Galbraith, P.S., Chassé, J., Caverhill, C., et al. 2016. Physical oceanographic conditions in the Gulf of St. Lawrence in 2015. DFO Can. Sci. Advis. Sec. Res. Doc. 2016/056. v+90 pp. http://waves-vagues.dfo-mpo.gc.ca/Library/365838.pdf.

Gillanders, B.M., and Kingsford, M.J. 2002. Impact of changes in flow of freshwater on estuarine and open coastal habitats and the associated organisms. *In* Oceanography and Marine Biology: An Annual Review, Volume 40. Edited by R. N. Gibson, et al. CRC Press. pp. 233-309.

Goosse, H., and Fichefet, T. 1999. Importance of ice-ocean interactions for the global ocean circulation: A model study. J. Geophys. Res. 104(C10): 23337–23355.

Gratton, Y., Mertz, G., and Gagne, J.A. 1988. Satellite observations of tidal upwelling and mixing in the St. Lawrence Estuary. J. Geophys. Res. 93(C6): 6947–6954.

Greisman, P., and Ingram, G. 1977. Nutrient distribution in the St. Lawrence estuary. J. Fish. Res. Board Can. 34(11): 2117–2123.

Hannah, C.G., Shore, J.A., Loder, J.W., and Naimie, C.E. 2001. Seasonal circulation on the western and central Scotian Shelf. J. Phys. Oceanogr. 31(2): 591–615.

Harrison, J.A., Frings, P.J., Beusen, A.H.W., Conley, D.J., and McCrackin, M.L. 2012. Global importance, patterns, and controls of dissolved silica retention in lakes and reservoirs. Global Biogeochem. Cycles 26(2): GB2037, doi: 10.1029/2011gb004228.

Hart, B.S., and Long, B.F. 1990. Recent evolution of the Outardes Estuary, Quebec, Canada: consequences of dam construction on the river. Sedimentology 37(3): 495–507.

Harvey, M., Galbraith, P.S., and Descroix, A. 2009. Vertical distribution and diel migration of macrozooplankton in the St. Lawrence marine system (Canada) in relation with the cold intermediate layer thermal properties. Prog. Oceanogr. 80(1–2): 1–21.

Hassan, E.M. 1975. Some effects of river regulation on marginal seas. Ocean Management 2(4): 333–344.

Hossain, F., Jeyachandran, I., and Pielke, R., Sr. 2009. Have large dams altered extreme precipitation patterns? EOS Trans. Am. Geophys. Union 90(48): 453–454.

Hudon, C., and Carigan, R. 2008. Cumulative impacts of hydrology and human activities on water quality in the St. Lawrence River (Lake Saint-Pierre, Quebec, Canada). Can. J. Fish. Aquat. Sci. 65(6): 1165–1180.

Humborg, C., Conley, D.J., Rahm, L., Wulff, F., Cociasu, A., and Ittekkot, V. 2000. Silicon retention in river basins: far-reaching effects on biogeochemistry and aquatic food webs in coastal marine environments. Ambio 29(1): 45–50.

Hydro-Québec 2007. Complexe de la Romaine, Étude d'impact sur l'environnement. Volume 8. Multiple pagination.

Hydro-Québec 2008. Complexe de la Romaine, Résumé de l'étude d'impact sur l'environnement. 119 pp.

Ingram, R.G., and El-Sabh, M.I. 1990. Fronts and mesoscale features in the St. Lawrence Estuary. *In* Oceanography of a Large-Scale Estuarine System: The St. Lawrence. Edited by M. I. El-Sabh and N. Silverberg. Springer-Verlag, Germany. pp. 71–93.

Ittekkot, V., Humborg, C., and Schaefer, P. 2000. Hydrological alterations and marine biogeochemistry: A silicate issue? Bioscience 50(9): 776–782.

Kaartvedt, S., and Svendsen, H. 1990. Advection of euphausiids in a Norwegian fjord system subject to altered freshwater input by hydro-electric power production. J. Plankton Res. 12(6): 1263–1277.

Koutitonsky, V.G., and Bugden, G.L. 1991. The physical oceanography of the Gulf of St. Lawrence: A review with emphasis on the synoptic variability of the motion. *In* The Gulf of St. Lawrence: Small Ocean or Big Estuary. Edited by J. C. Therriault. Can. Spec. Pub. Fish. Aquat. Sci. 113. pp. 57–60.

Lambert, N., Chassé, J., Perrie, W., Long, Z., Guo, L., and Morrison, J. 2013. Projection of future river runoffs in Eastern Atlantic Canada from global and regional climate models. Can. Tech. Rep. Hydrogr. Ocean Sci. 288: viii+234 pp.

Lavoie, D., Simard, Y., and Saucier, F.J. 2000. Aggregation and dispersion of krill at channel heads and shelf edges: the dynamics in the Saguenay-St. Lawrence Marine Park. Can. J. Fish. Aquat. Sci. 57(9): 1853–1869.

Lavoie, D., Chassé, J., Simard, Y., Lambert, N., Galbraith, P.S., Roy, N., and Brickman, D. 2016. Large-scale atmospheric and oceanic control on krill transport into the St. Lawrence estuary evidenced with 3D numerical modelling. Atmos.-Ocean 54(3): 299-325.

Le Fouest, V., Zakardjian, B., Saucier, F.J., and Çizmeli, S.A. 2006. Application of SeaWIFS- and AVHRR-derived data for mesoscale and regional validation of a 3-D high-resolution physical-biological model of the Gulf of St. Lawrence (Canada). J. Mar. Syst. 60(1–2): 30–50.

Loder, J.W., Hannah, C.G., Petrie, B.D., and Gonzalez, E.A. 2003. Hydrographic and transport variability on the Halifax section. J. Geophys. Res. 108(C11).

Maavara, T., Dürr, H.H., and Van Cappellen, P. 2014. Worldwide retention of nutrient silicon by river damming: From sparse data set to global estimate. Global Biogeochem. Cycles: 2014GB004875.

Madec, G., Delecluse, P., Imbard, M., and Lévy, C. 1998. OPA 8.1 Ocean General Circulation Model reference manual. Note du Pôle de modélisation de l'Institut Pierre-Simon Laplace, Volume 11, 91 pp.

Madec, G. 2012. NEMO ocean engine. Note du Pôle de modélisation de l'Institut Pierre-Simon Laplace, Volume 27, 367 pp.

Maps, F., Zakardjian, B.A., Plourde, S., and Saucier, F.J. 2011. Modeling the interactions between the seasonal and diel migration behaviors of Calanus finmarchicus and the circulation in the Gulf of St. Lawrence (Canada). J. Mar. Syst. 88(2): 183–202.

Maps, F., Plourde, S., Lavoie, D., McQuinn, I., and Chassé, J. 2013. Modelling the influence of daytime distribution on the transport of two sympatric krill species (Thysanoessa raschii and Meganyctiphanes norvegica) in the Gulf of St Lawrence, eastern Canada. ICES J. Mar. Sci. 71: 282–292.

Maps, F., Plourde, S., McQuinn, I.H., St-Onge-Drouin, S., Lavoie, D., Chasse, J., and Lesage, V. 2015. Linking acoustics and finite-time Lyapunov exponents reveals areas and mechanisms of krill aggregation within the Gulf of St. Lawrence, eastern Canada. Limnol. Oceanogr. 60(6): 1965–1975.

McQuinn, I.H., Plourde, S., St Pierre, J.F., and Dion, M. 2015. Spatial and temporal variations in the abundance, distribution, and aggregation of krill (Thysanoessa raschii and Meganyctiphanes norvegica) in the lower estuary and Gulf of St. Lawrence. Prog. Oceanogr. 131: 159–176.

Mendonça, R., Kosten, S., Sobek, S., Barros, N., Cole, J.J., Tranvik, L., and Roland, F. 2012. Hydroelectric carbon sequestration. Nature Geoscience 5(12): 838–840.

MPO 2008. Projet hydroélectrique du complexe La Romaine -Examen scientifique de l'étude d'impact, volet marin. Secr. Can. de Consult. Sci. du MPO. Rép. des Sci. 2008/012. 14 pp.

Neu, H.J.A. 1970. A study on mixing and circulation in the St. Lawrence estuary up to 1964. Bedford Institute of Oceanography Report Series 1970-9. 31 pp.

Neu, H.J.A. 1976. Runoff regulation for hydro-power and its effect on the ocean environment. Hydrol. Sci. Bull. 21(3): 433–444.

Neu, H.J.A. 1982. Man-made storage of water resources – a liability to the ocean environment? Part 1. Mar. Pollut. Bull. 13(1): 7–12.

Ohashi, K., and Sheng, J.Y. 2013. Influence of St. Lawrence River discharge on the circulation and hydrography in Canadian Atlantic waters. Cont. Shelf Res. 58: 32–49.

Pellerin, G., Lefaivre, L., Houtekamer, P., and Girard, C. 2003. Increasing the horizontal resolution of ensemble forecasts at CMC. Nonlinear Proc. Geoph. 10: 463–468.

Petrie, B., Pettipas, R., and Petrie, W.M. 2008. An overview of meteorological, sea ice and sea-surface temperature conditions off eastern Canada during 2007. DFO Can. Sci. Advis. Sec. Res. Doc. 2008/16. iv+38 pp.

Plourde, S., Joly, P., Runge, J.A., Zakardjian, B., and Dodson, J.J. 2001. Life cycle of Calanus finmarchicus in the lower St. Lawrence estuary: The imprint of circulation and late timing of the spring phytoplankton bloom. Can. J. Fish. Aquat. Sci. 58(4): 647–658.

Plourde, S., McQuinn, I.H., Maps, F., St-Pierre, J.F., Lavoie, D., and Joly, P. 2013. Daytime depth and thermal habitat of two sympatric krill species in response to surface salinity variability in the Gulf of St Lawrence, eastern Canada. ICES J. Mar. Sci. 71(2): 272–281.

Reid, S.J. 1977. Circulation and mixing in the St. Lawrence Estuary near Ilet Rouge. Bedford Institute of Oceanography Report Series, BI-R-77-1. 36 pp.

Robitaille, P. 1998. Qualité des eaux des rivières aux Outardes, Manicouagan et Moisie, 1979 à 1996 Envirodoq no. EN9800xx 28 pp. + 24 annexes.

Rosenberg, D.M., Berkes, F., Bodaly, R.A., Hecky, R.E., Kelly, C.A., and Rudd, J.W.M. 1997. Large-scale impacts of hydroelectric development. Environ. Rev. 5(1): 27–54.

Rosenberg, D.M., McCully, P., and Pringle, C.M. 2000. Global-scale environmental effects of hydrological alterations: Introduction. Bioscience 50(9): 746–751.

Runge, J.A., and Simard, Y. 1990. Zooplankton of the St. Lawrence Estuary: the imprint of physical processes on its composition and distribution. *In* Oceanography of a Large-Scale Estuarine System: The St. Lawrence. Edited by M. I. El-Sabh and N. Silverberg. Springer-Verlag, Germany. pp. 296–320.

Runge, J.A., Castonguay, M., De Lafontaine, Y., Ringuette, M., and Beaulieu, J.L. 1999. Covariation in climate, zooplankton biomass and mackerel recruitment in the southern Gulf of St. Lawrence. Fish. Oceanogr. 8(2): 139–149.

Saucier, F.J., Roy, F., Senneville, S., Smith, G., Lefaivre, D., Zakardjian, B., and Dumais, J.-F. 2009. Modélisation de la circulation dans l'estuaire et le golfe du Saint-Laurent en réponse aux variations du débit d'eau douce et des vents. Rev. Sci. Eau 22(2): 159–176.

Savenkoff, C., Comtois, S., and Chabot, D. 2013. Trophic interactions in the St. Lawrence Estuary (Canada): Must the blue whale compete for krill? Estuar. Coast. Shelf Sci. 129: 136–151.

Sheng, J. 2001. Dynamics of a buoyancy-driven coastal jet: The Gaspe Current. J. Phys. Oceanogr. 31(11): 3146–3162.

Simard, Y., and Lavoie, D. 1999. The rich krill aggregation of the Saguenay - St. Lawrence Marine Park: Hydroacoustic and geostatistical biomass estimates, structure, variability, and significance for whales. Can. J. Fish. Aquat. Sci. 56(7): 1182–1197.

Simard, Y. 2009. Le Parc Marin Saguenay–Saint-Laurent: processus océanographiques à la base de ce site d'alimentation unique des baleines du Nord-Ouest Atlantique. Rev. Sci. Eau 22(2): 177–197.

Simard, Y., and Harvey, M. 2010. Predation on Northern Krill (Meganyctiphanes norvegica Sars). *In* Advances in Marine Biology. Edited by A. T. Geraint. Academic Press. pp. 277–306.

Sinclair, M., Budgen, G.L., Tang, C.L., Therriault, J.-C., and Yeats, P.A. 1986. Assessment of effects of freshwater runoff variability on fisheries production in coastal waters. *In* The role of freshwater outflow in coastal marine ecosystems. Edited by S. Skreslet. Springer-Verlag, Berlin. pp. 139–160.

Sutcliffe, W.H., Loucks, R.H., and Drinkwater, K.F. 1976. Coastal circulation and physical oceanography of Scotian Shelf and Gulf of Maine. J. Fish. Res. Board Can. 33(1): 98–115.

Syvitski, J.P.M., Vorosmarty, C.J., Kettner, A.J., and Green, P. 2005. Impact of humans on the flux of terrestrial sediment to the global coastal ocean. Science 308(5720): 376–380.

Teodoru, C.R., Bastien, J., Bonneville, M.-C., et al. 2012. The net carbon footprint of a newly created boreal hydroelectric reservoir. Global Biogeochem. Cycles 26(2): GB2016, doi:10.1029/2011GB004187.

Therriault, J.C., and Lacroix, G. 1976. Nutrients, chlorophyll, and internal tides in the St. Lawrence estuary. J. Fish. Res. Board Can. 33(12): 2747–2757.

Urrego-Blanco, J., and Sheng, J.Y. 2014a. Formation and distribution of sea ice in the Gulf of St. Lawrence: A process-oriented study using a coupled ocean-ice model. J. Geophys. Res. 119(10): 7099–7122.

Urrego-Blanco, J., and Sheng, J.Y. 2014b. Study on subtidal circulation and variability in the Gulf of St. Lawrence, Scotian Shelf, and Gulf of Maine using a nested-grid shelf circulation model. Ocean Dyn. 64(3): 385–412.

Table 1. Watershed size, mean annual runoff, flow type, and years of dam construction for the seven rivers under study.

Name	**Watershed size (km^2)**	**Mean runoff (m^3/s)**	**Flow type**
Betsiamites[1]	18,699	402	Dammed for hydroelectricity; two dams between 1955 and 1959
Manicouagan[2]	45,908	1,002	Dammed for hydroelectricity; four main dams with large reservoirs built between 1951 and 1975
Outardes[2]	19,057	389	Dammed for hydroelectricity; three main dams with large reservoirs built between 1969 and 1978
Little Mecatina	19,294	421	Natural (construction planned)
Romaine[3]	15,400	327	Natural (under construction for hydroelectricity 2014–2020)
Saguenay[4]	85,500	2,110	Dammed for hydroelectricity: Ile-Maligne (1923–1926), Chute-à-Caron (1926–1931), Shipshaw (1941–1943)
St. Lawrence (mean runoff estimated near Quebec City)[5]	1,300,000	12,600[6]	Dammed for hydroelectricity and water level/flood control. The two major power dams were built between 1954 and 1958 (Moses-Saunders, Great Lakes) and 1959 and 1964 (Carillon, Ottawa River)

[1]BAPE (2001), [2]Robitaille (1998), [3]Hydro-Québec (2008), [4]Fortin and Pelletier (1995), [5]Bourgault and Koutitonsky (1999),[6]Hudon and Carigan (2008).

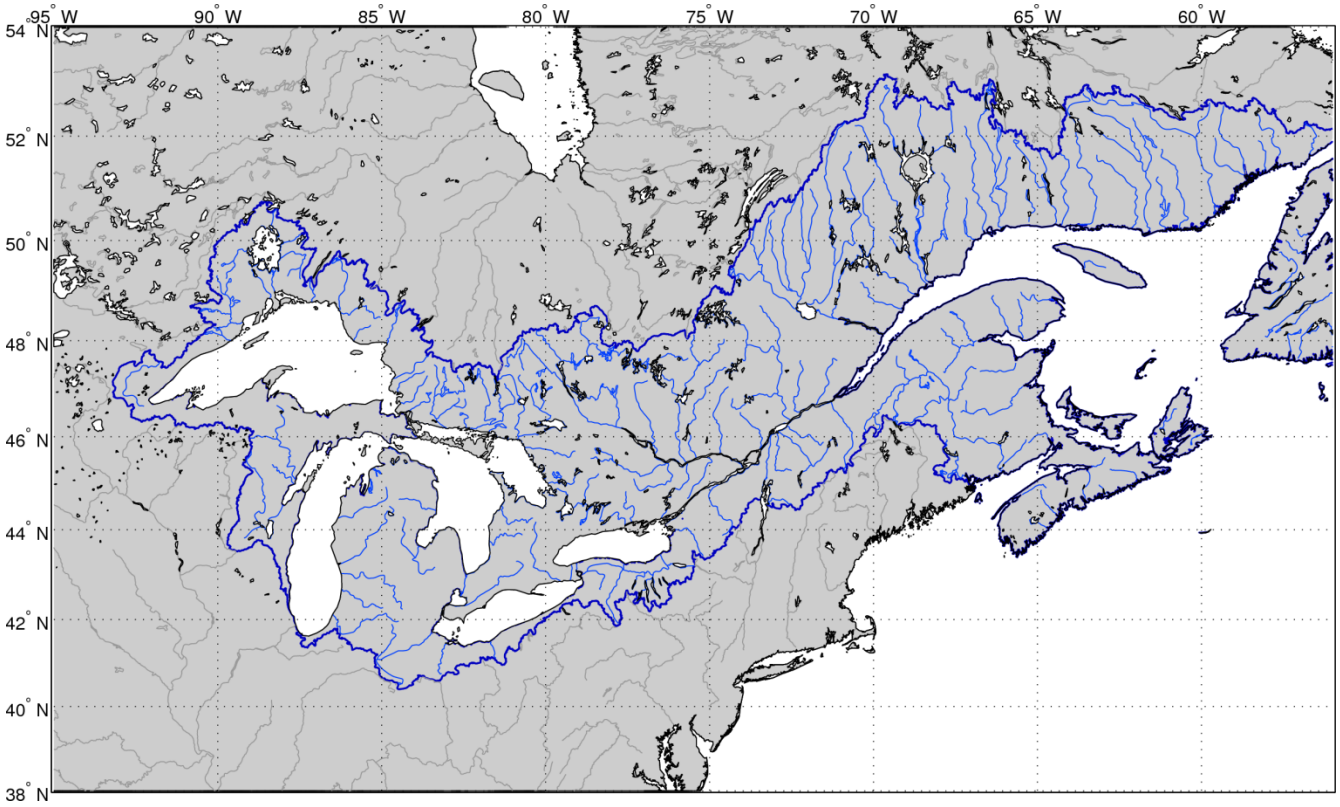

Figure 1. Rivers flowing into the St. Lawrence system (in blue). The data used for map production were obtained from the National Oceanic and Atmospheric Administration (NOAA, http://www.ngdc.noaa.gov/mgg/shorelines/shorelines.html) and from Natural Resources Canada (http://ftp.geogratis.gc.ca/pub/nrcan_rncan/vector/canvec/). Smaller rivers are not displayed on the map.

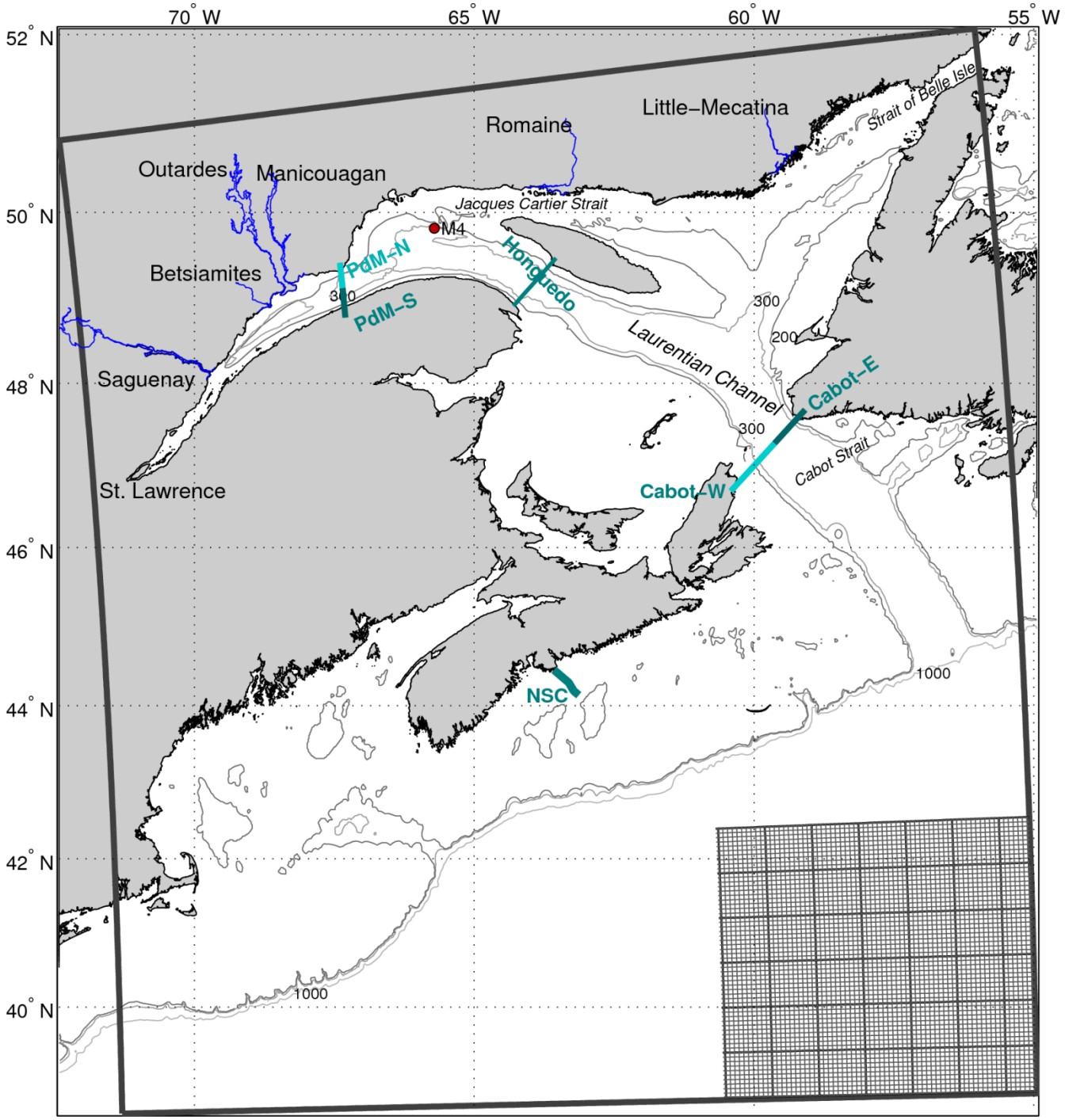

Figure 2. Map of the study area showing the model domain with a small subarea of the grid on the lower right corner. The seven rivers under study are depicted in blue (except for the St. Lawrence River). The 200, 300, and 1000 m depth contours are shown. The red dot (M4) shows the location of the ADCP mooring. The northern and southern halves of the Pointe-des-Monts cross section (PdM-N, PdM-S), western and eastern halves of the Cabot Strait cross section (Cabot-W and Cabot-E), Honguedo Strait, and the inner Halifax line (NSC) are also shown (turquoise lines).

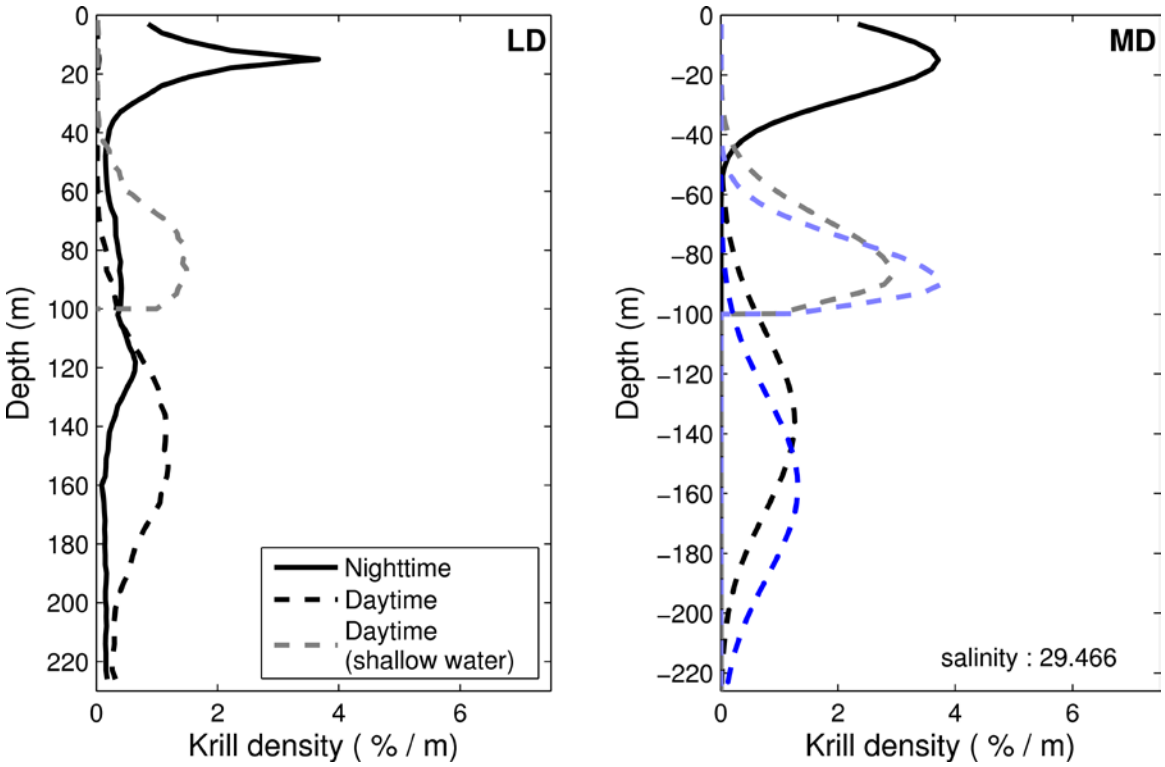

Figure 3. Vertical distributions of krill during the day and at night for LD and MD. The LD distribution is obtained from ADCP data at M4 in July 2009. The MD distribution depicted is for a mean sea surface salinity of 29.5. The shallow-water curve represents the case where the bottom depth is 100 m. In the MD panel, the blue curves are for *M. norvegica* while the gray curves are for *T. raschii*.

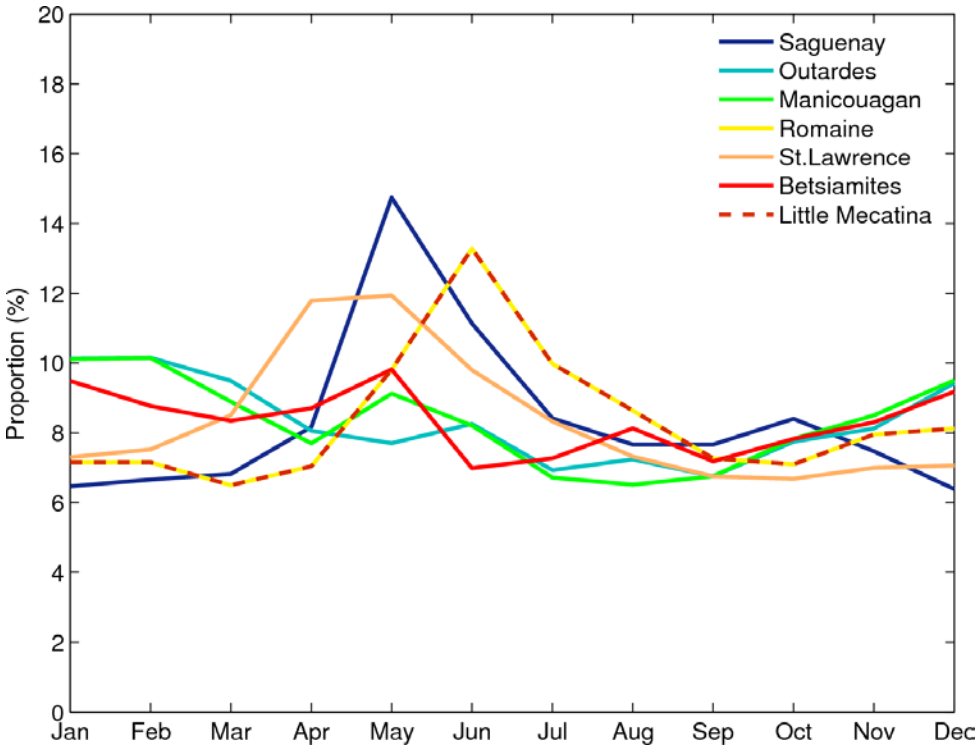

Figure 4. Proportions of the annual runoff released each month at the dams. In the case of the St. Lawrence River, the curve represents the monthly proportions of the natural cycle estimated by S. Senneville (Institut des Sciences de la Mer, UQAR, Rimouski, QC; pers. comm.).

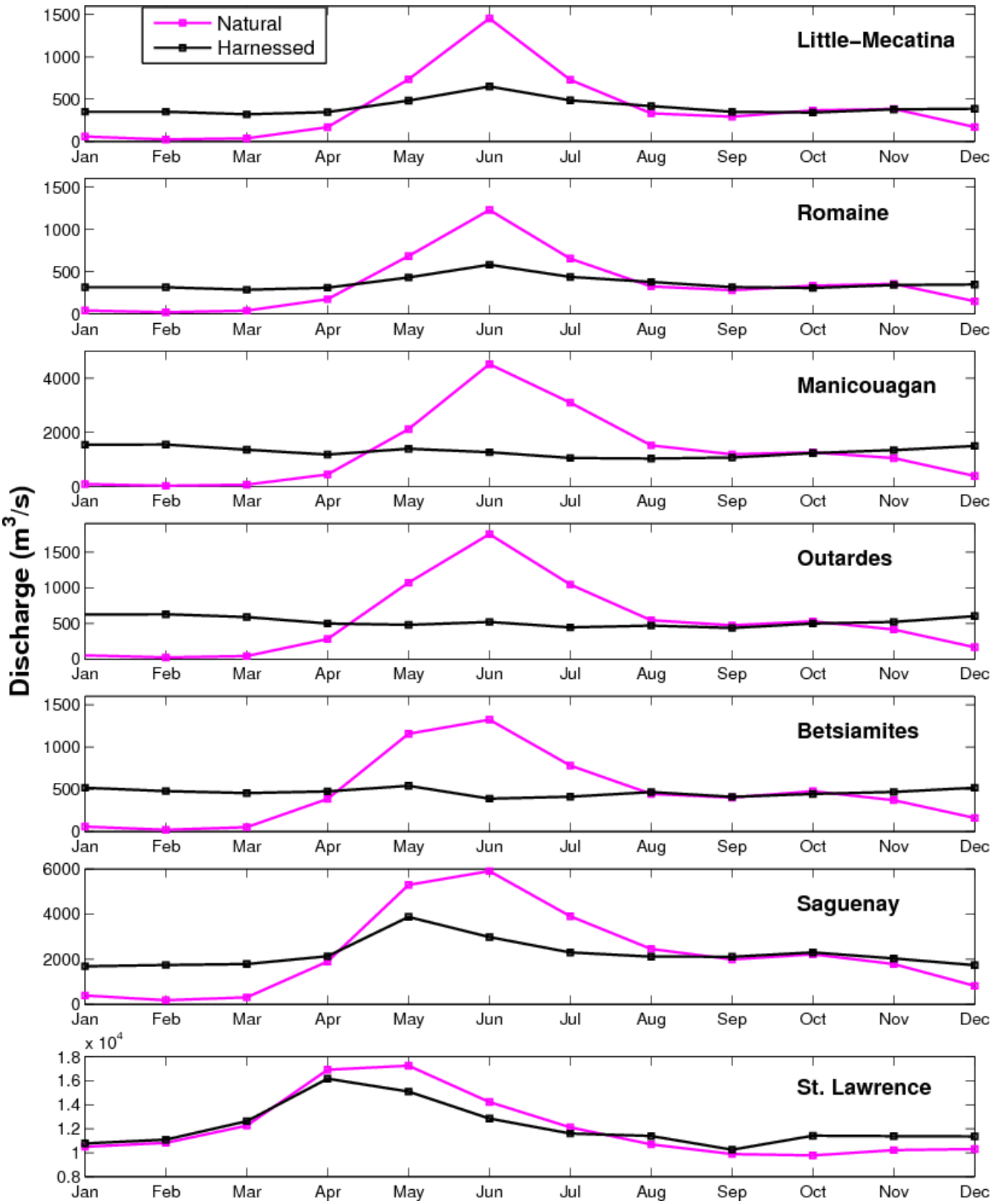

Figure 5. Mean 2006–2011 monthly runoff for natural (pink curve) and harnessed (black curve) conditions.

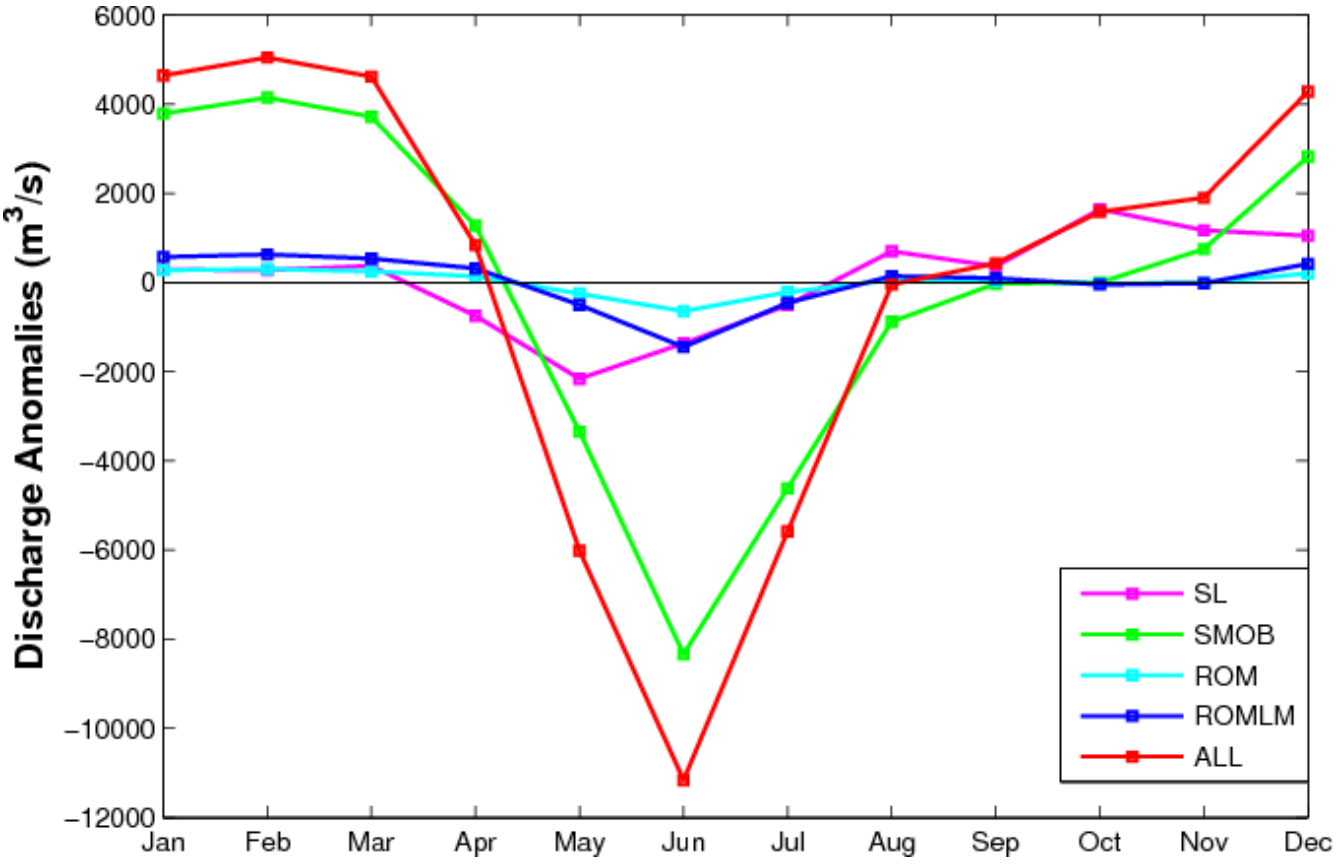

Figure 6. Monthly anomalies (harnessed minus natural scenarios) for the mean runoffs displayed in Figure 5.

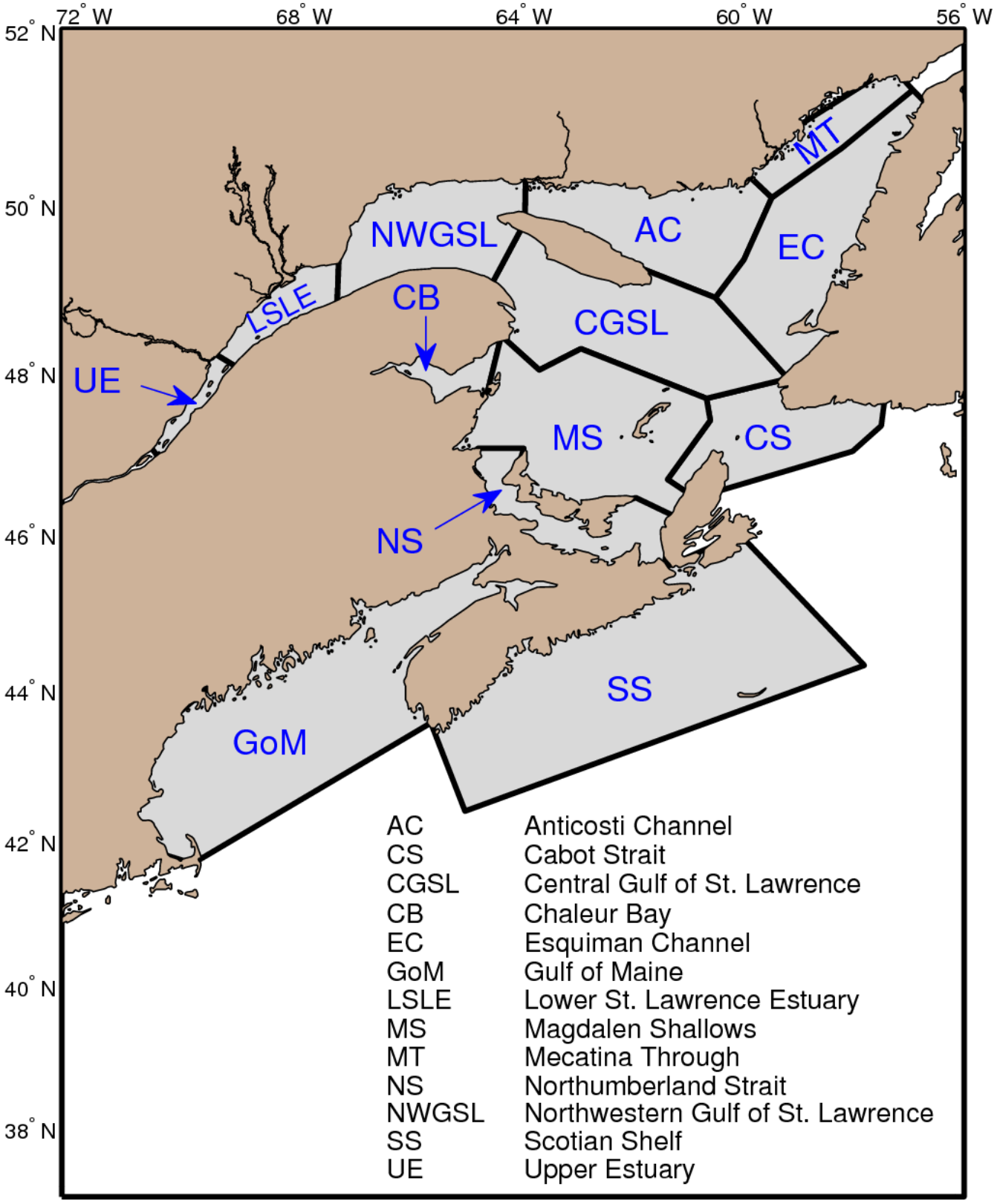

Figure 7. Subdivisions of the model domain used for the statistical analyses.

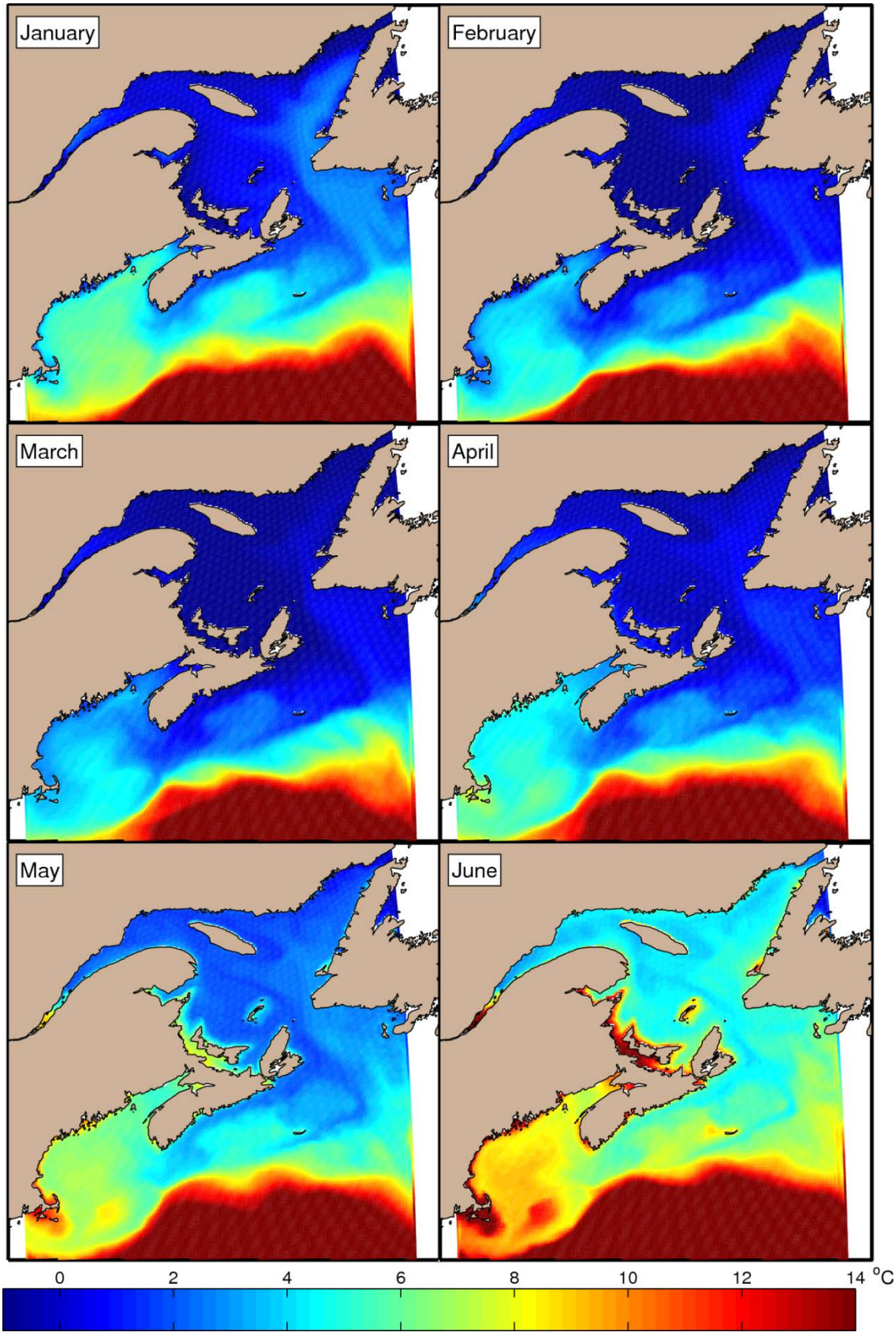

Figure 8. Mean 0–50 m temperature over the six-year period for January to June for the base simulation (natural conditions).

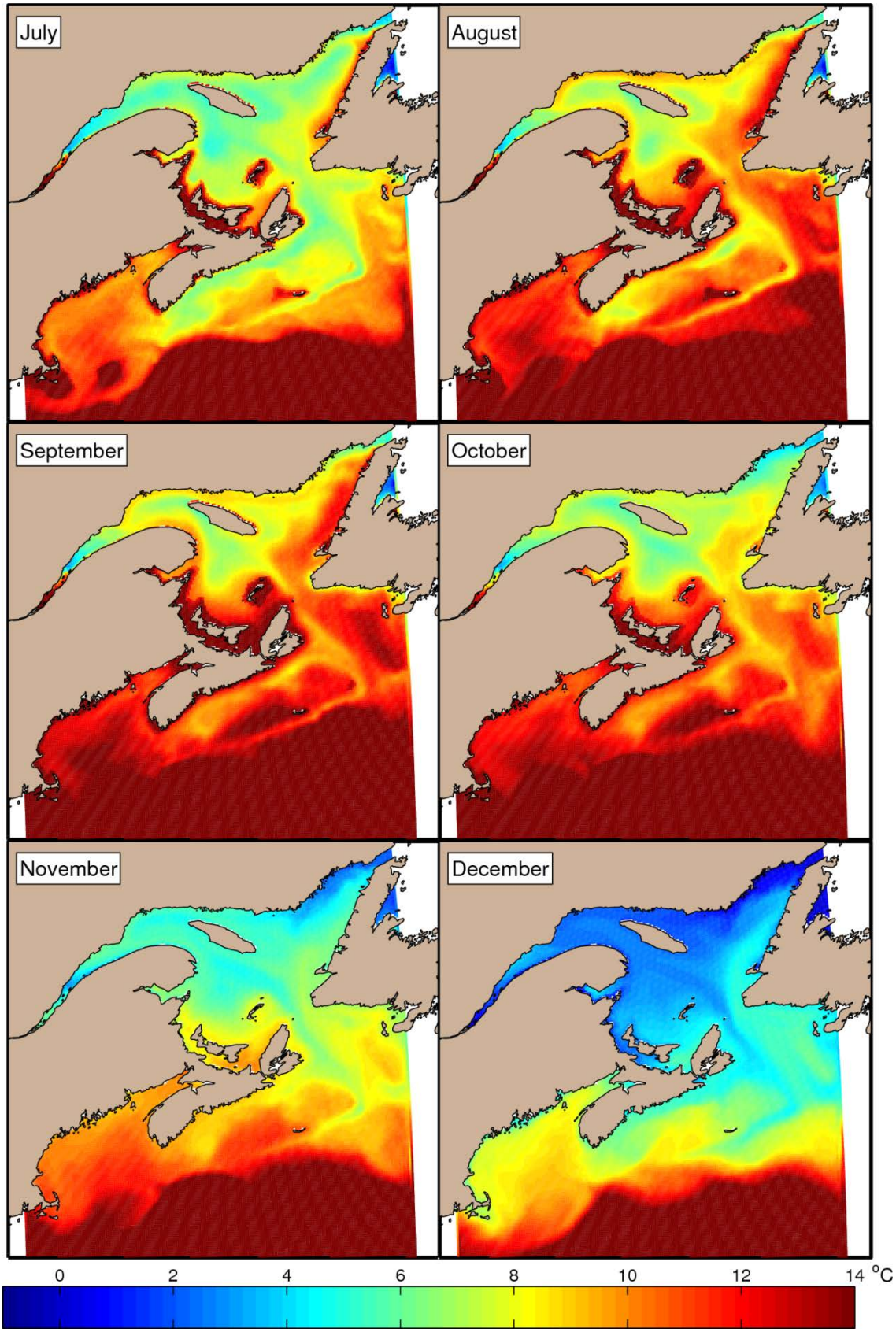

Figure 9. Mean 0–50 m temperature over the six-year period for July to December for the base simulation (natural conditions).

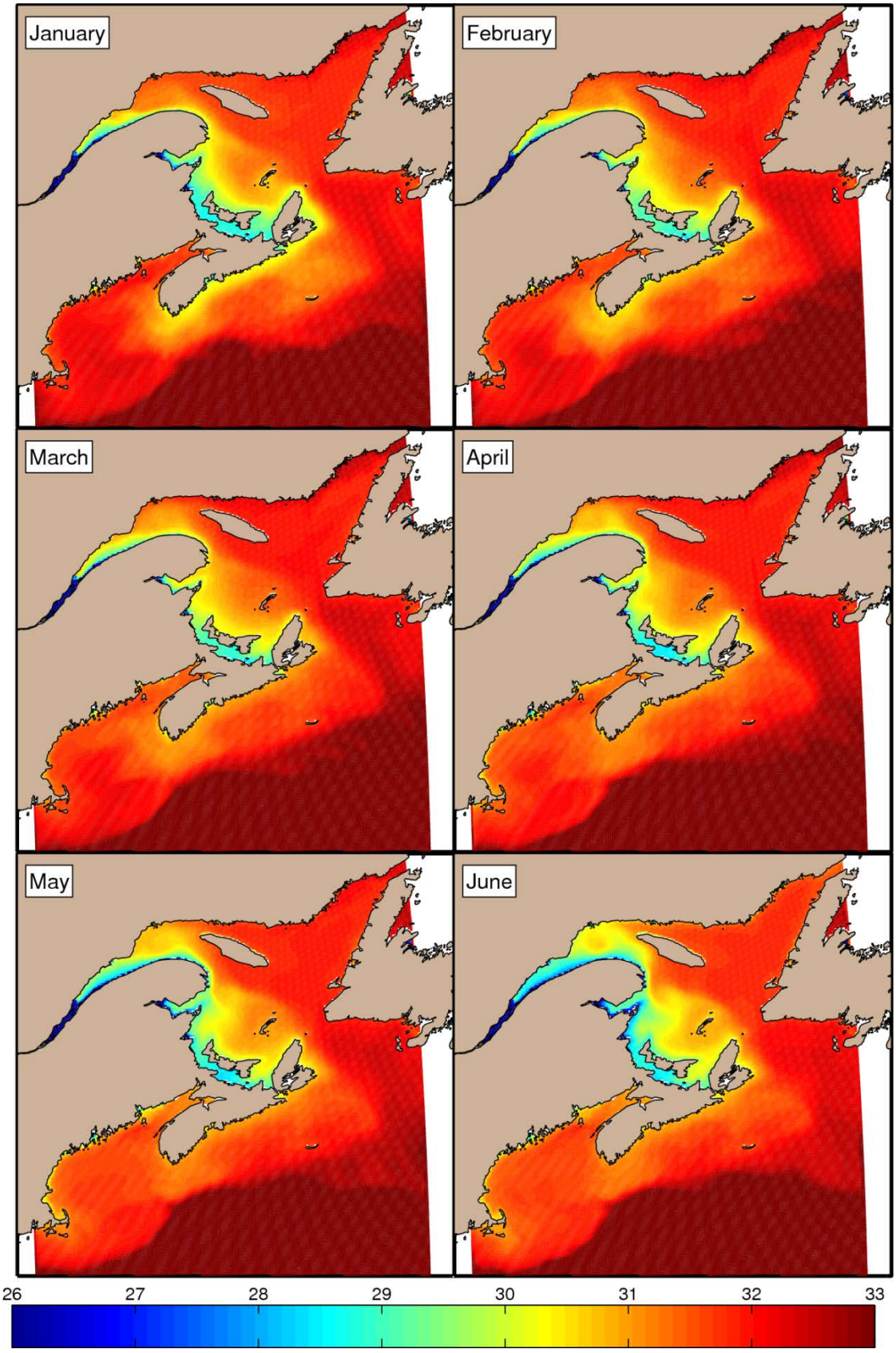

Figure 10. Mean 0–50 m salinities over the six-year period for January to June for the base simulation (natural conditions).

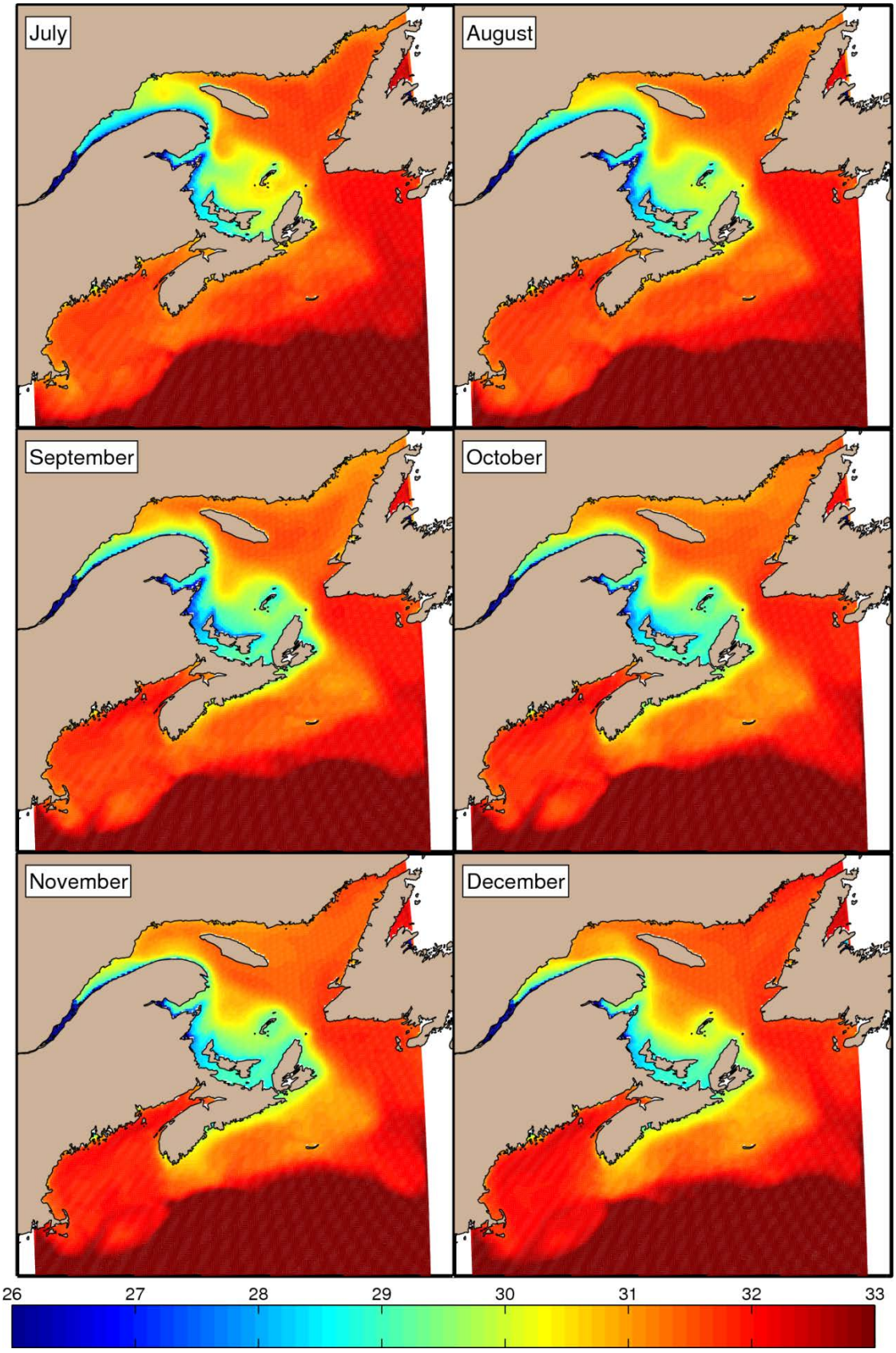

Figure 11. Mean 0–50 m salinities over the six-year period for July to December for the base simulation (natural conditions).

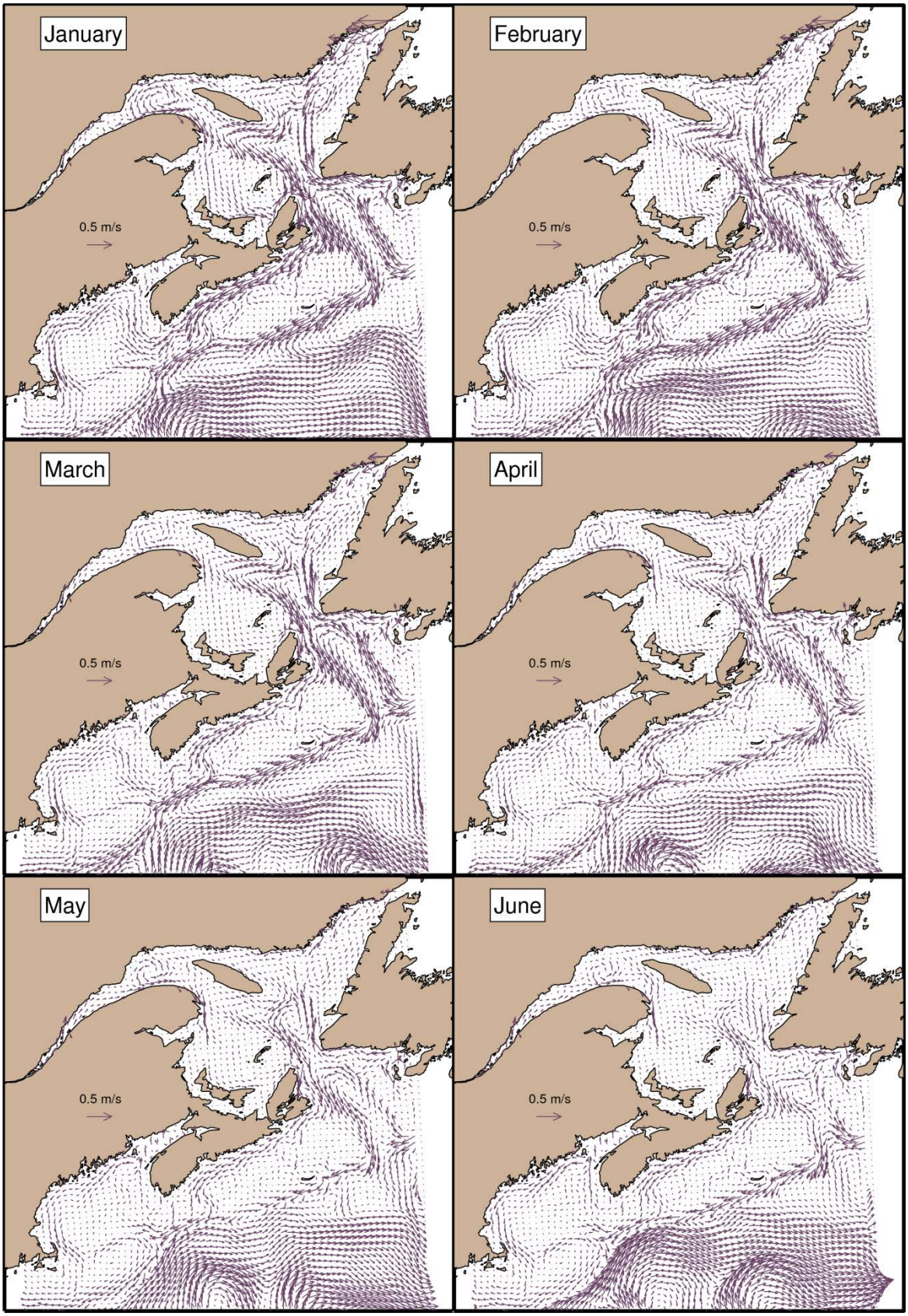

Figure 12. Mean simulated surface currents (0–50 m) over the six-year period for the months of January to June for the base simulation (natural conditions). Only every other cell is represented to improve figure clarity.

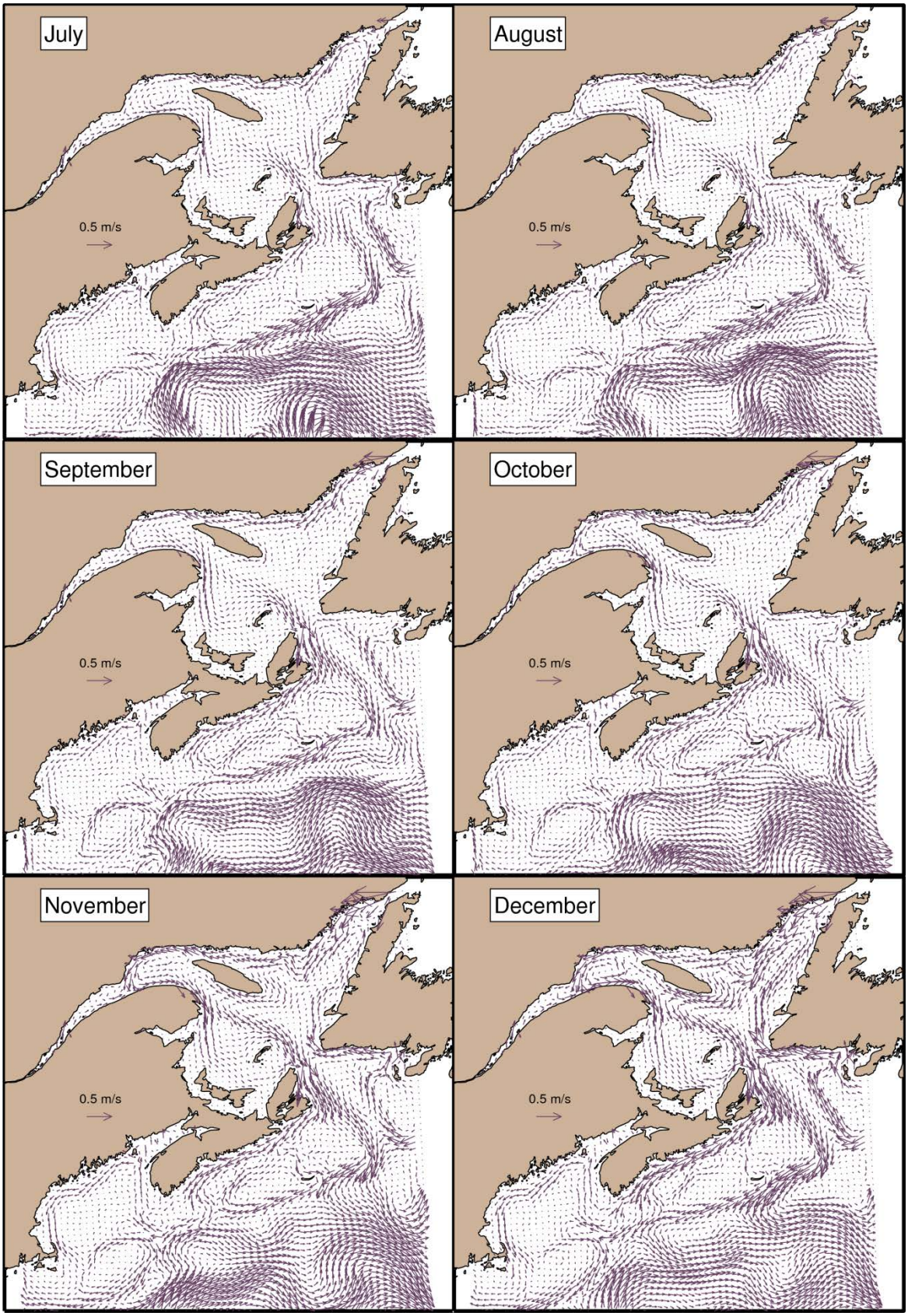

Figure 13**.** Mean simulated surface currents (0–50 m) over the six-year period for the months of July to December for the base simulation (natural conditions). Only every other cell is represented to improve figure clarity.

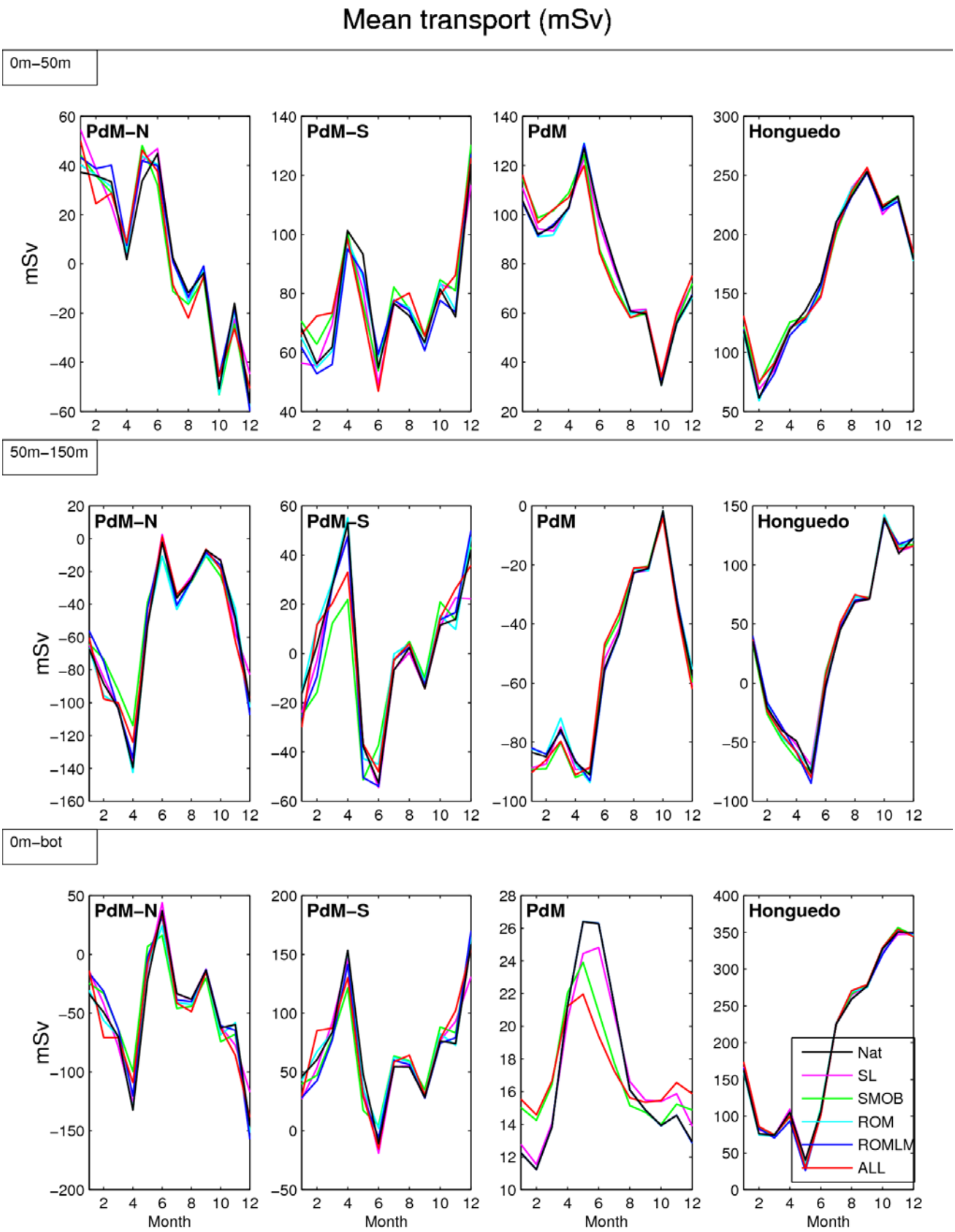

Figure 14. Mean transport (1 mSv = 1 milli-Sverdrup = 10^3 m^3/s) across different cross sections (Pointe-des-Monts [PdM], PdM-N, and PdM-S [northern and southern half of PdM] and Honguedo Strait; see Figure 1) for the different scenarios over the six-year period. Positive transport indicates eastward transport (outflow), while negative transport indicates westward transport (inflow).

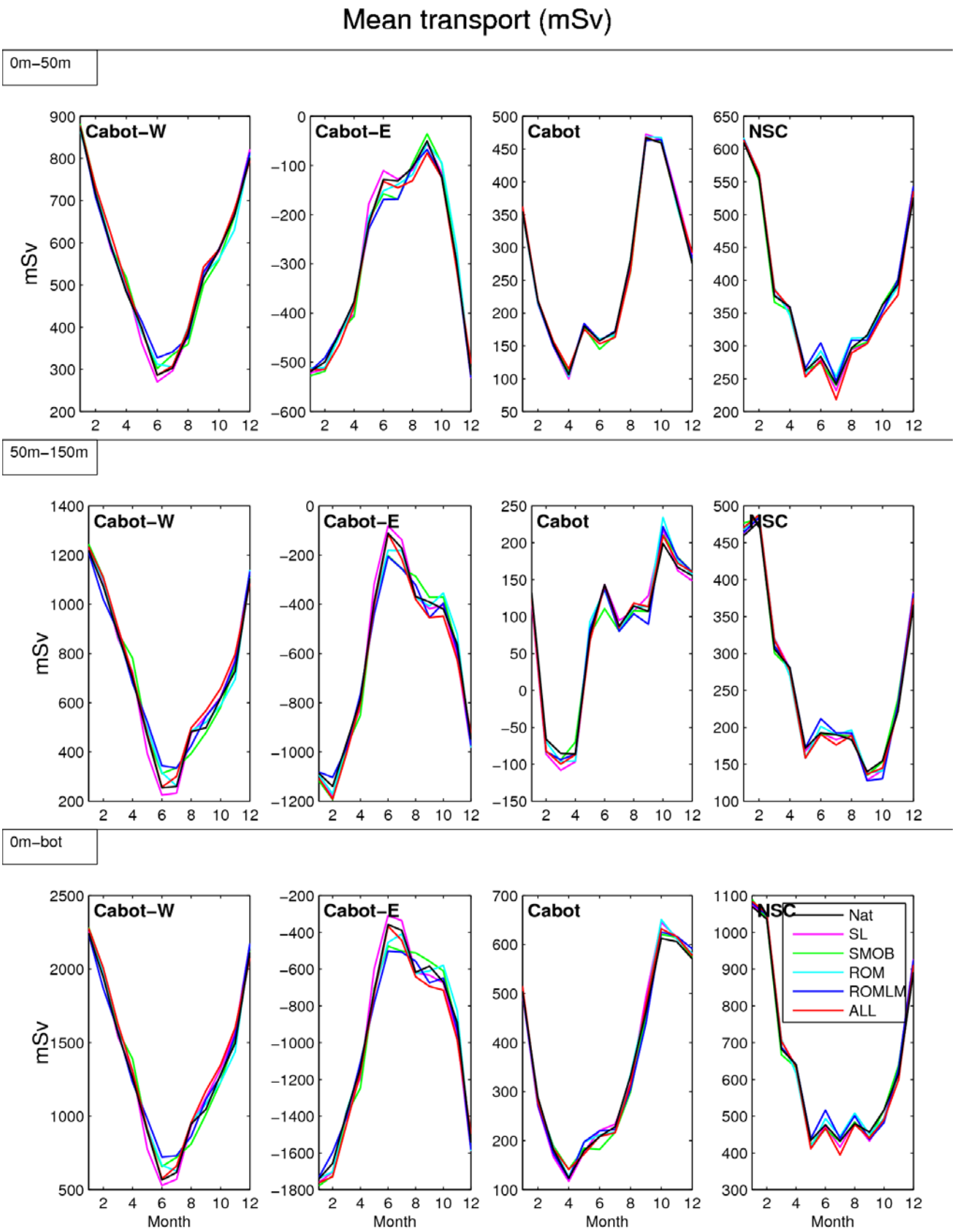

Figure 15. Mean transport (1 mSv = 1 milli-Sverdrup = 10^3 m^3/s) across different cross sections (Cabot Strait, Cabot-W, Cabot-E, and the Nova Scotian Current [NSC]; see Figure 1) for the different scenarios over the six-year period. Positive transport indicates outflow from the GSL, while negative transport indicates inflow. At NSC, positive transport indicates southward transport.

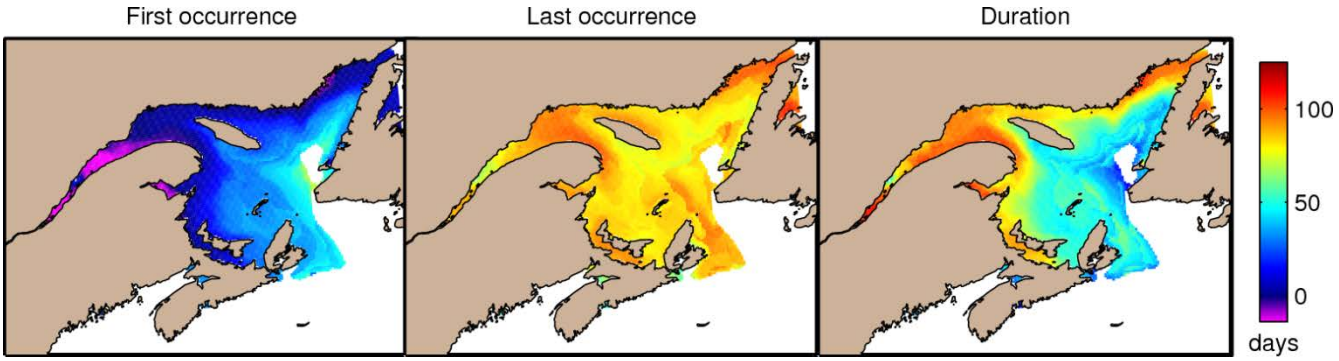

Figure 16. Mean sea-ice first occurrence, sea-ice last occurrence, and sea-ice duration for the 2006–2011 period for the base simulation (0 d = January 1st). Only cells with monthly mean sea-ice concentration greater than 5% are considered.

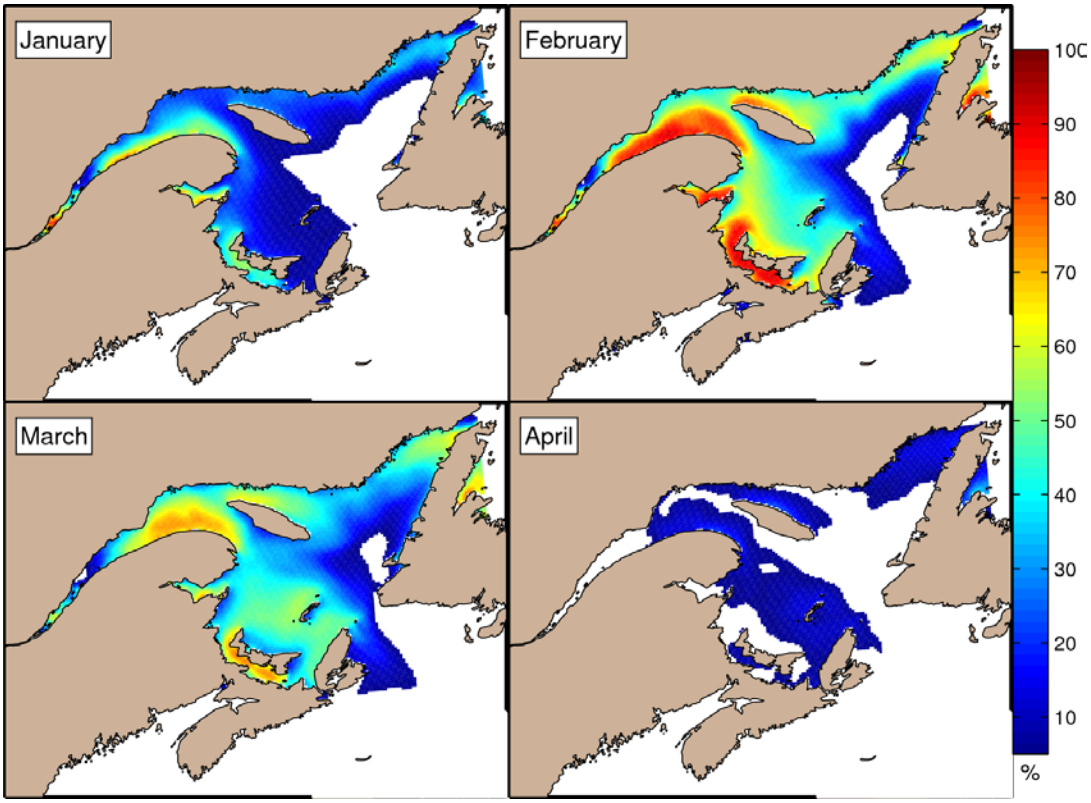

Figure 17. Mean simulated sea-ice concentration (>5%) over the six-year period for the natural conditions from January to April.

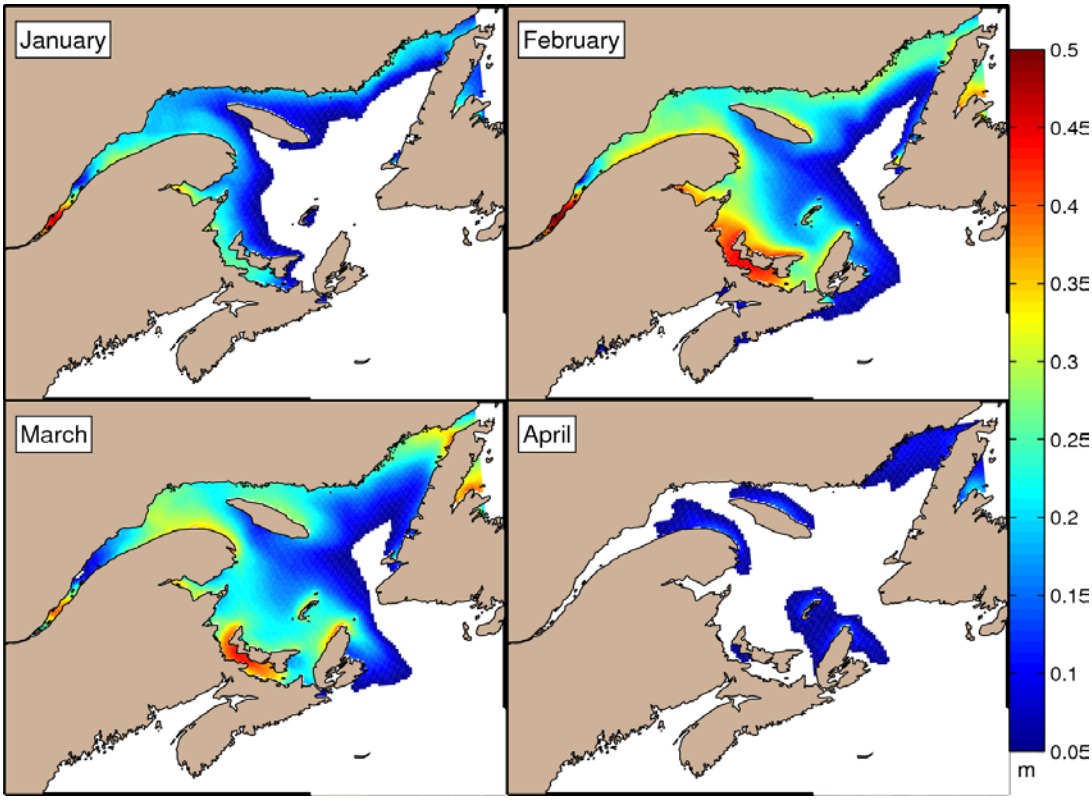

Figure 18. Mean simulated sea-ice thickness (> 5 cm) over the six-year period for the natural conditions from January to April.

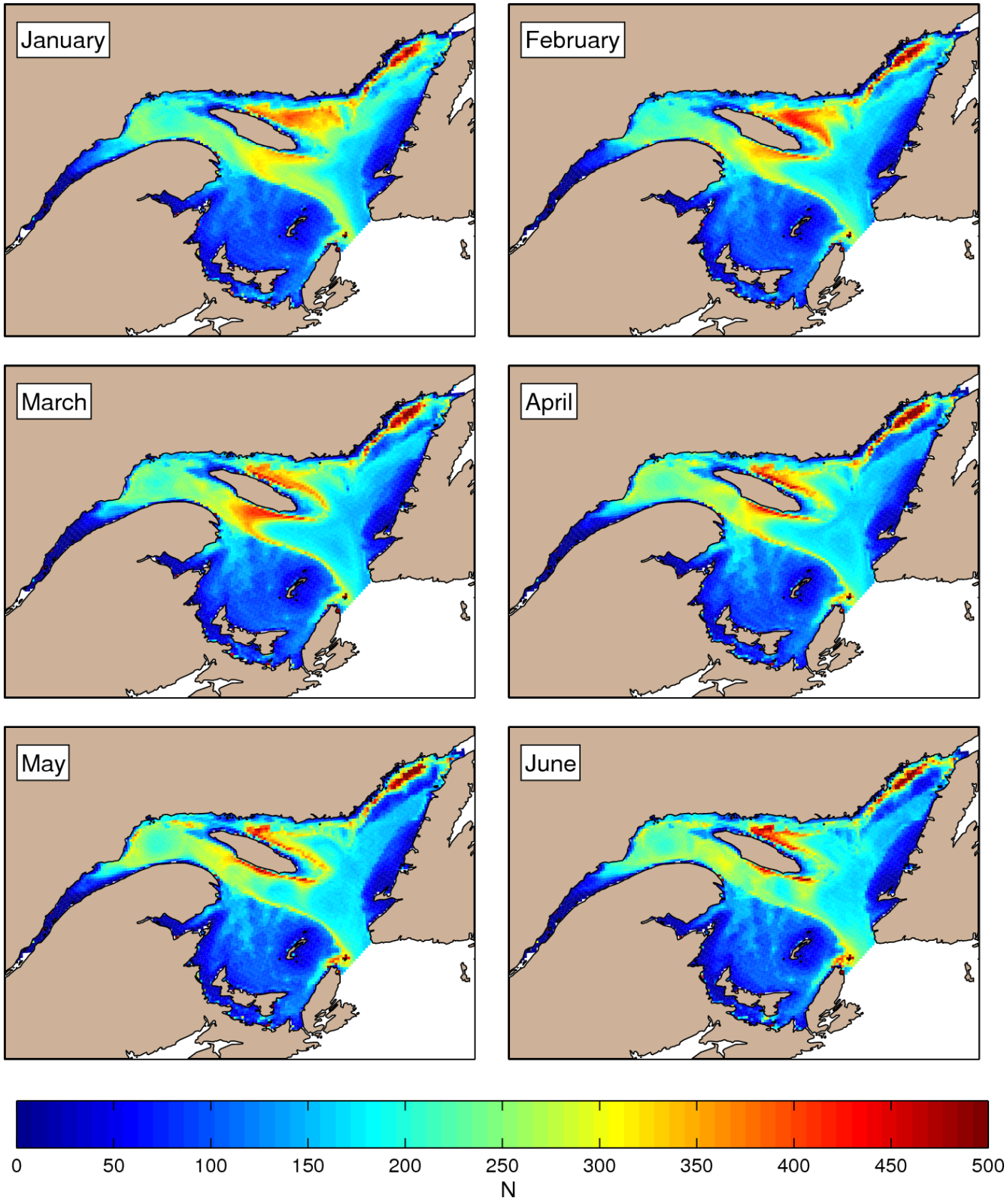

Figure 19. Mean krill density (number of particles per grid cell) with the LD vertical distribution over the five-year period (2007–2011) for the base simulation for January to June.

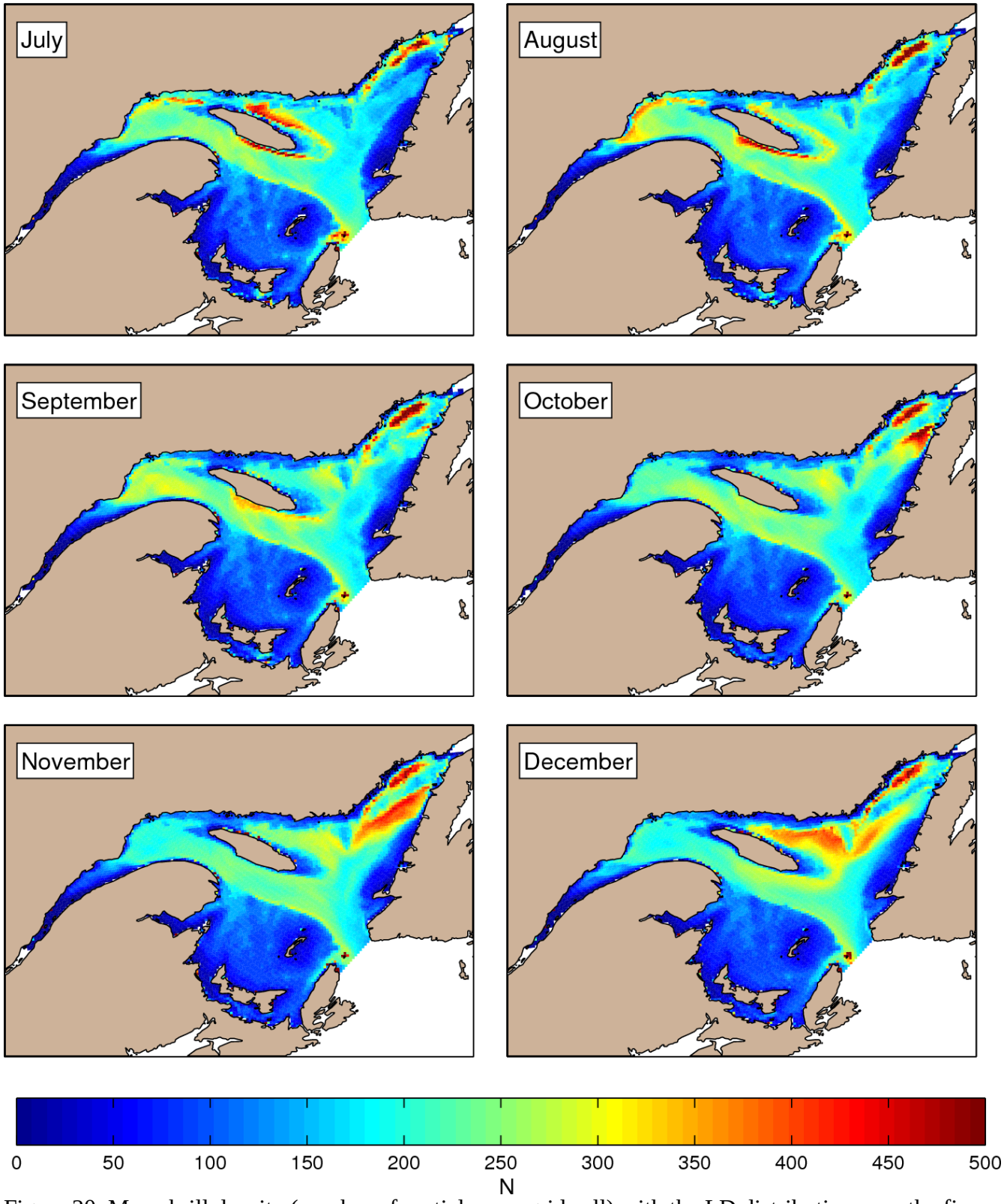

Figure 20. Mean krill density (number of particles per grid cell) with the LD distribution over the five-year period (2007–2011) for the base simulation for July to December.

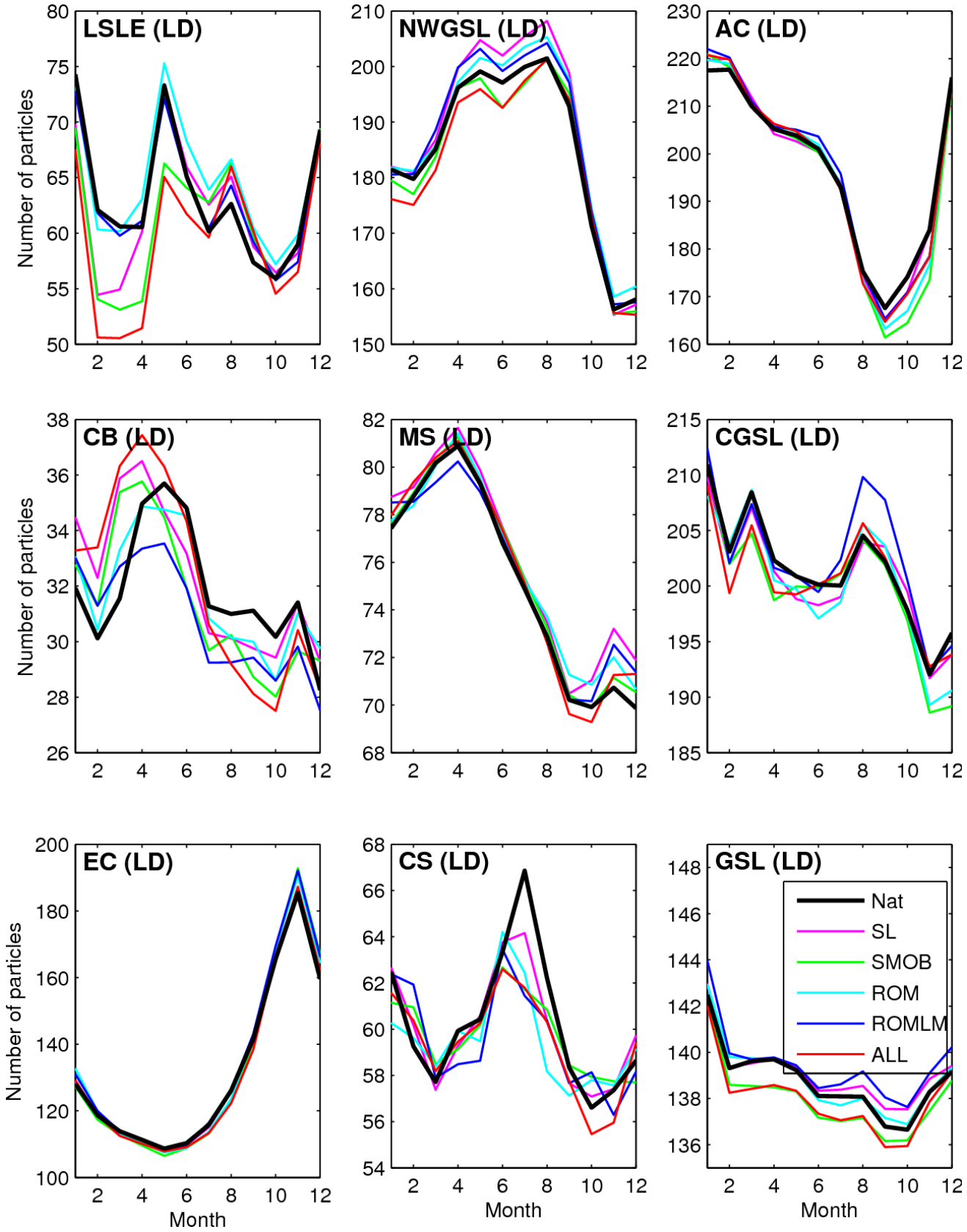

Figure 21. Monthly mean krill density with the harnessed and natural conditions with the LD vertical distribution over the different regions (mean number of particles in the regions described in Figure 7).

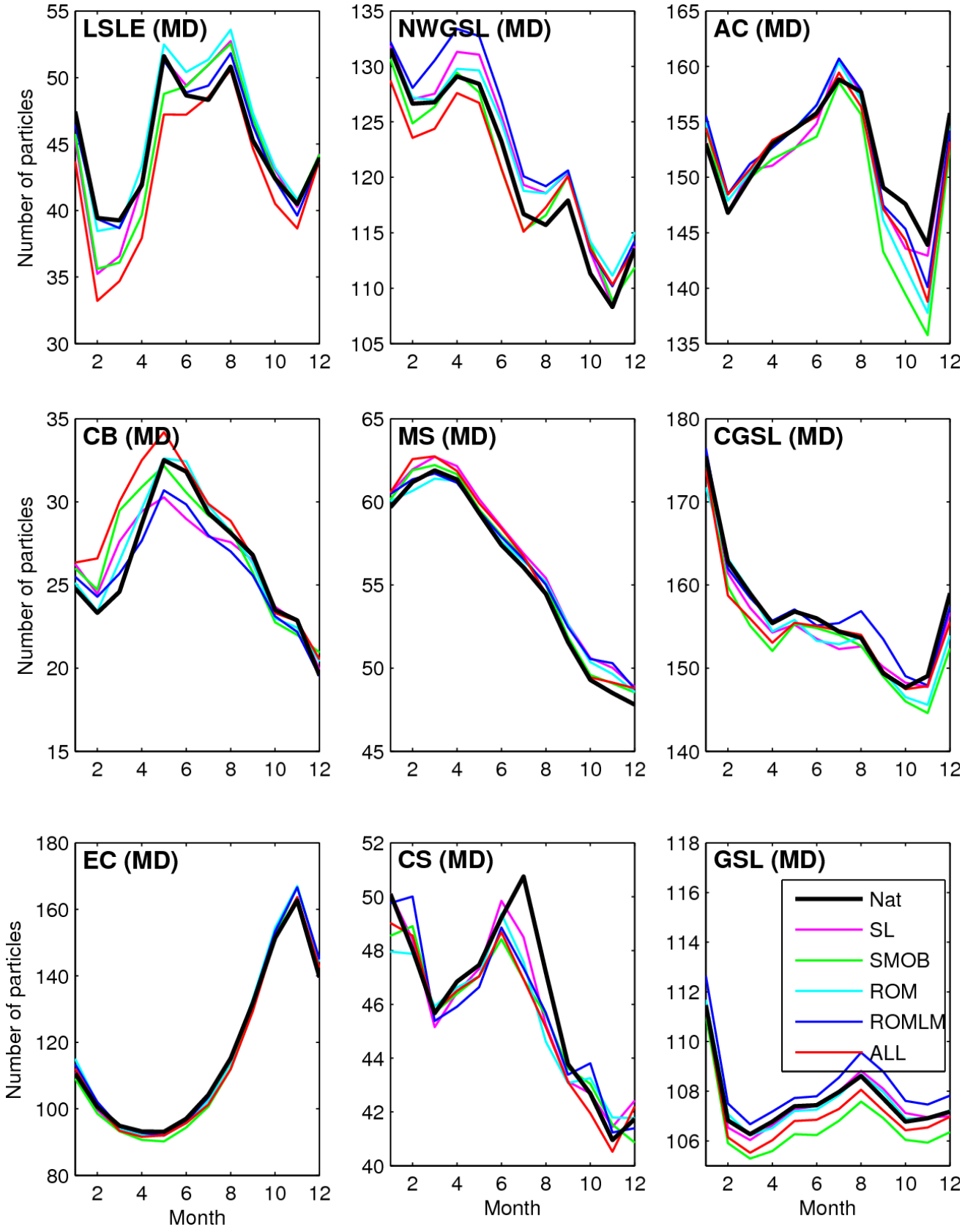

Figure 22. Monthly mean krill density with the harnessed and natural conditions with the MD vertical distribution over the different regions (mean number of particles in the regions described in Figure 7).

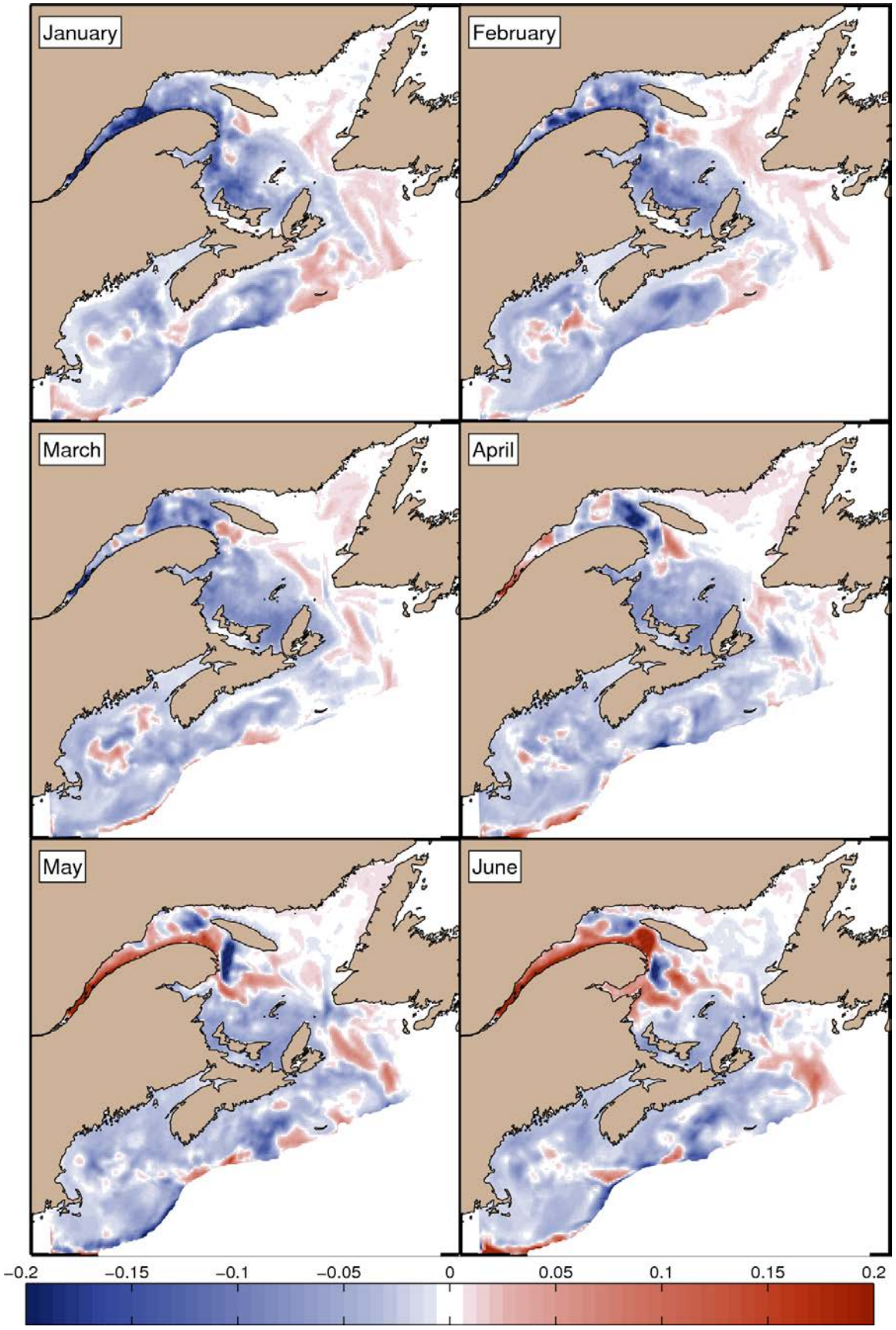

Figure 23. Differences in monthly mean 0–50 m salinities over the six-year period between the St. Lawrence River scenario (SL) and the base simulation for January to June.

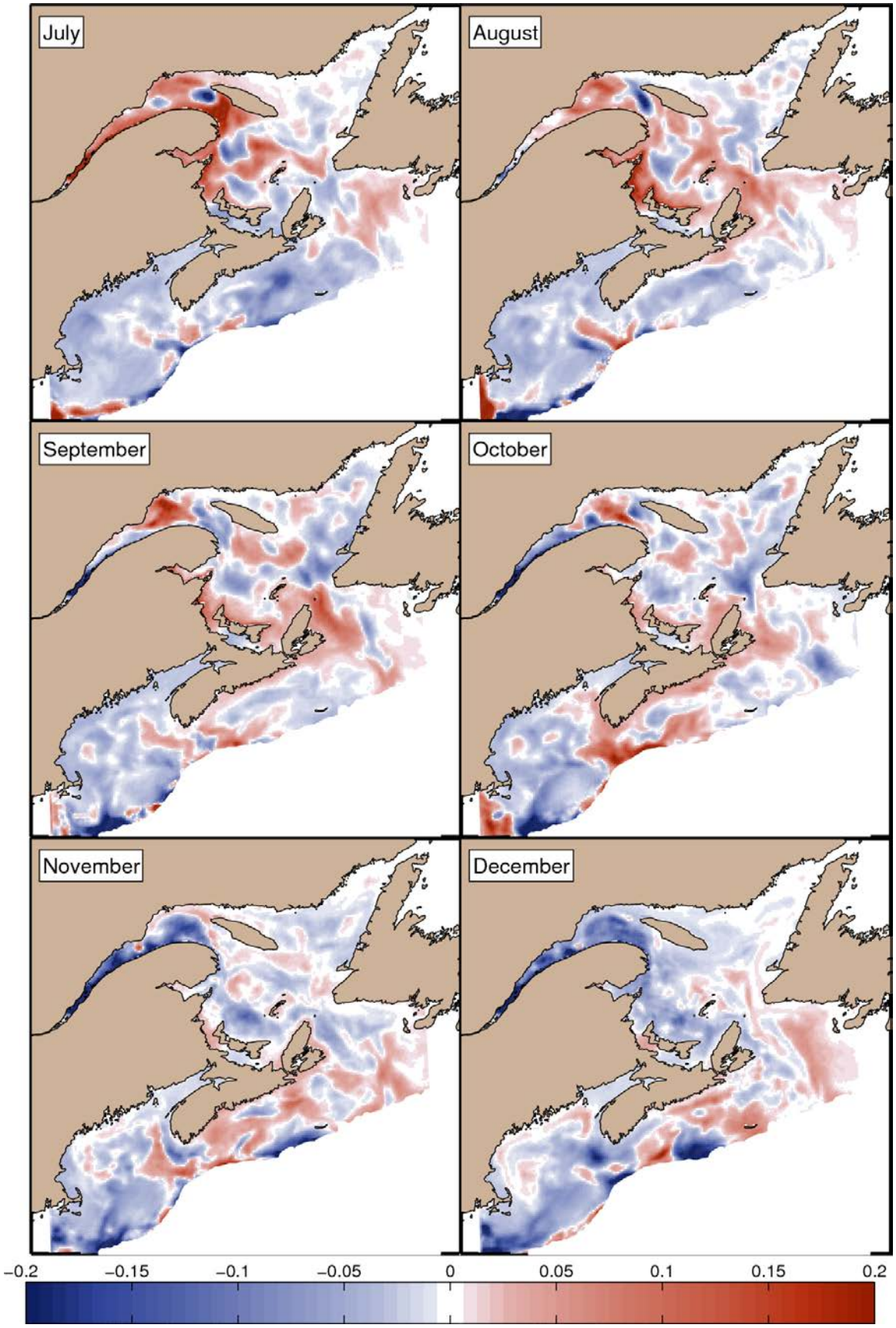

Figure 24. Differences in monthly mean 0–50 m salinities over the six-year period between the St. Lawrence River scenario (SL) and the base simulation for July to December.

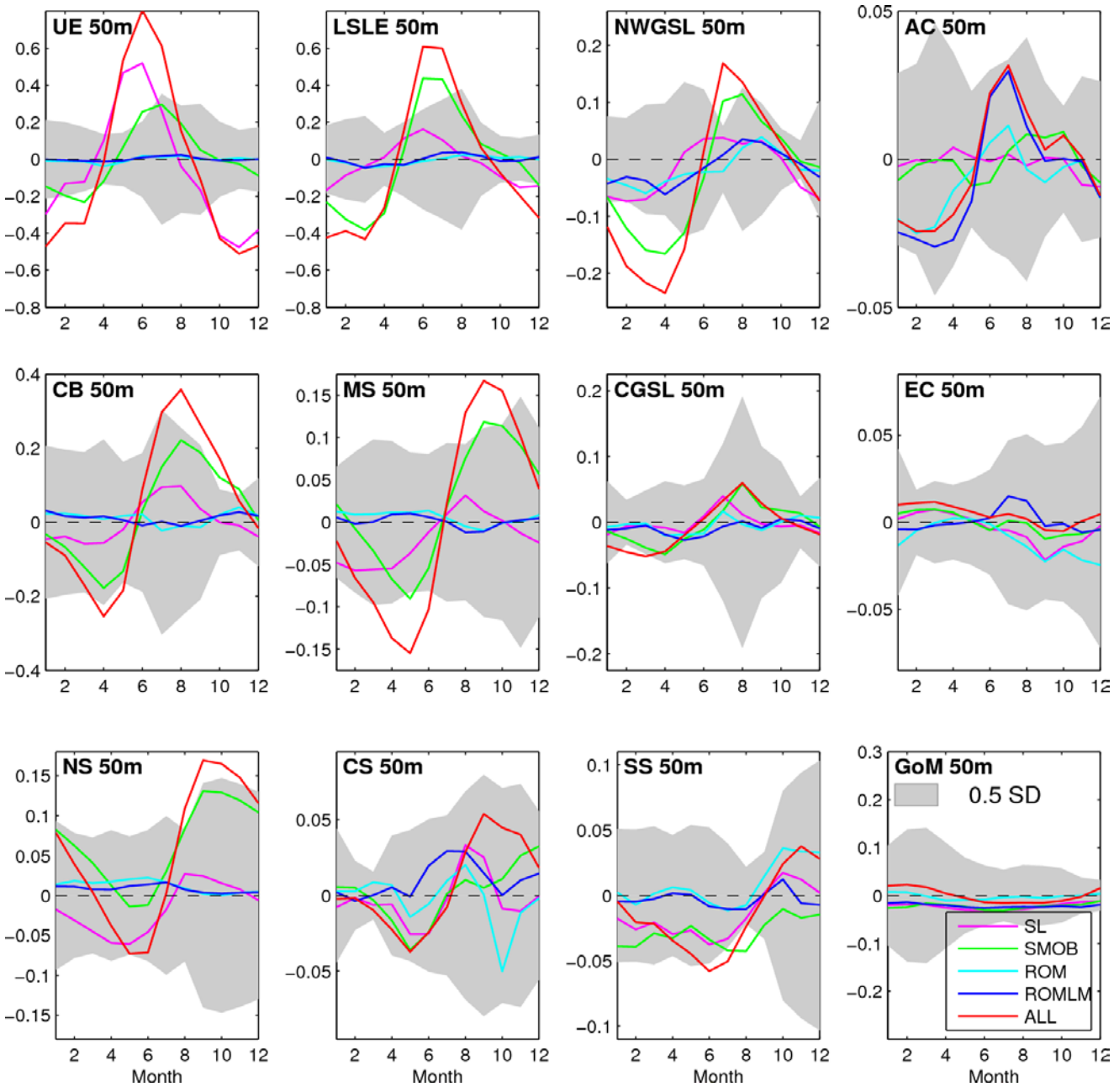

Figure 25. Differences (harnessed minus natural conditions) in monthly mean 0–50 m salinity averaged over twelve regions defined on Figure 7. The grey areas represent half the standard deviations (0.5 SD) among years for each month of the reference simulation (NATURAL).

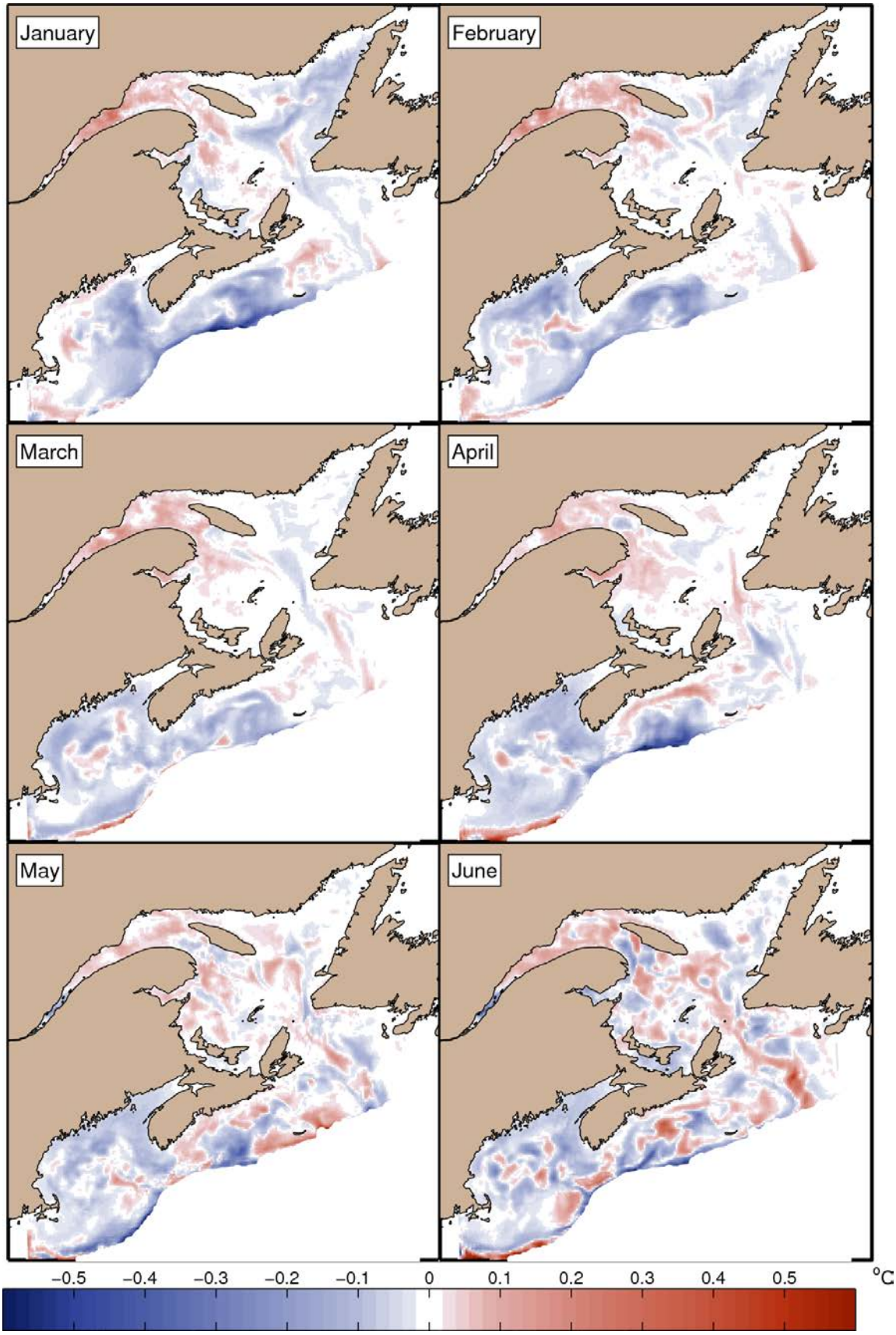

Figure 26. Differences in monthly mean 0–50 m temperatures over the six-year period between the St. Lawrence River scenario (SL) and the base simulation for January to June.

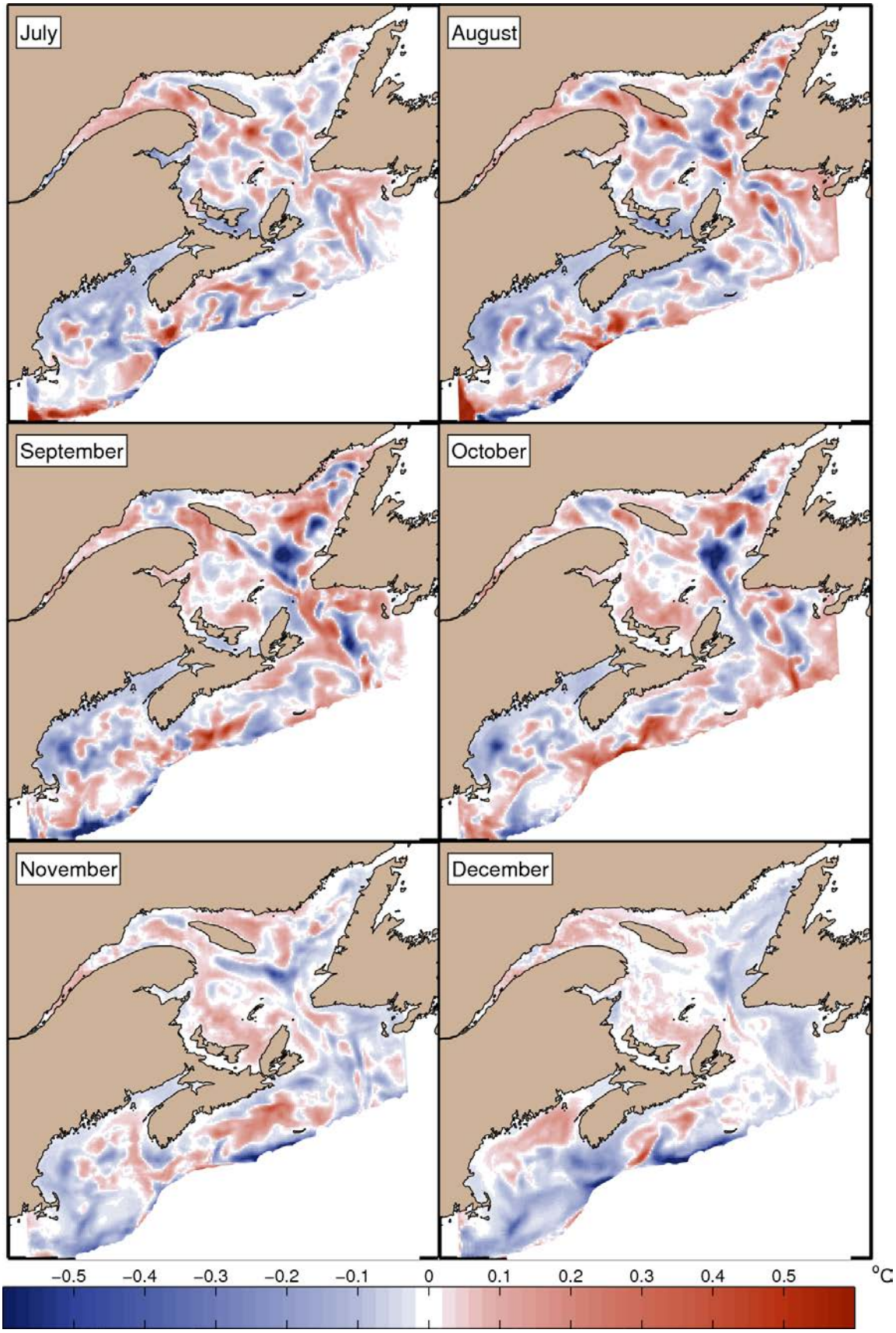

Figure 27. Differences in monthly mean 0–50 m temperatures over the six-year period between the St. Lawrence River scenario (SL) and the base simulation for July to December.

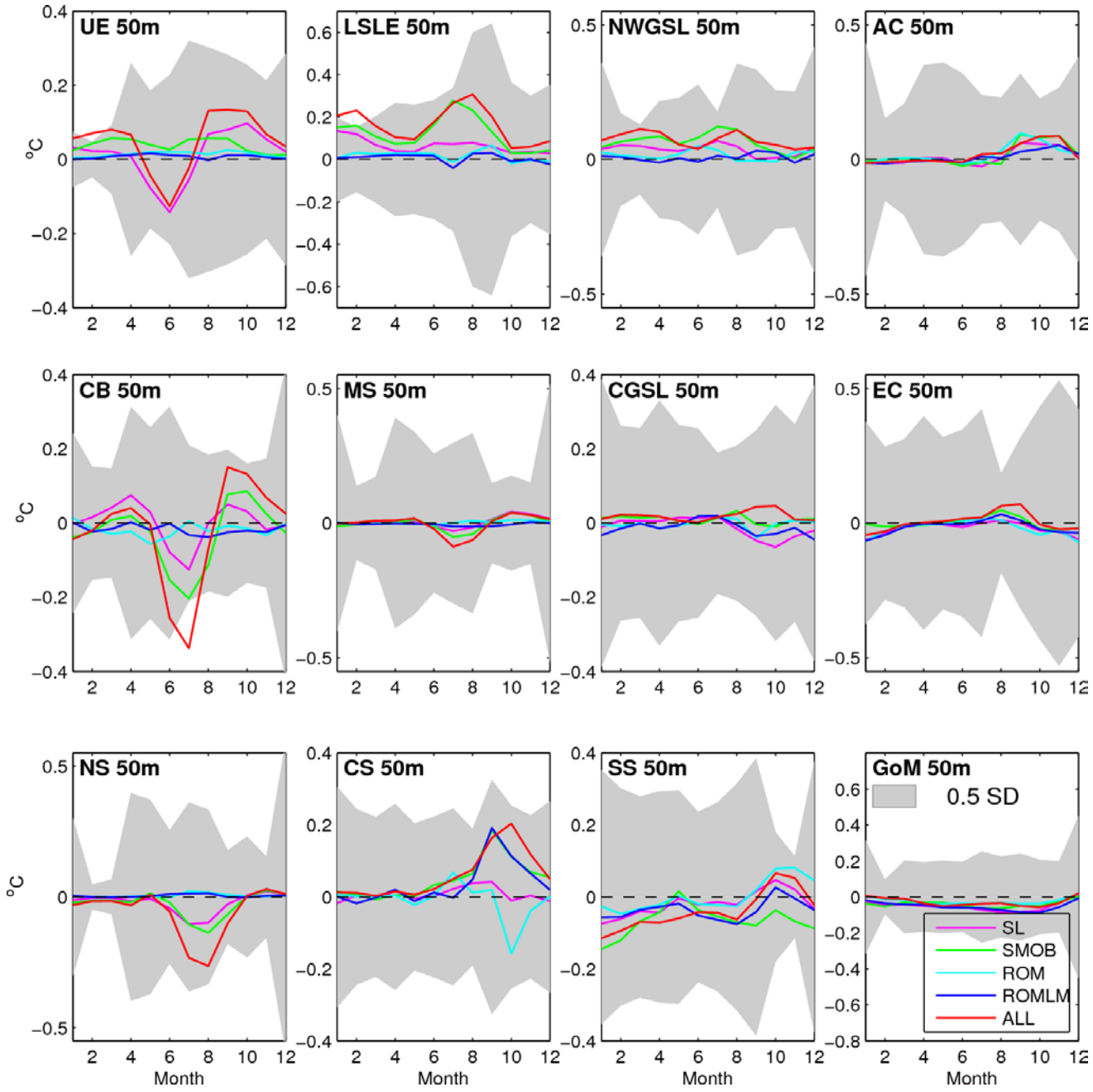

Figure 28. Differences (harnessed minus natural conditions) in monthly mean temperature averaged over the 0–50 m layer and over twelve regions defined on Figure 7. The grey areas represent half the standard deviations (0.5 SD) among years for each month of the reference simulation (NATURAL).

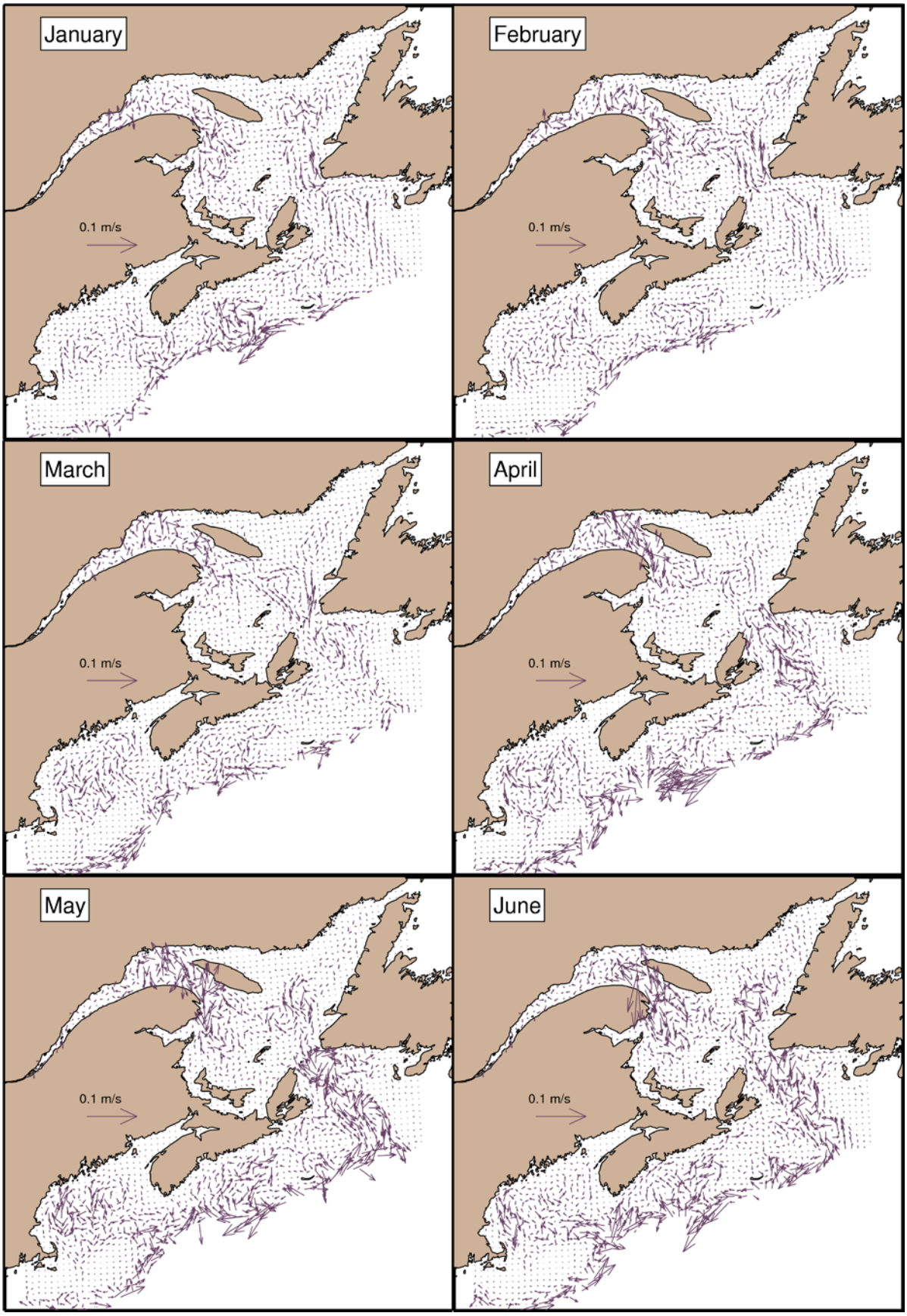

Figure 29. Differences in monthly mean 0–50 m currents over the six-year period between the St. Lawrence River scenario (SL) and the base simulation for January to June.

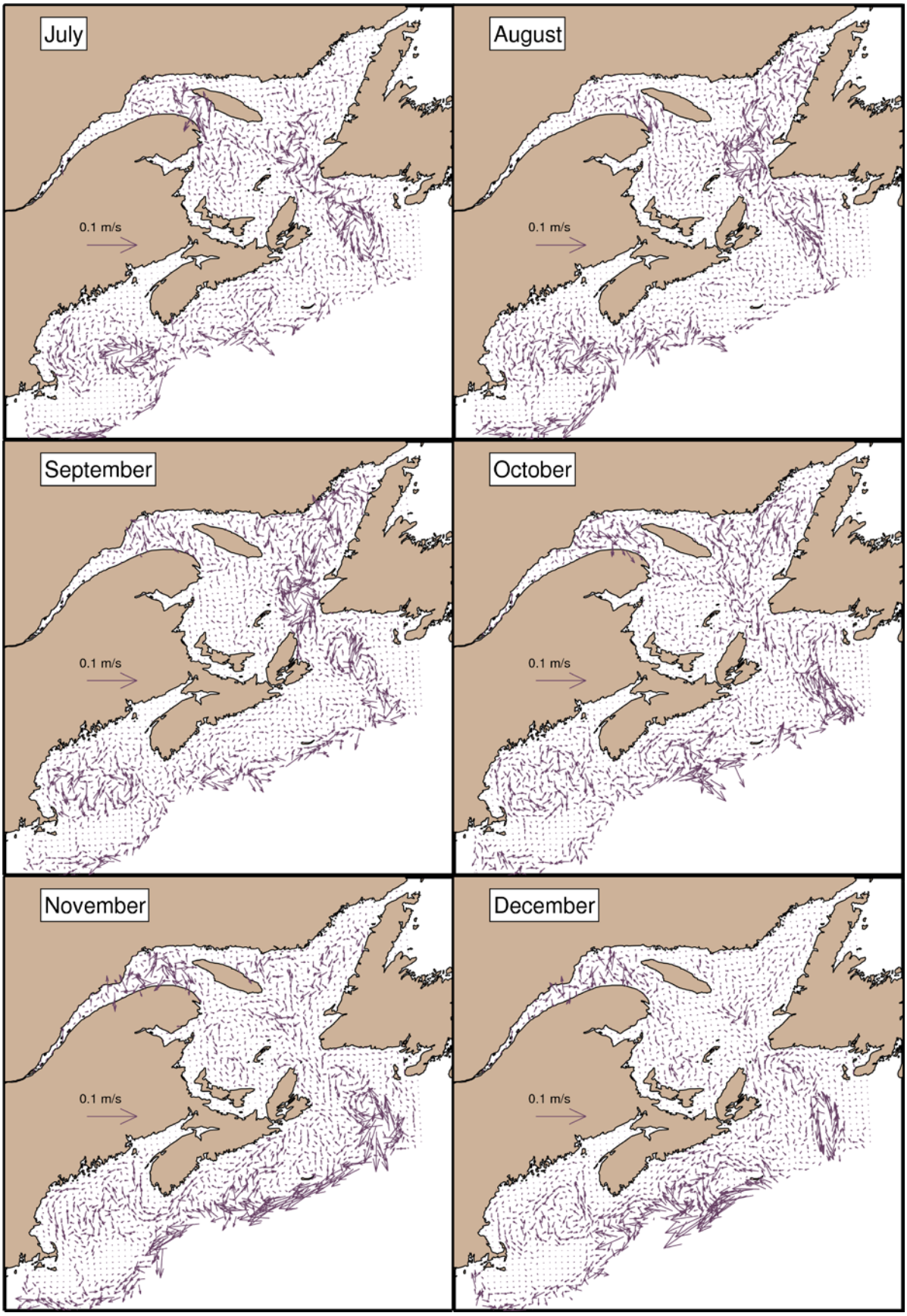

Figure 30. Differences in monthly mean 0–50 m currents over the six-year period between the St. Lawrence River scenario (SL) and the base simulation for July to December.

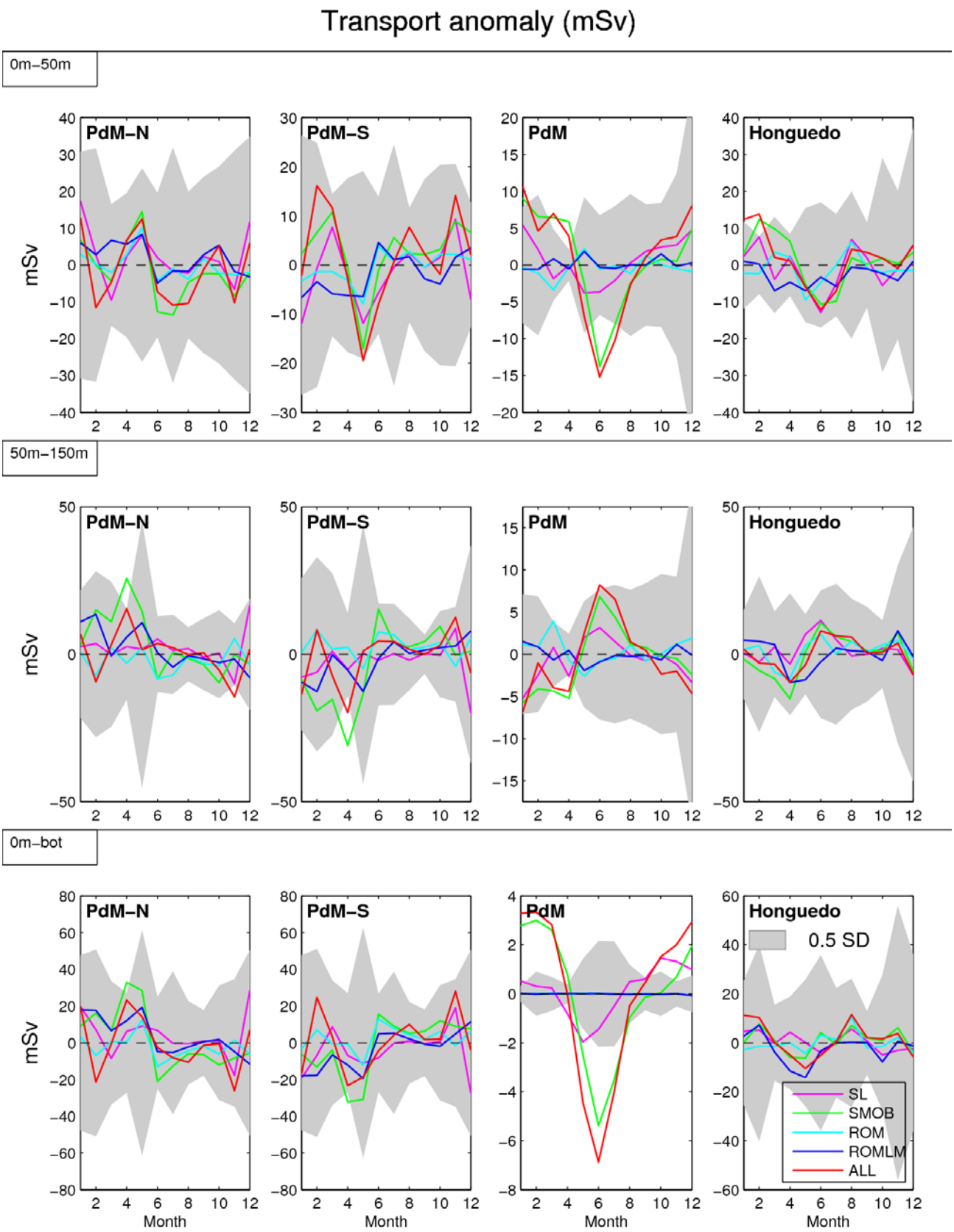

Figure 31. Transport anomaly (harnessed minus natural conditions) for PdM-N, PdM-S, PdM and Honguedo Strait (1 mSv = 1 milli-Sverdrup=10^3 m^3/s). The grey areas represent half the standard deviations (0.5 SD) among years for each month of the reference simulation (NATURAL). See also the mean transport in Figure 14.

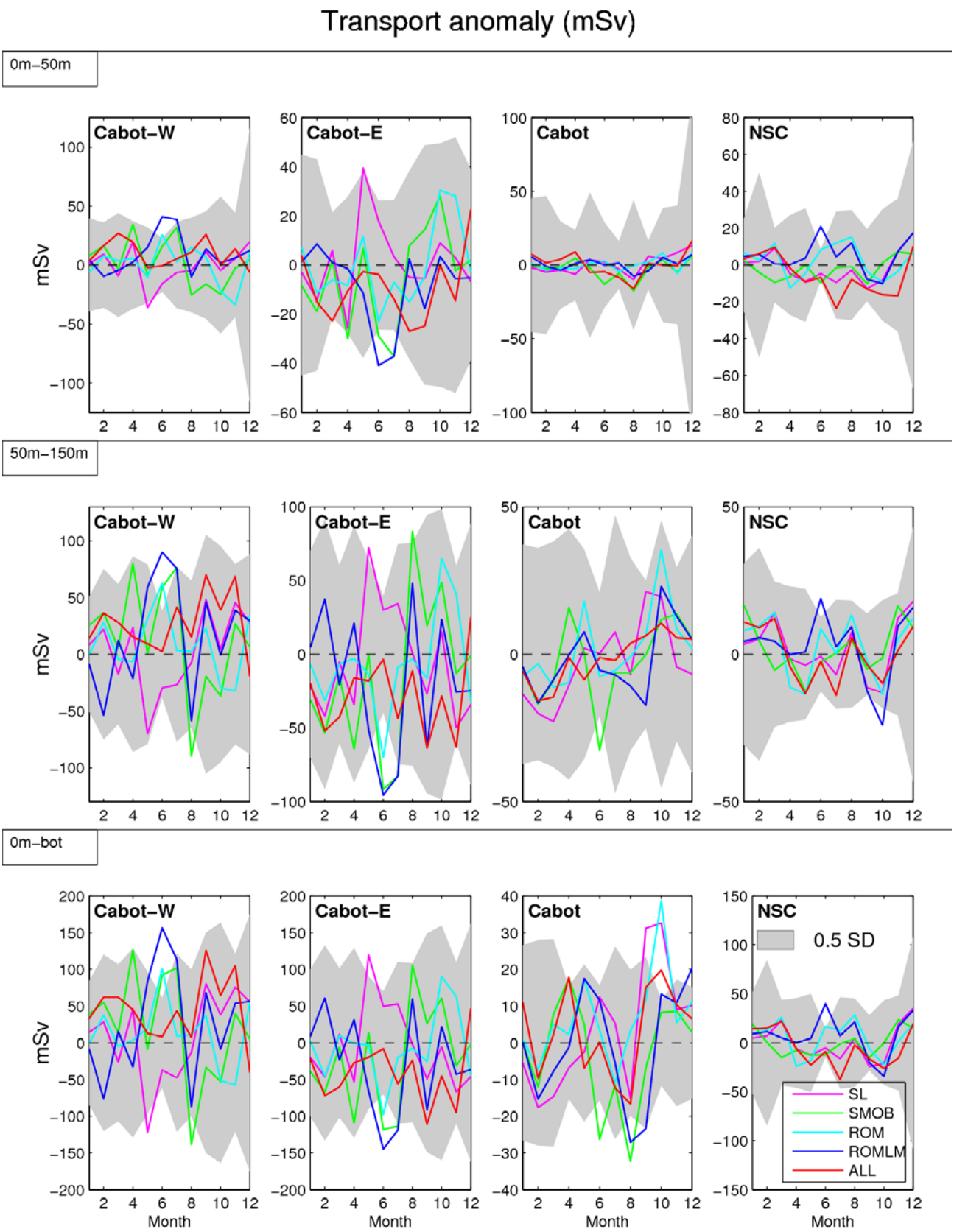

Figure 32. Transport anomaly (harnessed minus natural conditions) for Cabot-W, Cabot-E, Cabot and NSC (1 mSv = 1 milli-Sverdrup=10^3 m^3/s). The grey areas represent half the standard deviations (0.5 SD) among years for each month of the reference simulation (NATURAL). See also the mean transport in Figure 15.

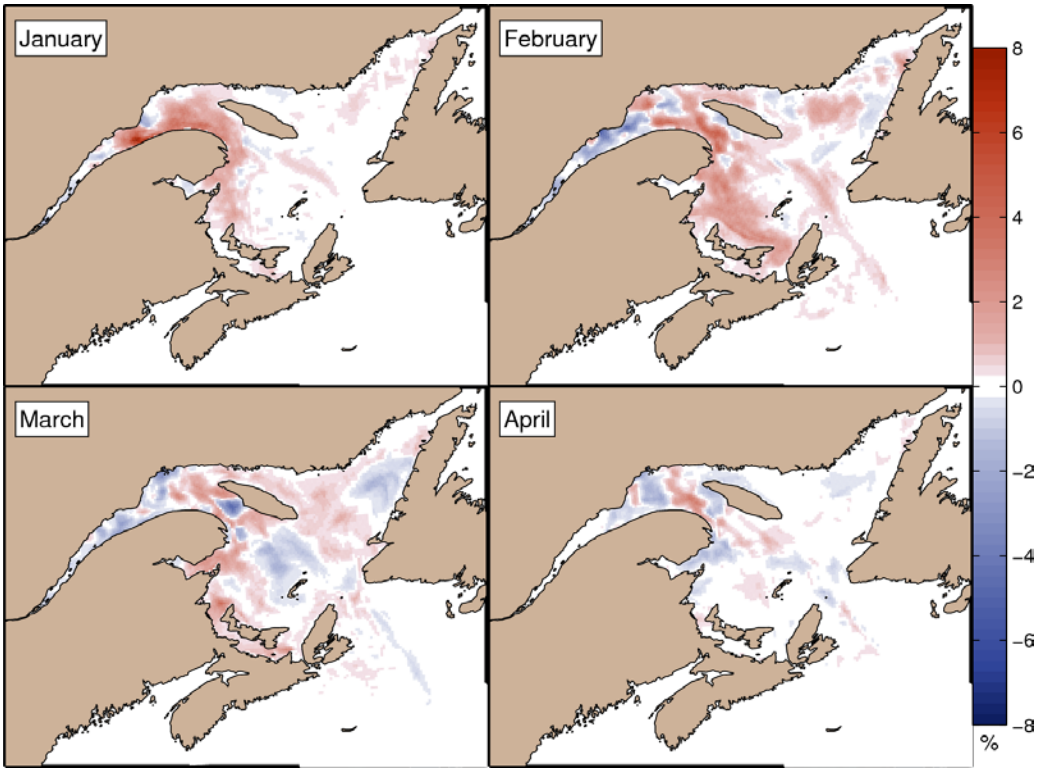

Figure 33. Differences in monthly mean sea-ice concentration over the six-year period between the St. Lawrence River scenario (SL) and the base simulation for January to April.

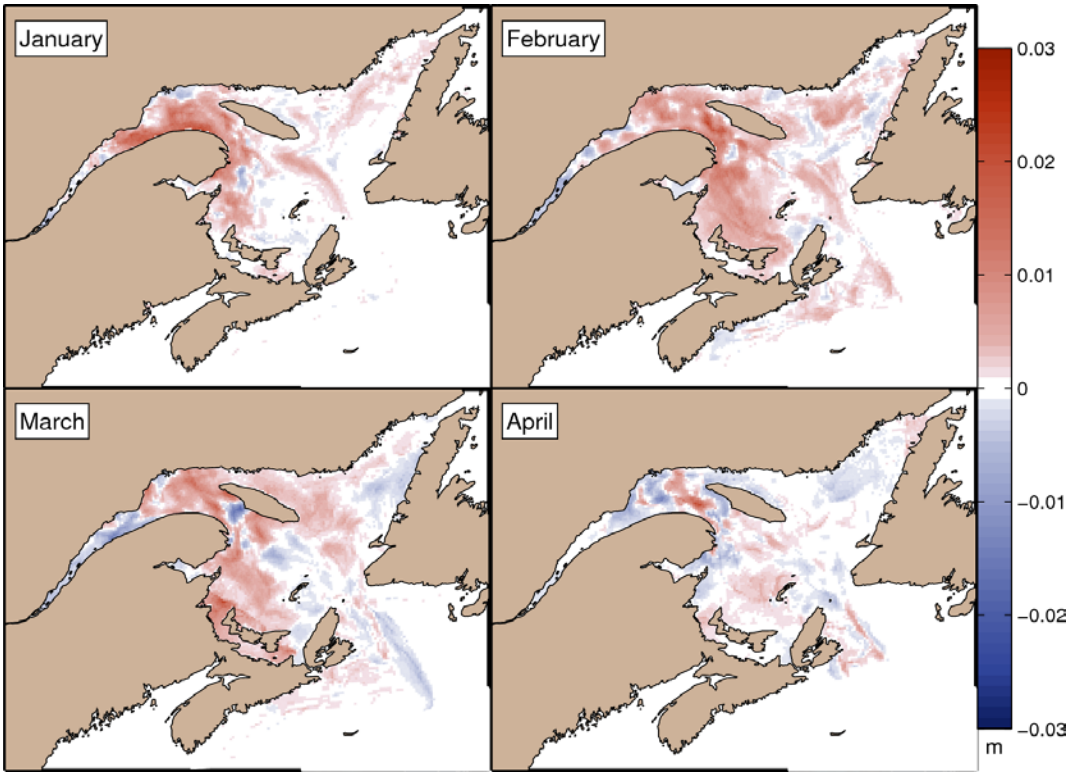

Figure 34. Differences in monthly mean sea-ice thickness over the six-year period between the St. Lawrence River scenario (SL) and the base simulation for January to April.

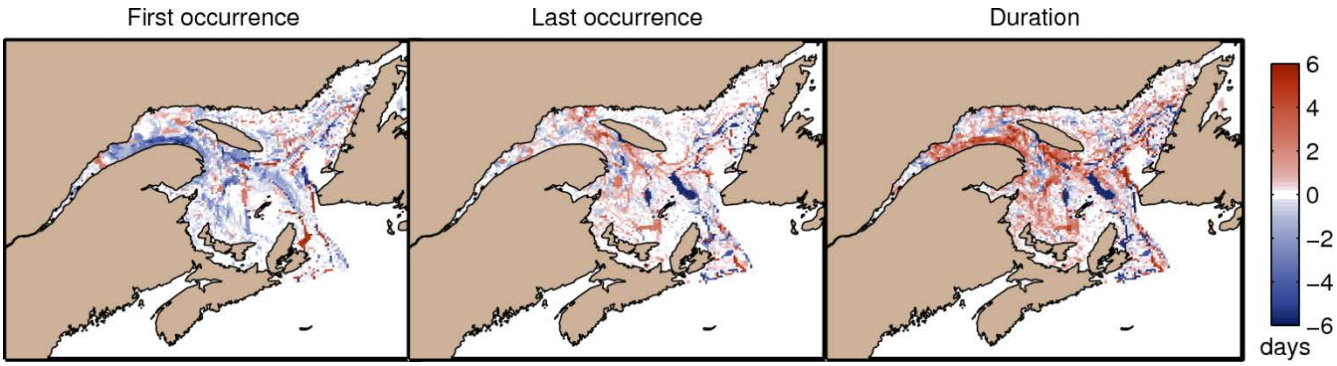

Figure 35. Differences in the 2006–2011 mean of start, end, and length of the sea-ice period (concentration > 5%) between the St. Lawrence River scenario (SL) and the base simulation.

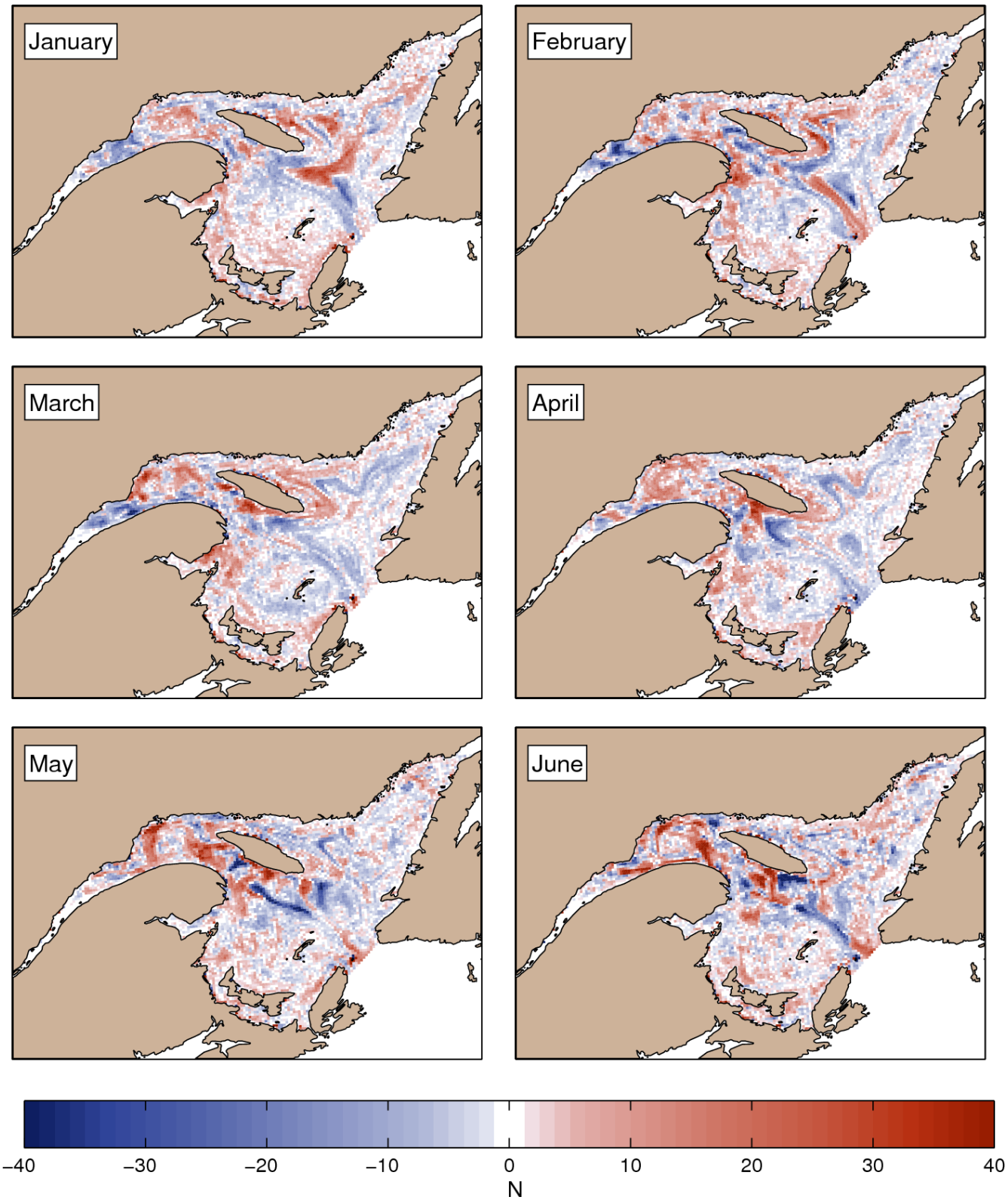

Figure 36. Differences in monthly mean krill density (number of particles per grid cell) with the LD vertical distribution over the five-year period (2007–2011) between the St. Lawrence River scenario (SL) and the base simulation for January to June.

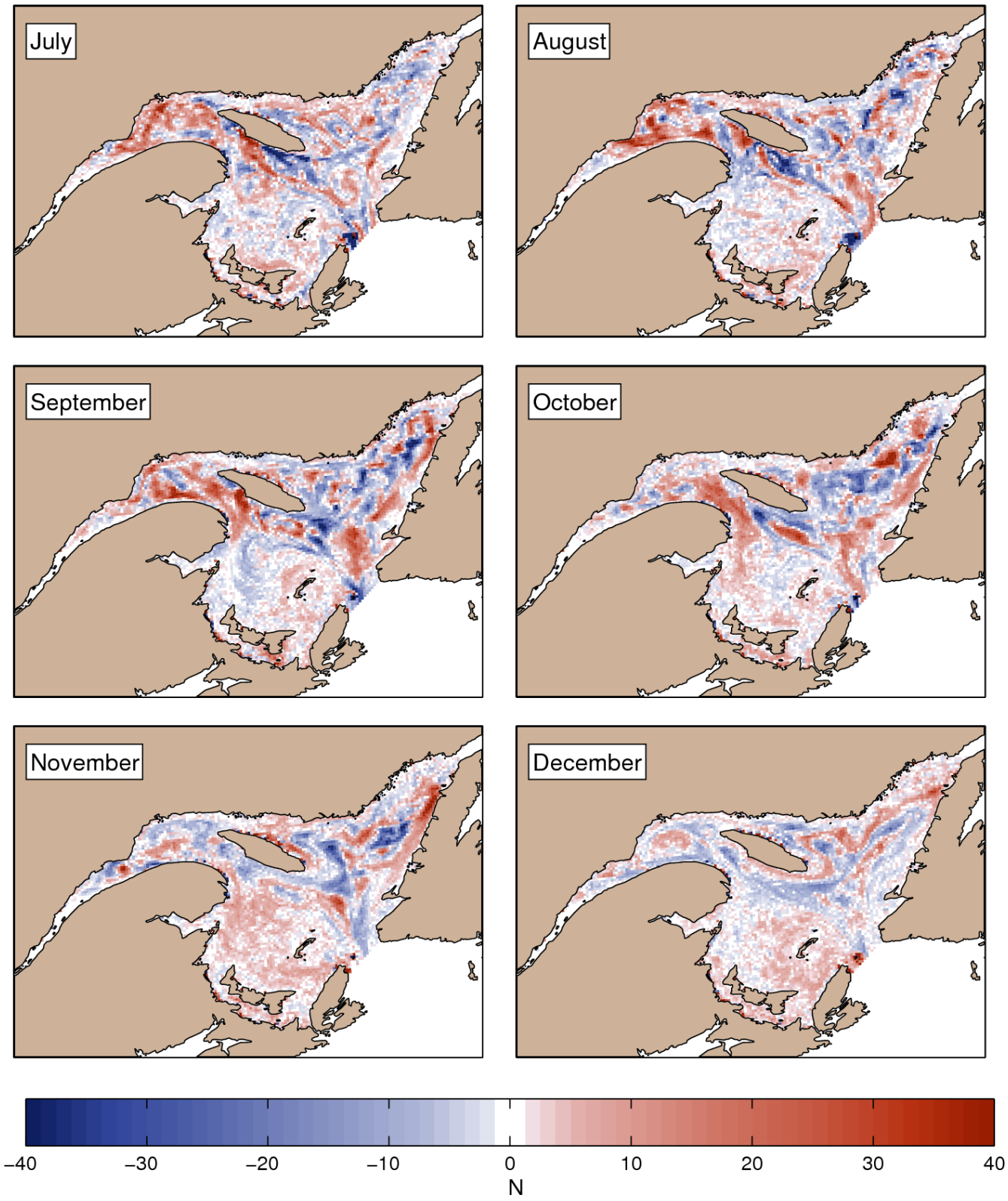

Figure 37. Differences in monthly mean krill density (number of particles per grid cell) with the LD vertical distribution over the five-year period (2007–2011) between the St. Lawrence River scenario (SL) and the base simulation for July to December.

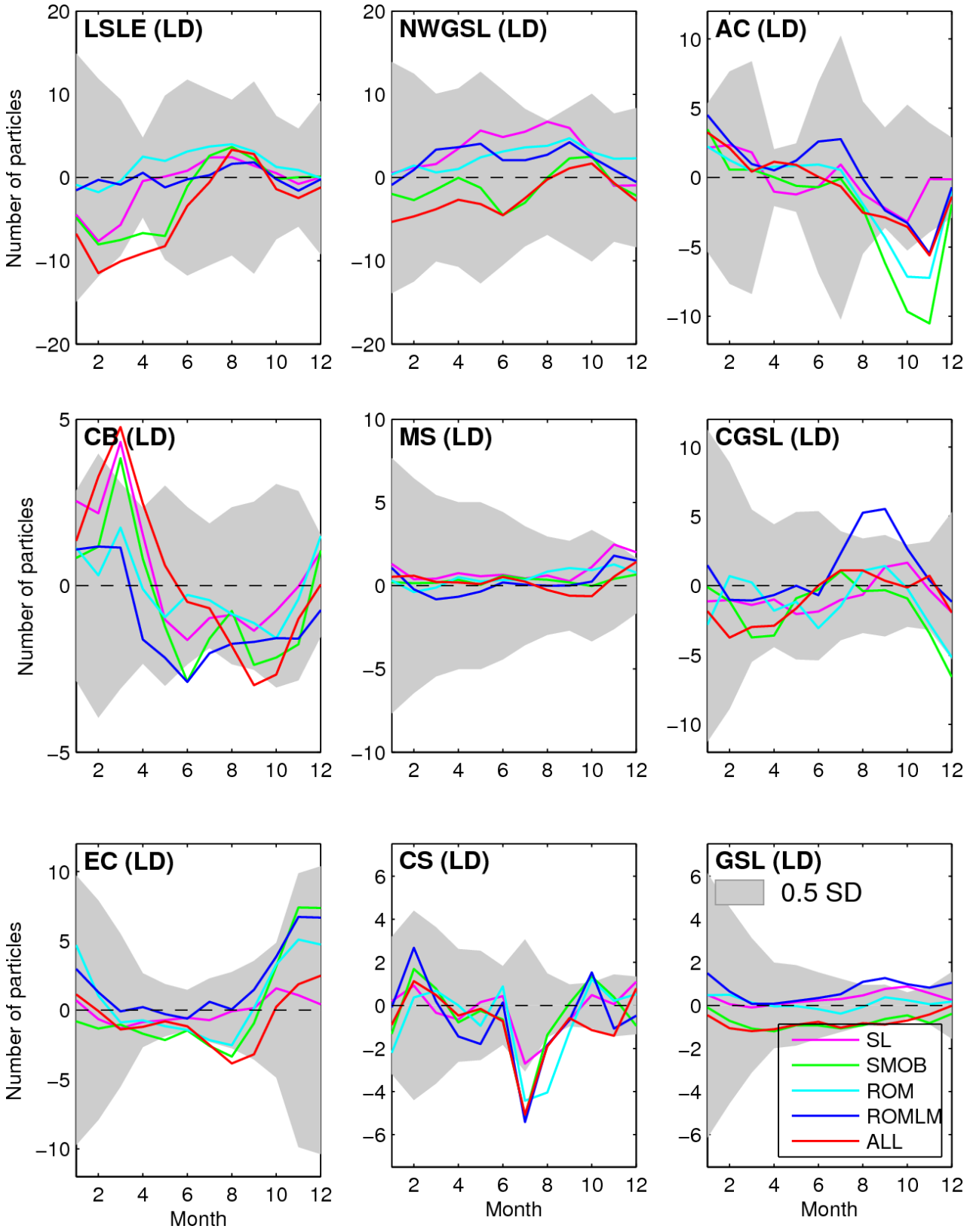

Figure 38. Differences (harnessed minus natural conditions) in monthly mean depth-integrated krill density (LD vertical distribution) averaged over the eight regions defined on Figure 7 and the whole GSL, which includes all the regions up to Cabot Strait. The grey areas represent half the standard deviations (0.5 SD) among years for each month of the reference simulation (NATURAL).

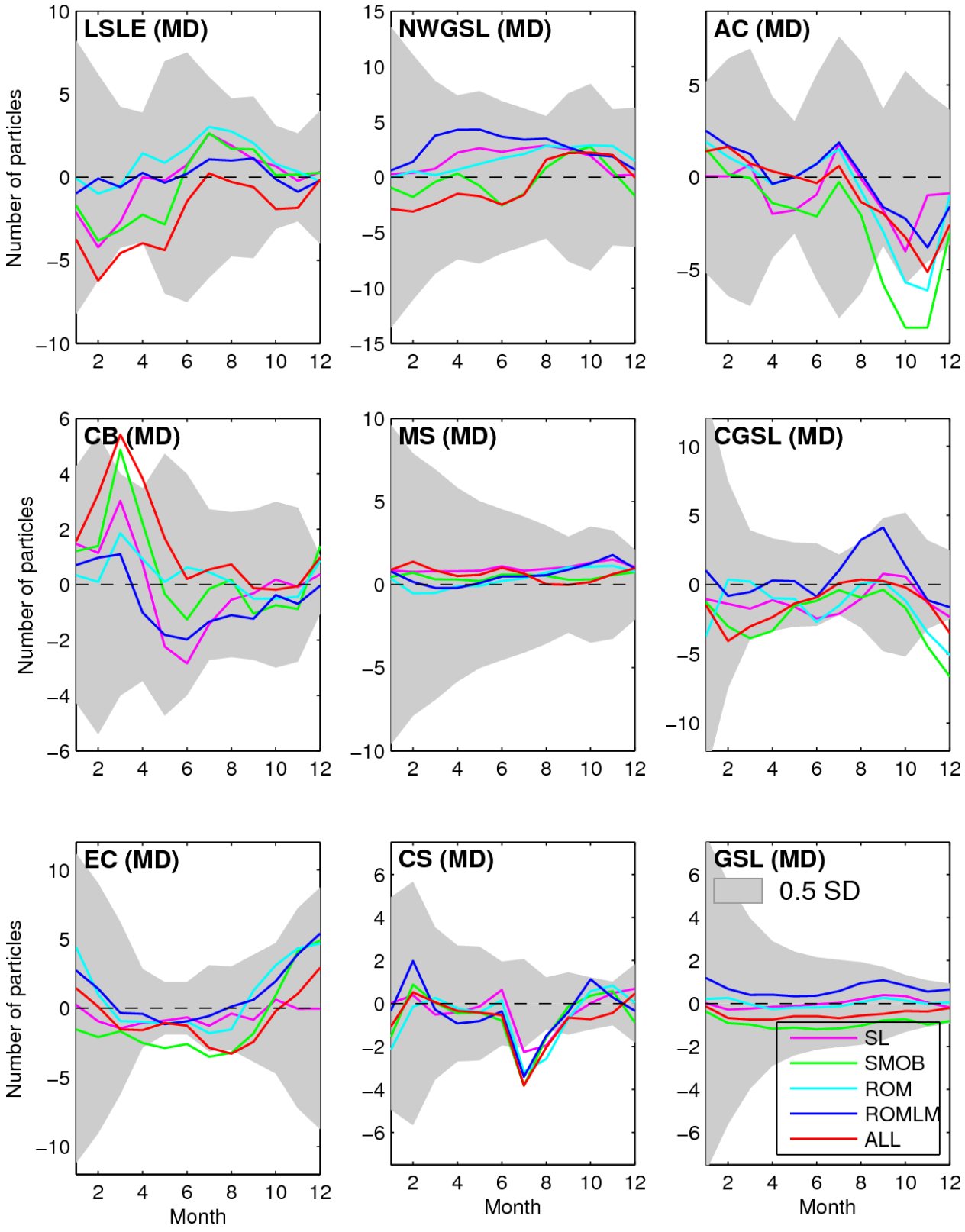

Figure 39. Differences (harnessed minus natural conditions) in monthly mean depth-integrated krill density (MD vertical distribution) averaged over eight regions defined on Figure 7 and the whole GSL, which includes all the regions up to Cabot Strait. The grey areas represent half the standard deviations (0.5 SD) among years for each month of the reference simulation (NATURAL).

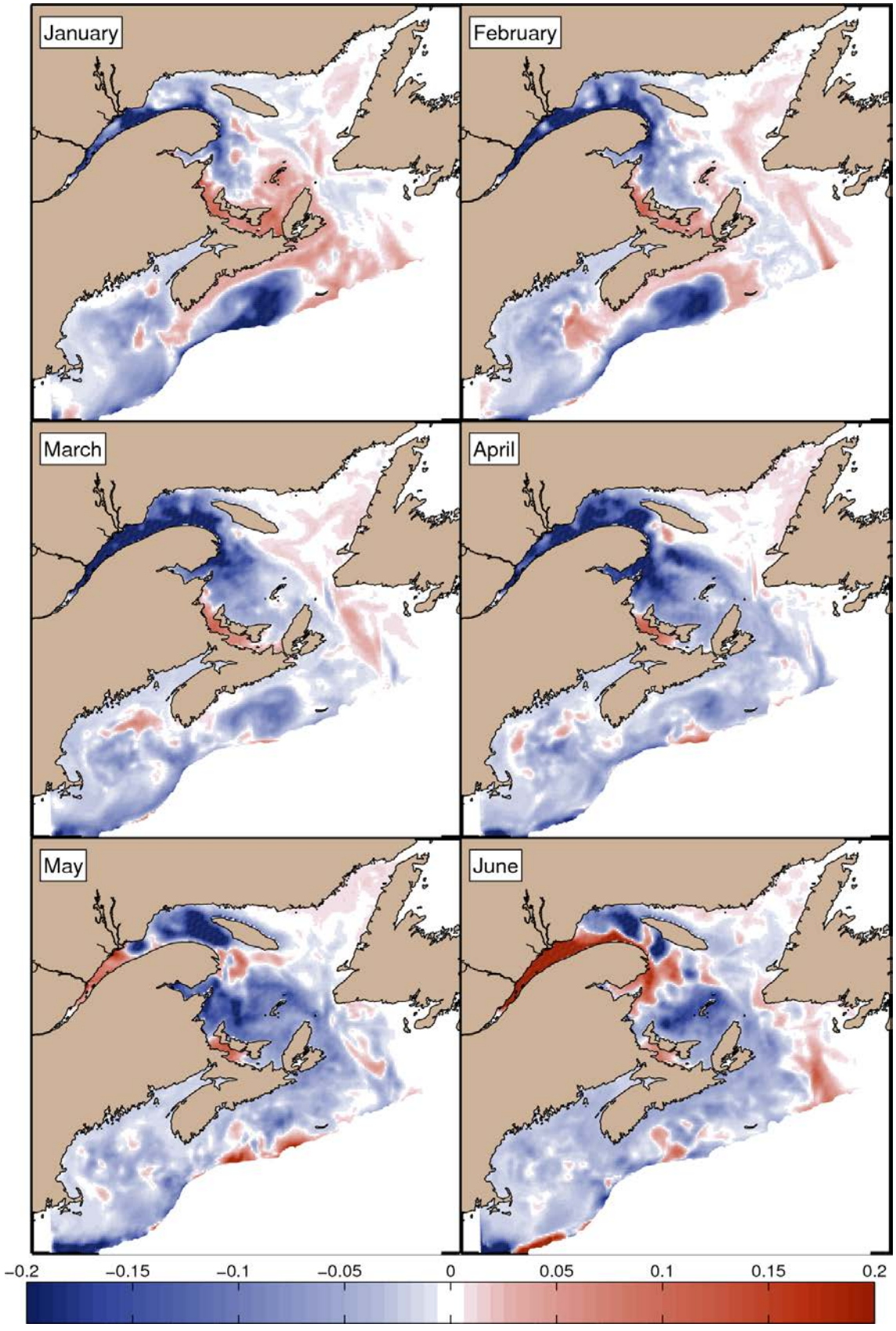

Figure 40. Differences in monthly mean 0–50 m salinities over the six-year period between the Saguenay, Manicouagan, Outardes, and Betsiamites rivers scenario (SMOB) and the base simulation for January to June.

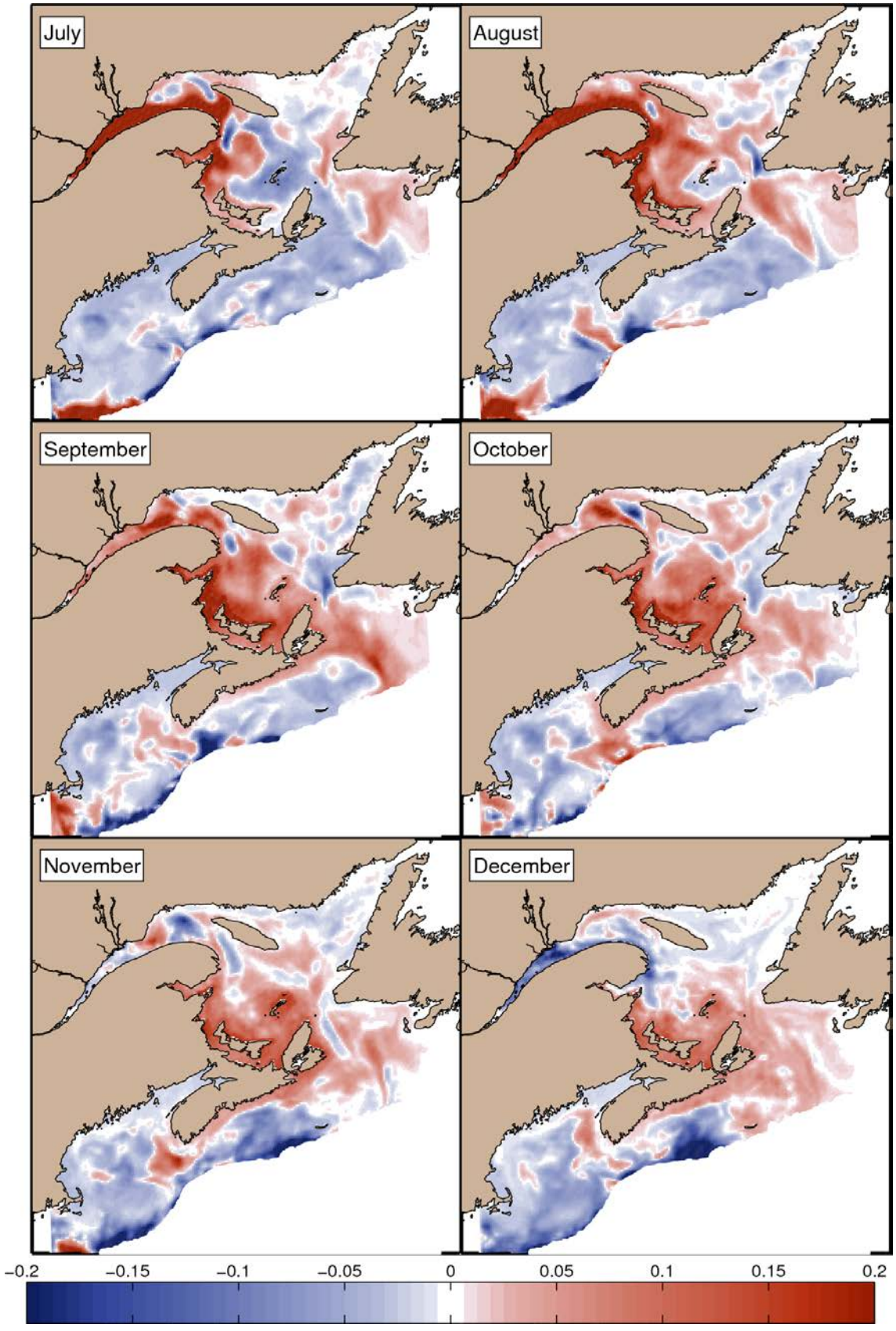

Figure 41. Differences in monthly mean 0–50 m salinities over the six-year period between the Saguenay, Manicouagan, Outardes, and Betsiamites rivers scenario (SMOB) and the base simulation for July to December.

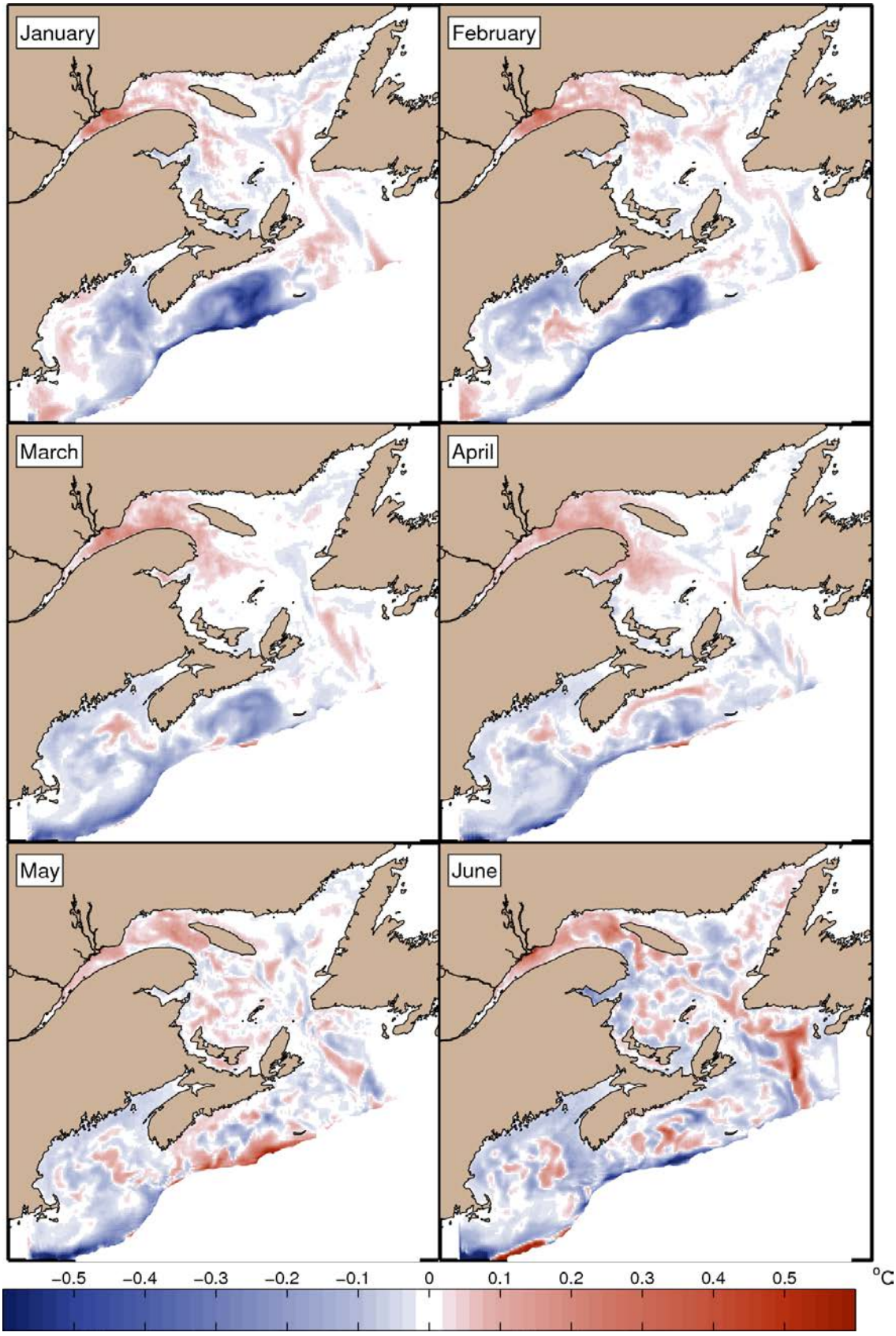

Figure 42. Differences in monthly mean 0–50 m temperatures over the six-year period between the Saguenay, Manicouagan, Outardes, and Betsiamites rivers scenario (SMOB) and the base simulation for January to June.

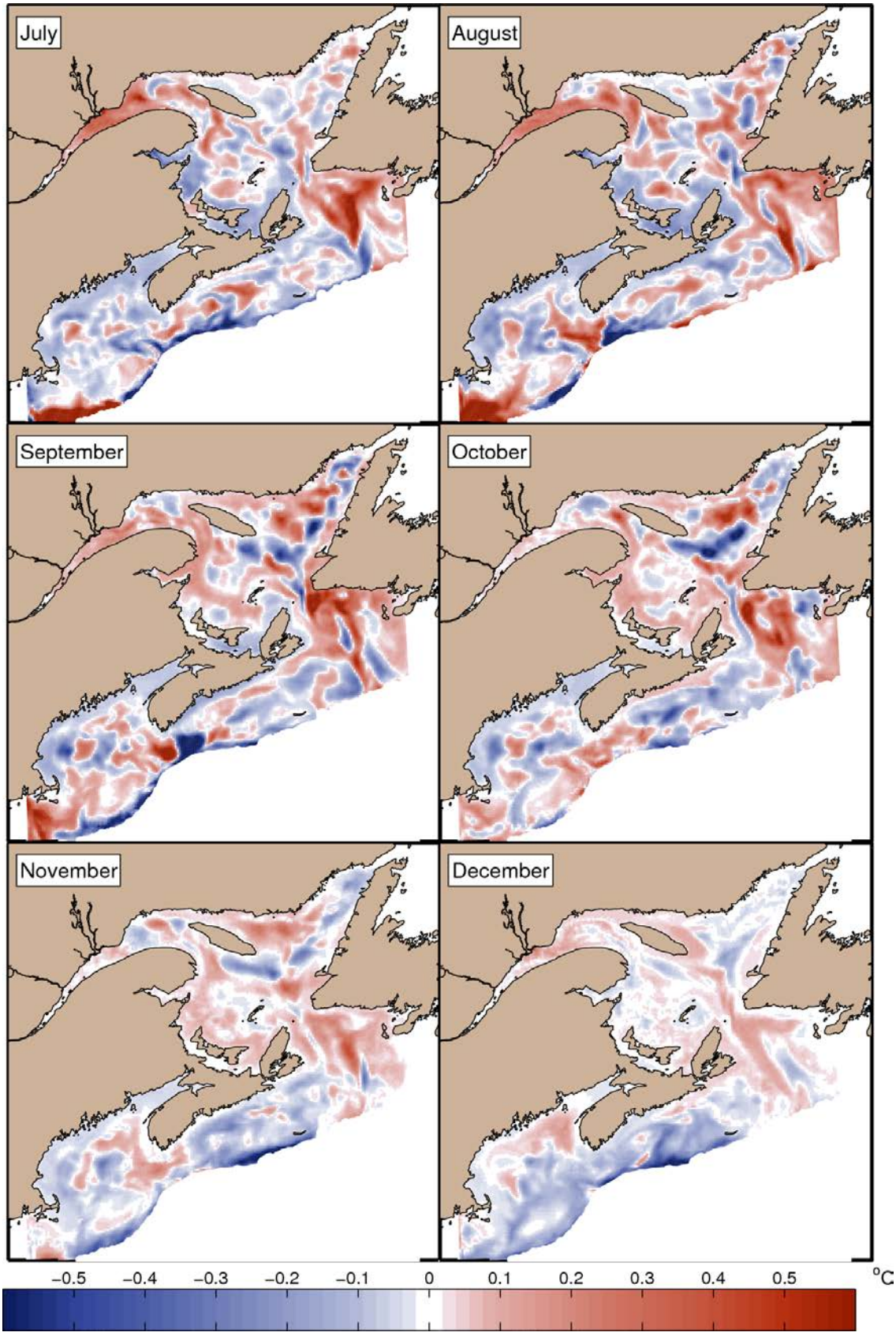

Figure 43. Differences in monthly mean 0–50 m temperatures over the six-year period between the Saguenay, Manicouagan, Outardes, and Betsiamites rivers scenario (SMOB) and the base simulation for July to December.

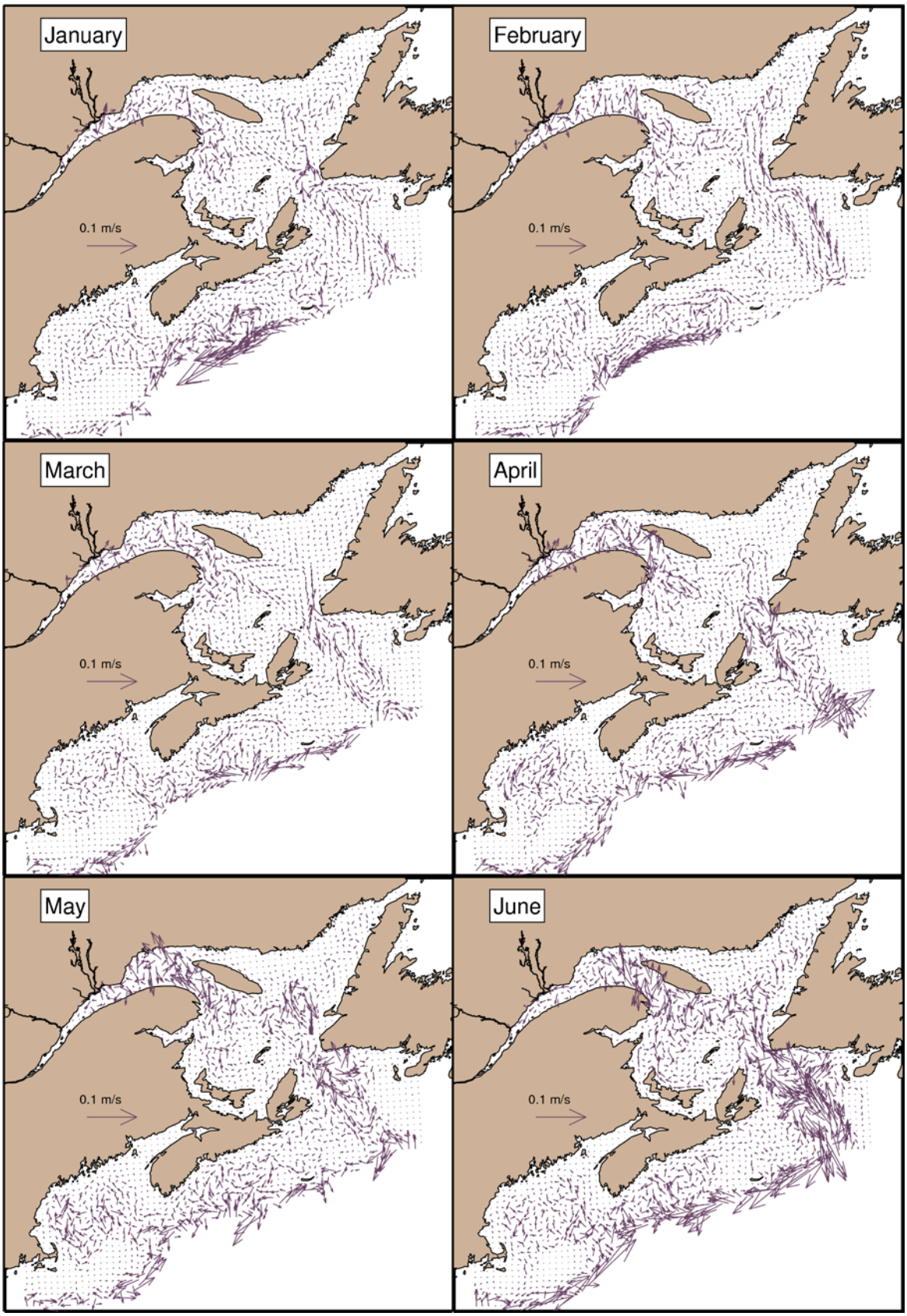

Figure 44**.** Differences in monthly mean 0–50 m currents over the six-year period between the Saguenay, Manicouagan, Outardes, and Betsiamites rivers scenario (SMOB) and the base simulation for January to June.

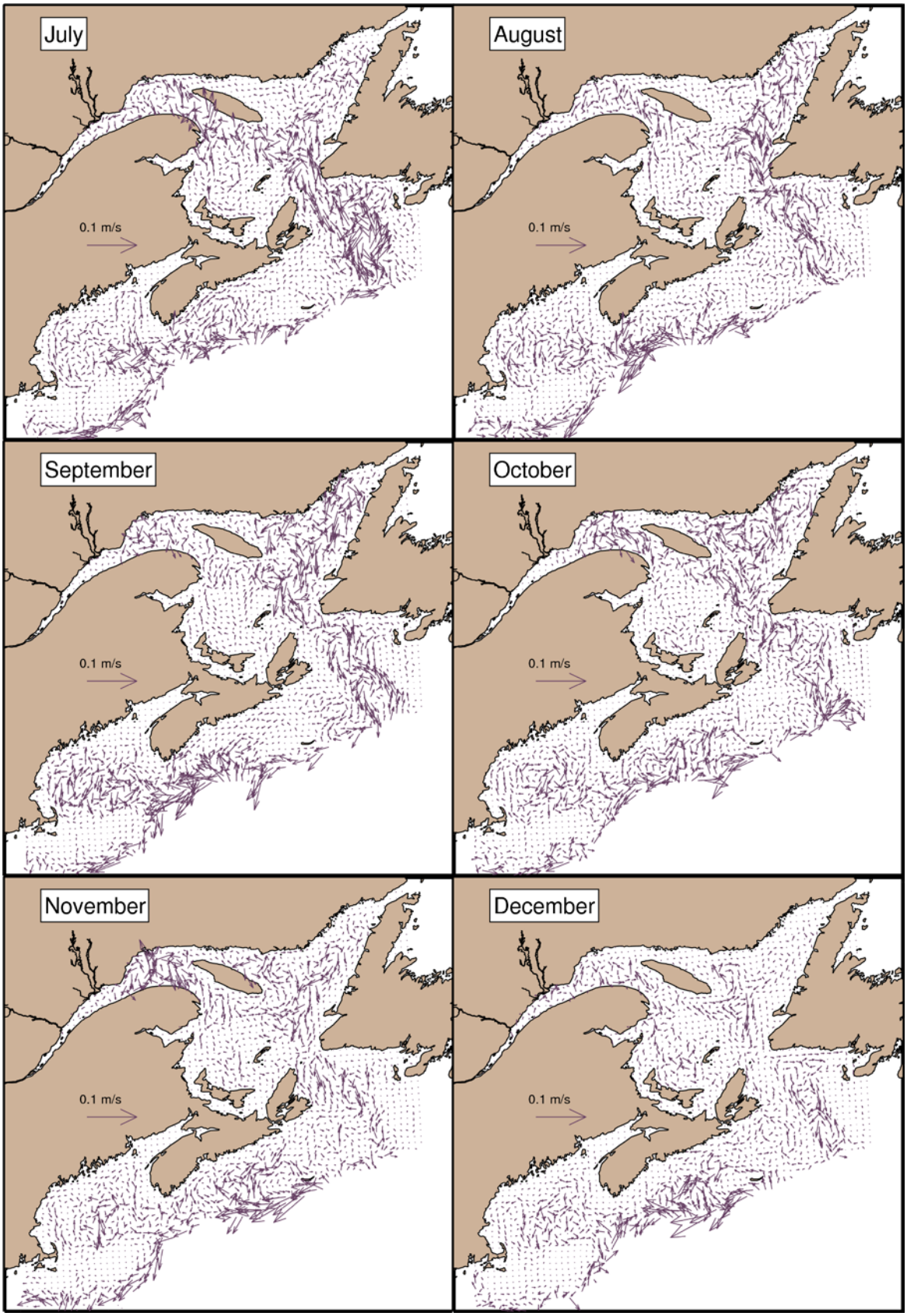

Figure 45**.** Differences in monthly mean 0–50 m currents over the six-year period between the the Saguenay, Manicouagan, Outardes, and Betsiamites rivers scenario (SMOB) simulation and the natural conditions (July to December).

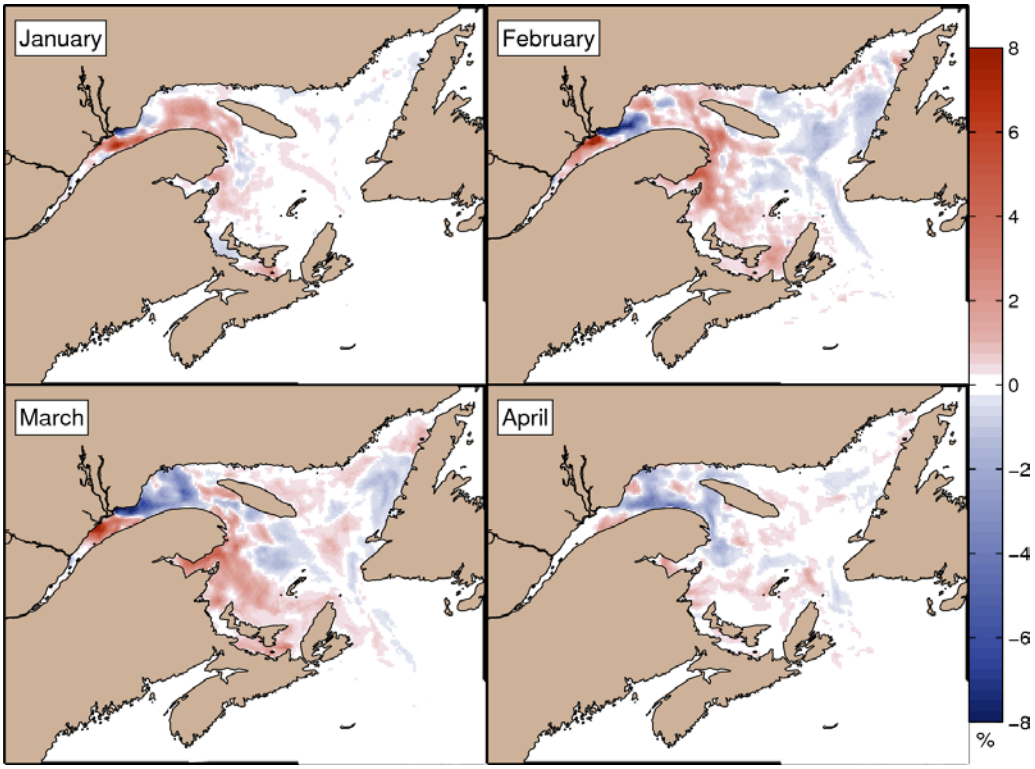

Figure 46. Differences in monthly mean sea-ice concentration over the six-year period between the Saguenay, Manicouagan, Outardes, and Betsiamites rivers scenario (SMOB) and the base simulation for January to April.

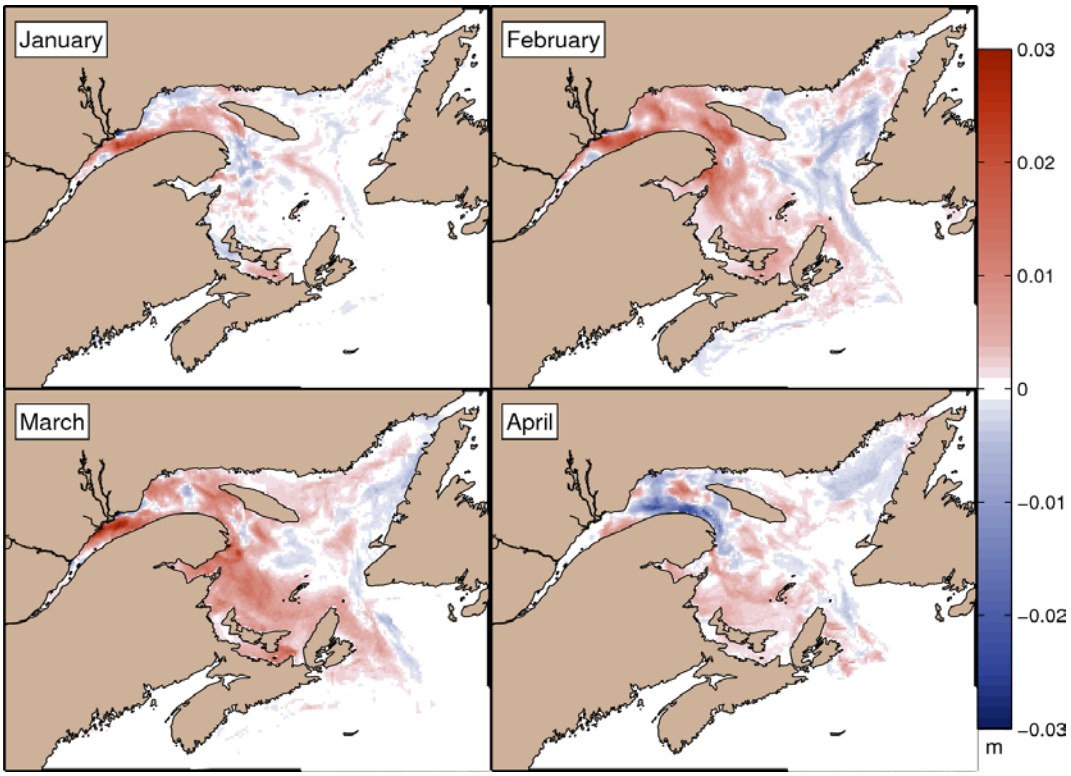

Figure 47. Differences in monthly mean sea-ice thickness over the six-year period between the Saguenay, Manicouagan, Outardes, and Betsiamites rivers scenario (SMOB) and the base simulation for January to April.

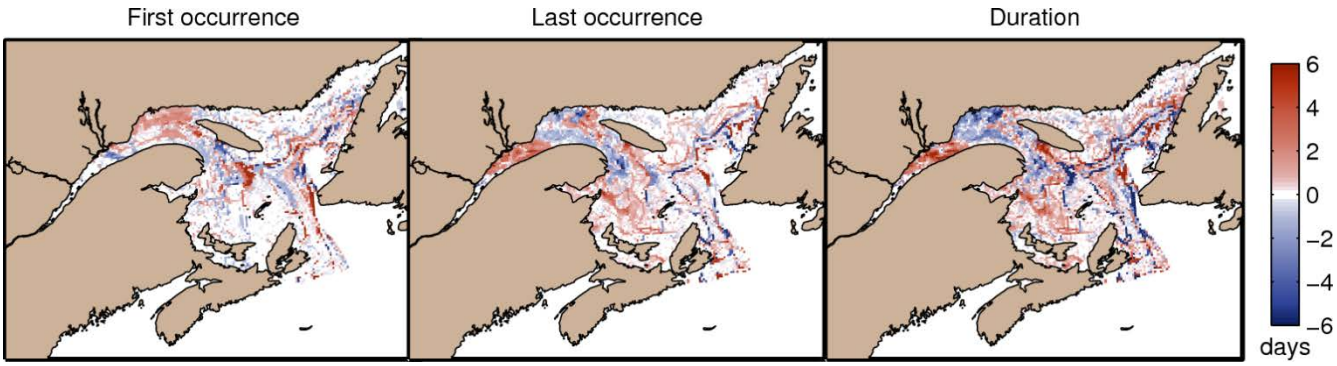

Figure 48. Differences in the 2006–2011 mean of start, end, and length of the sea-ice period (concentration > 5%) between the Saguenay, Manicouagan, Outardes, and Betsiamites rivers scenario (SMOB) and the base simulation.

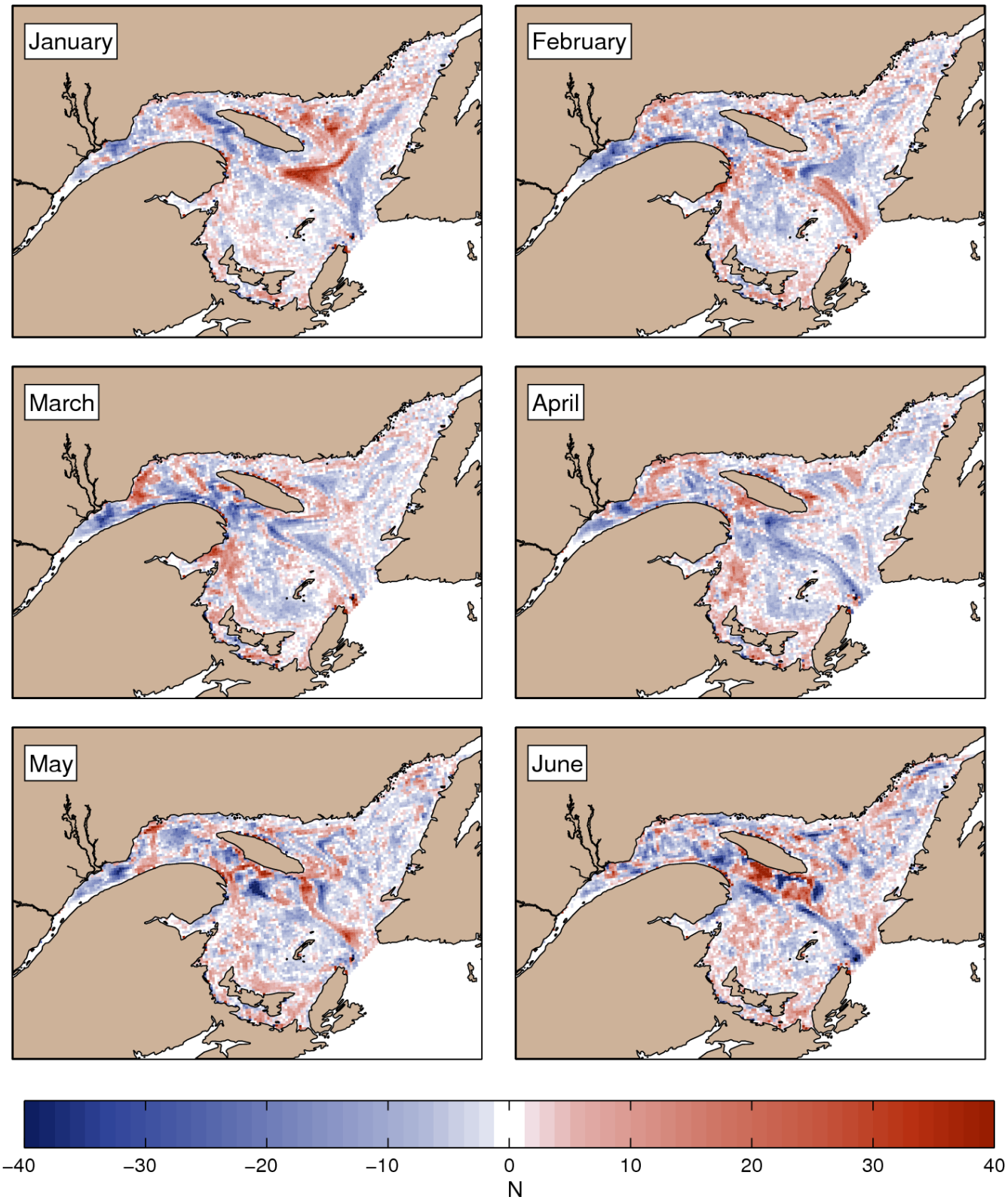

Figure 49. Differences in monthly mean krill density (number of particles per grid cell) with the LD vertical distribution over the five-year period (2007–2011) between the Saguenay, Manicouagan, Outardes, and Betsiamites rivers scenario (SMOB) and the base simulation for January to June.

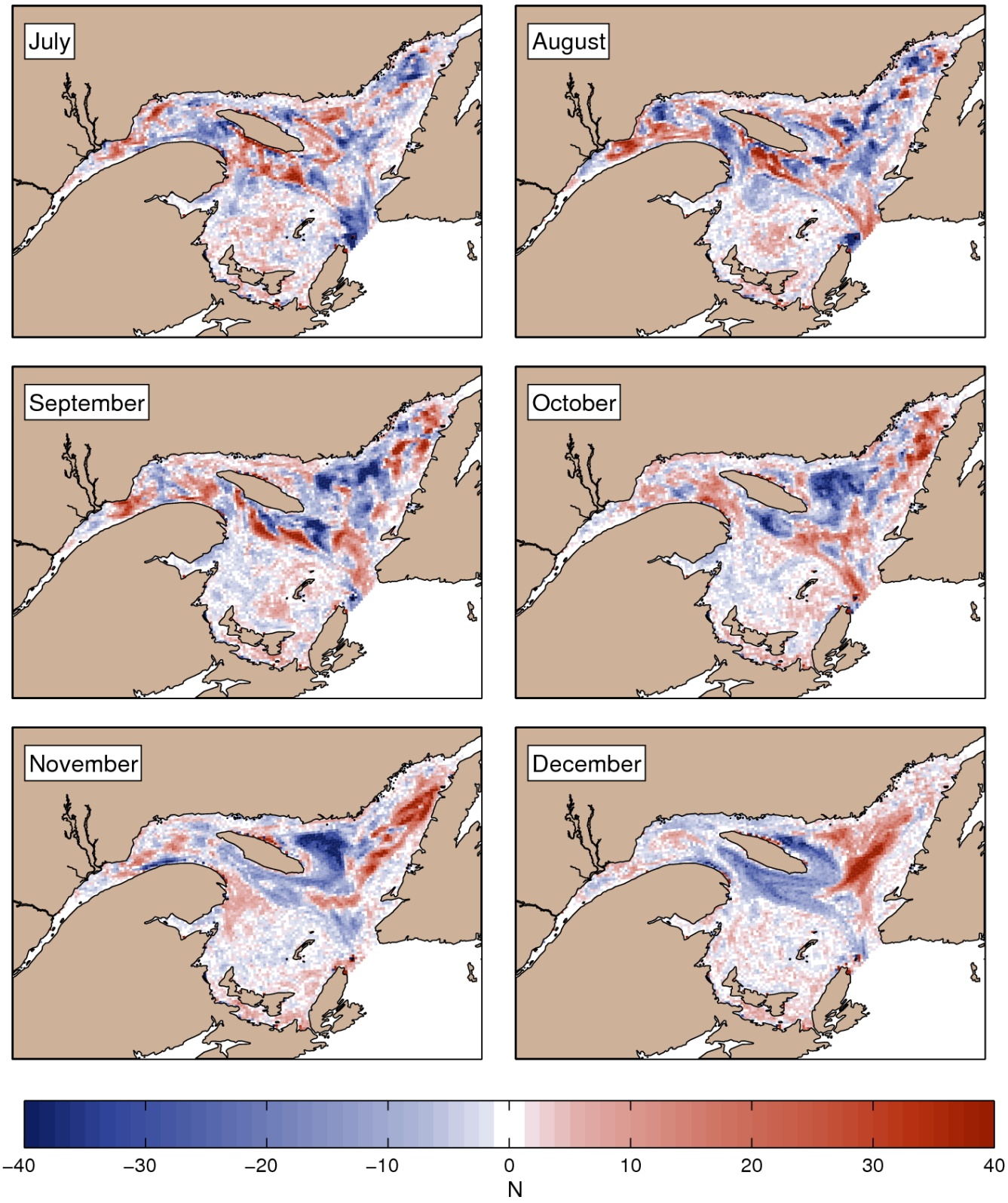

Figure 50. Differences in monthly mean krill density (number of particles per grid cell) with the LD vertical distribution over the five-year period (2007–2011) between the Saguenay, Manicouagan, Outardes, and Betsiamites rivers scenario (SMOB) and the base simulation for July to December.

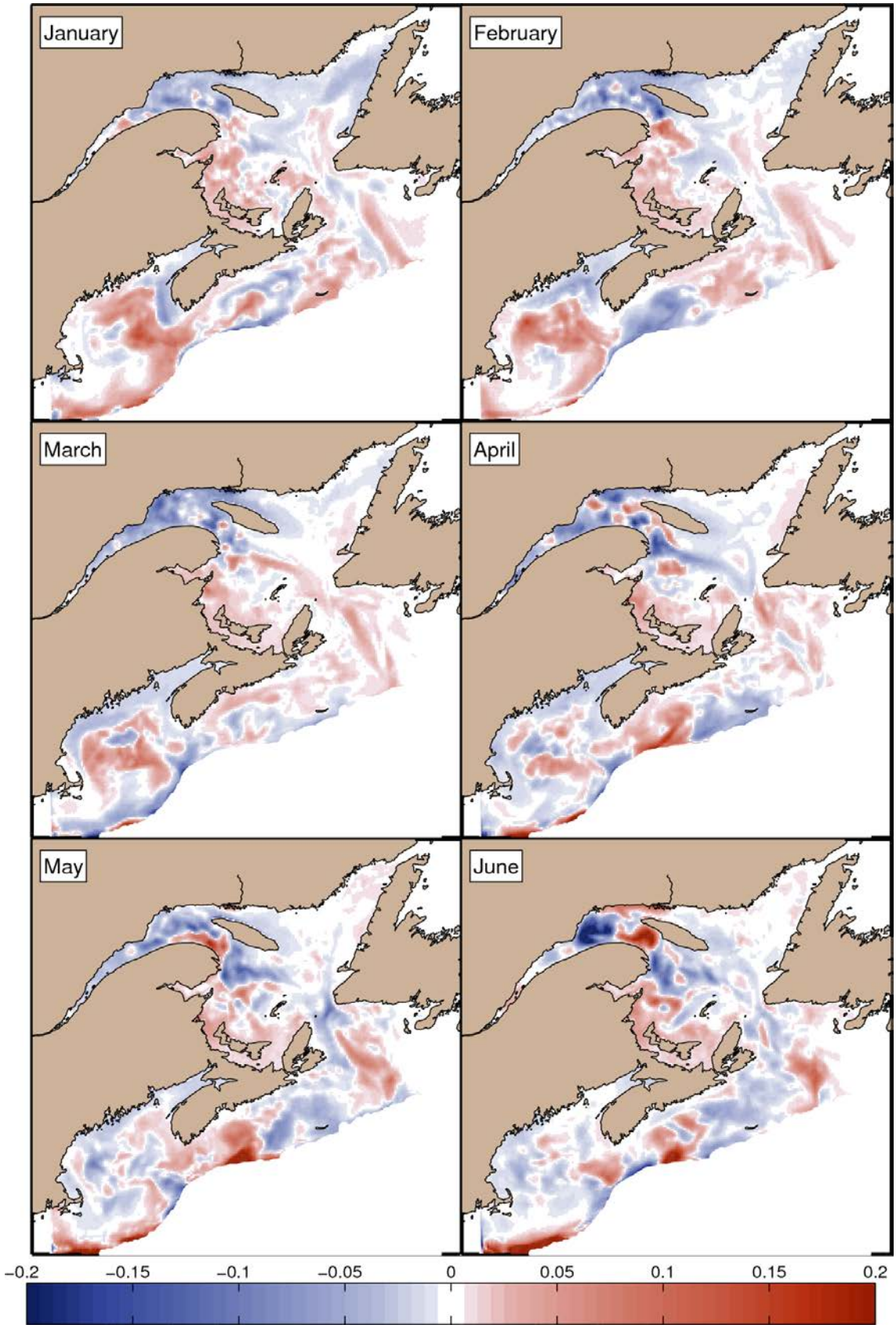

Figure 51. Differences in monthly mean 0–50 m salinities over the six-year period between the Romaine River scenario (ROM) and the base simulation for January to June.

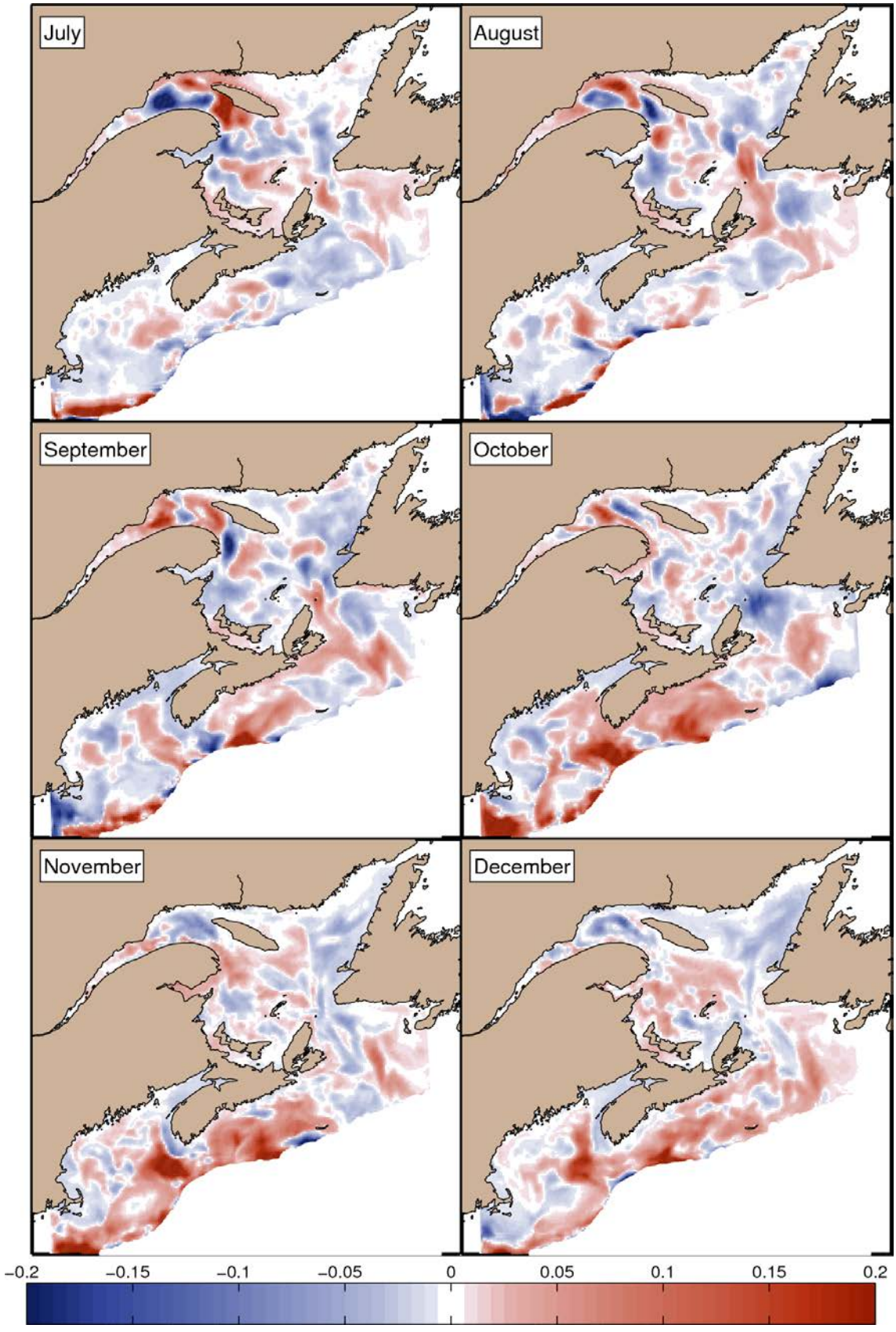

Figure 52. Differences in monthly mean 0–50 m salinities over the six-year period between the Romaine River scenario (ROM) and the base simulation for July to December.

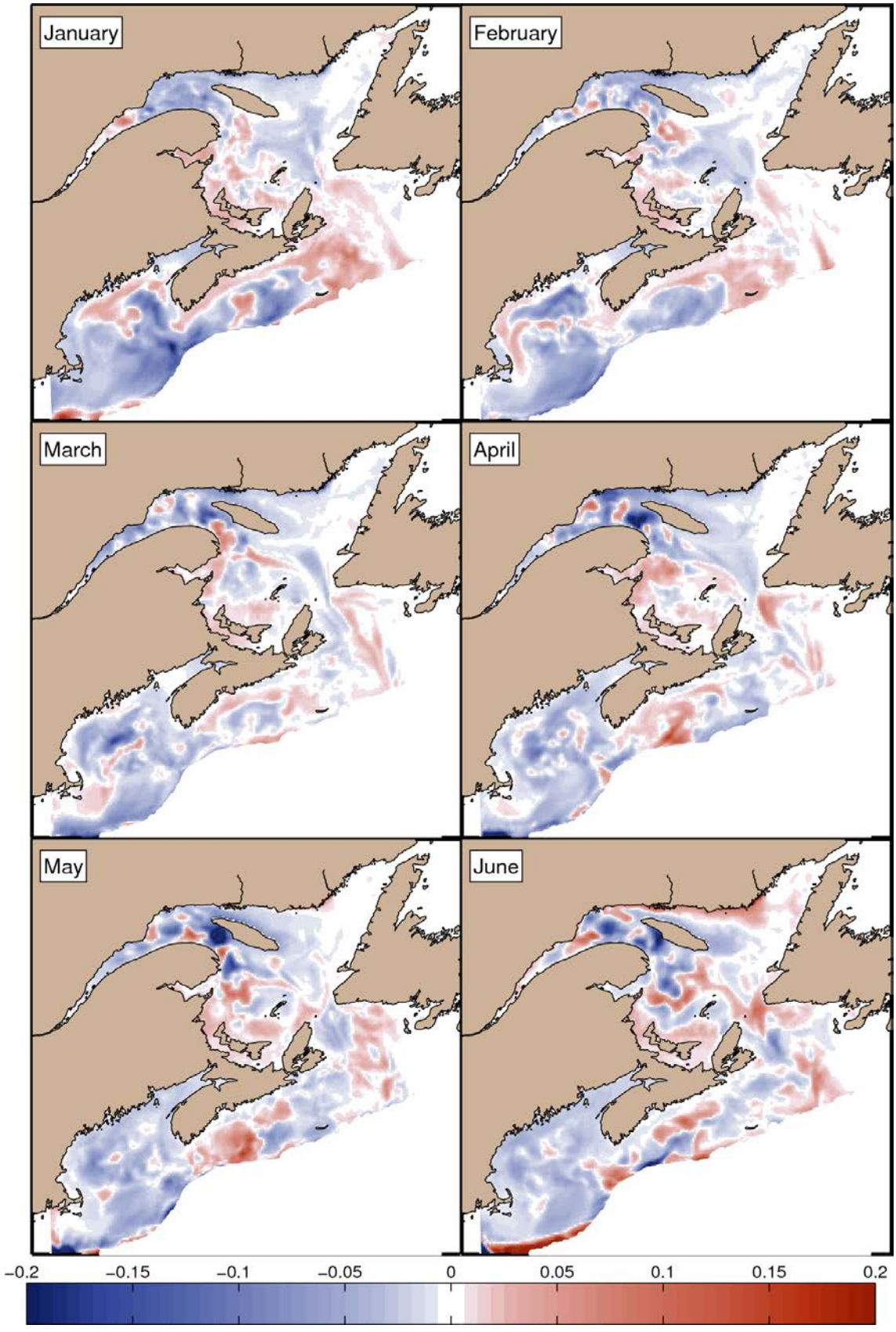

Figure 53. Differences in monthly mean 0–50 m salinities over the six-year period between the Romaine and Little Mecatina rivers (ROMLM) and the base simulation for January to June.

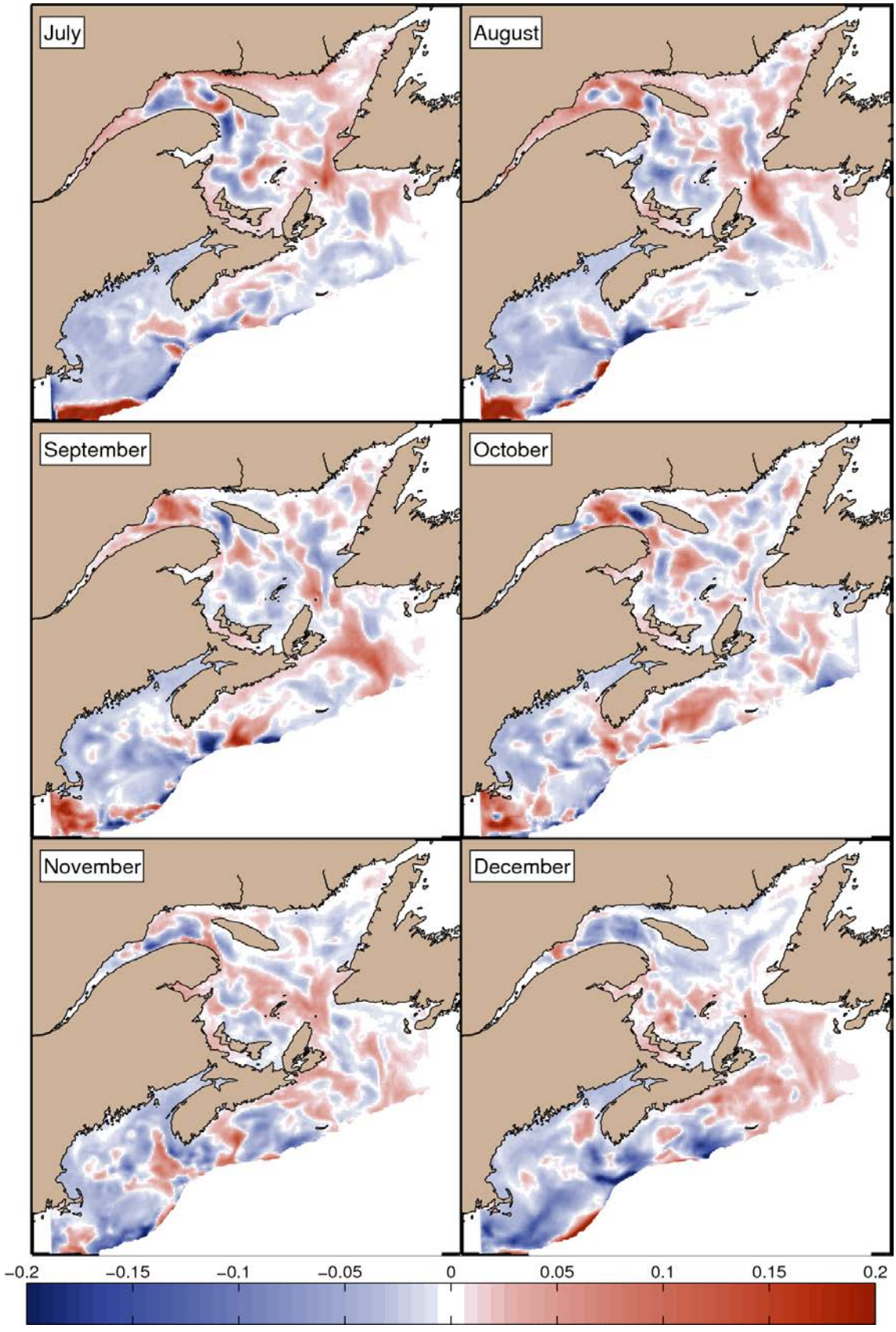

Figure 54. Differences in monthly mean 0–50 m salinities over the six-year period between the Romaine and Little Mecatina rivers (ROMLM) and the base simulation for July to December.

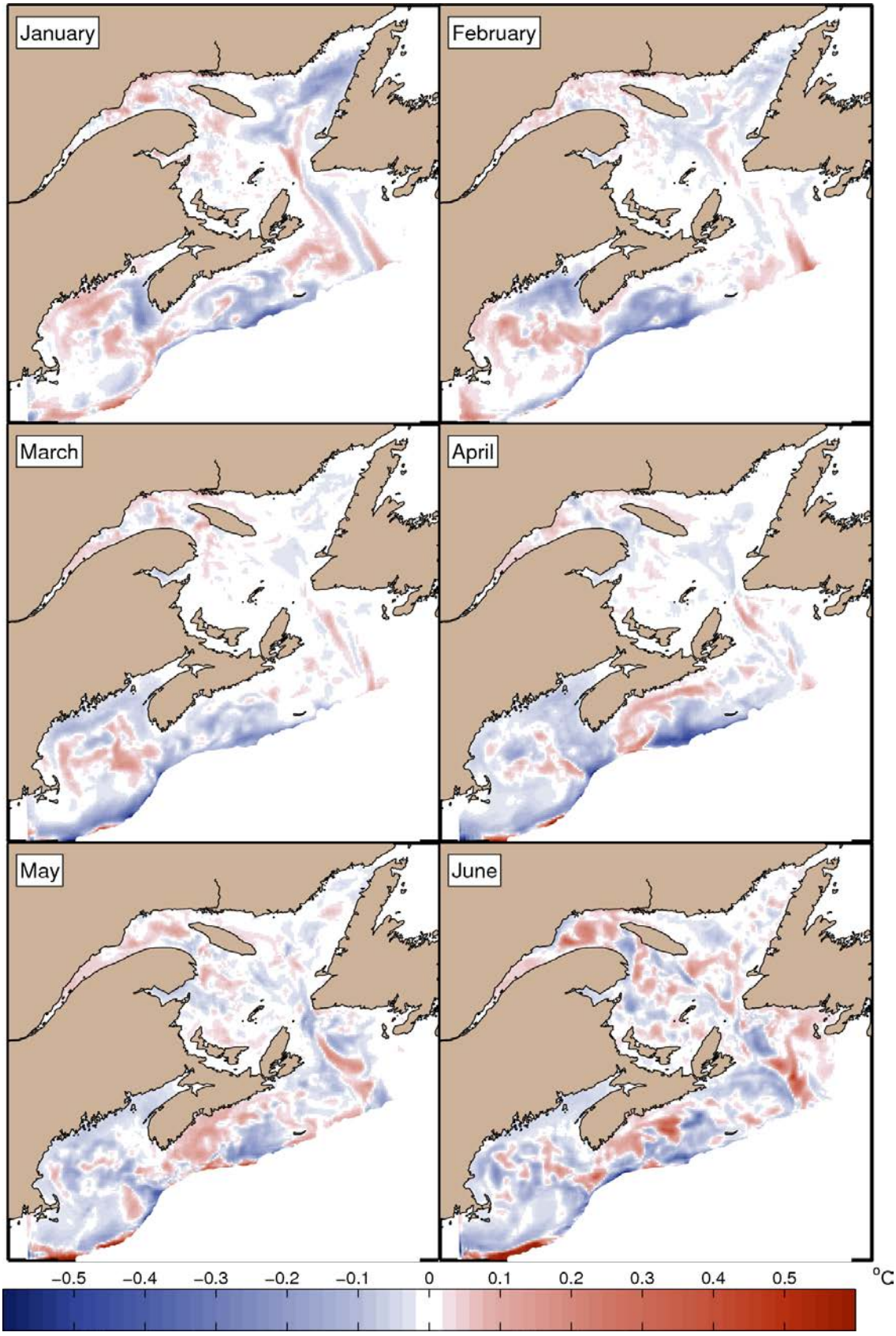

Figure 55. Differences in monthly mean 0–50 m temperatures over the six-year period between the Romaine River scenario (ROM) and the base simulation for January to June.

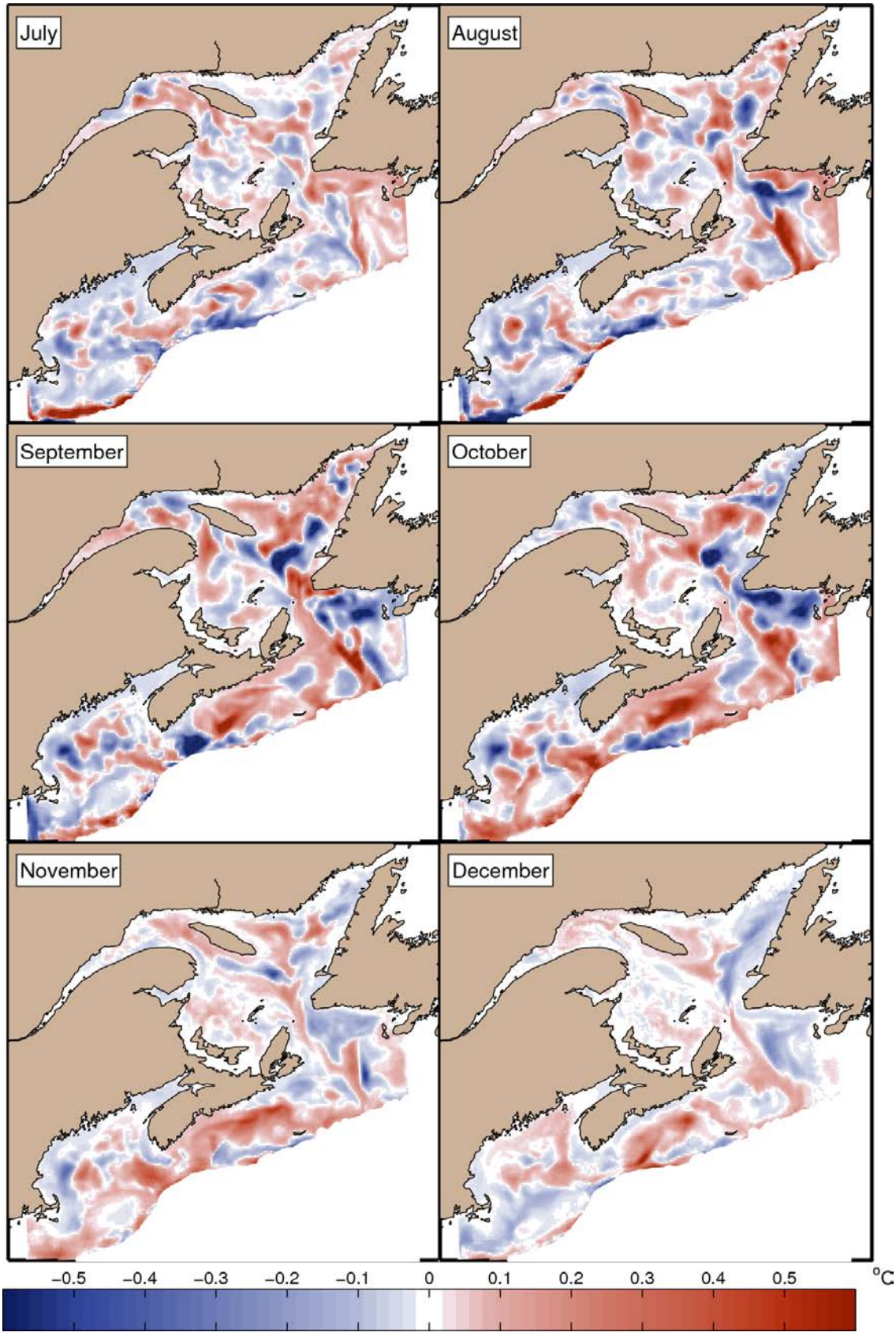

Figure 56. Differences in monthly mean 0–50 m temperatures over the six-year period between the Romaine River scenario (ROM) and the base simulation for July to December.

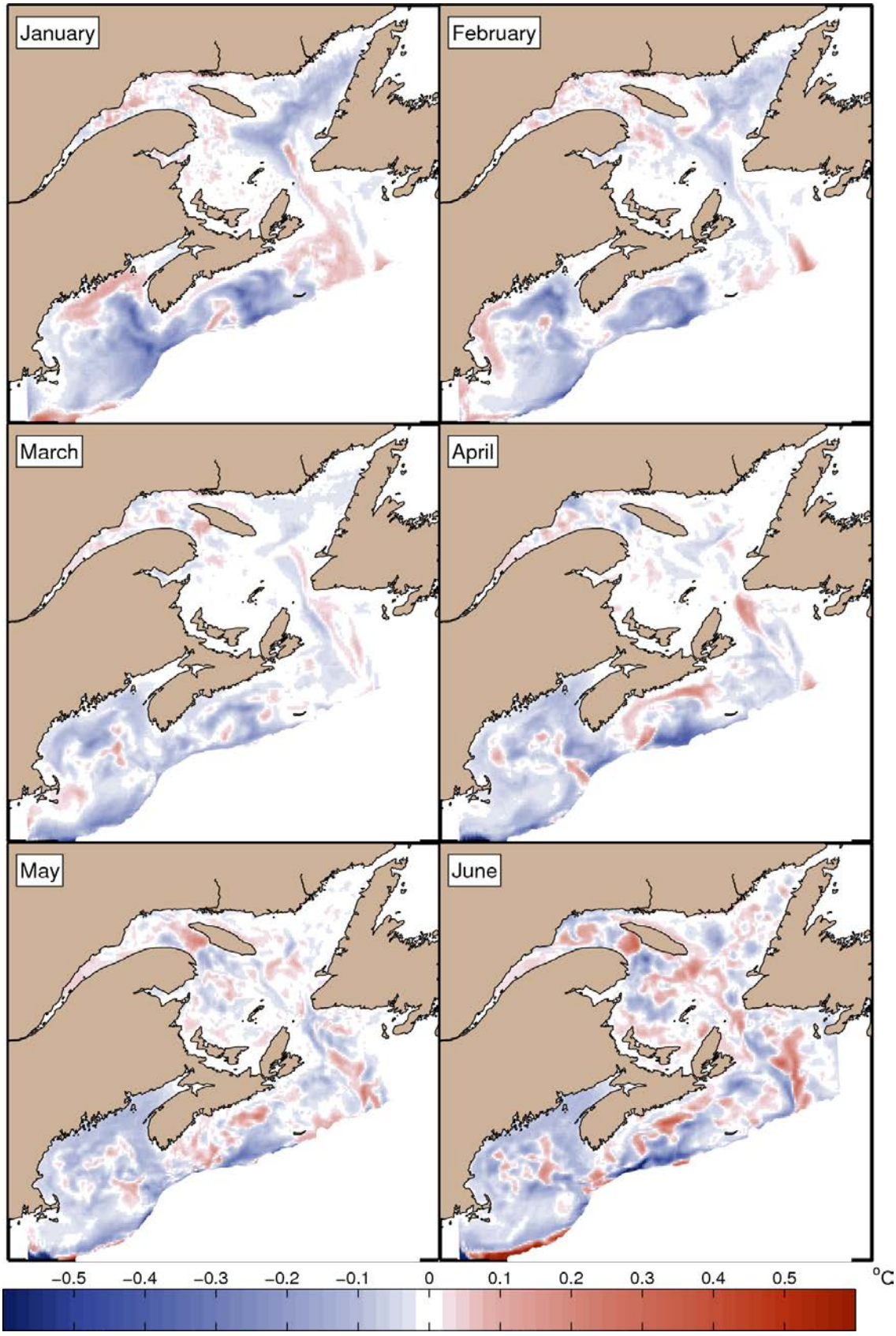

Figure 57. Differences in monthly mean 0–50 m temperatures over the six-year period between the Romaine and Little Mecatina rivers (ROMLM) and the base simulation for January to June.

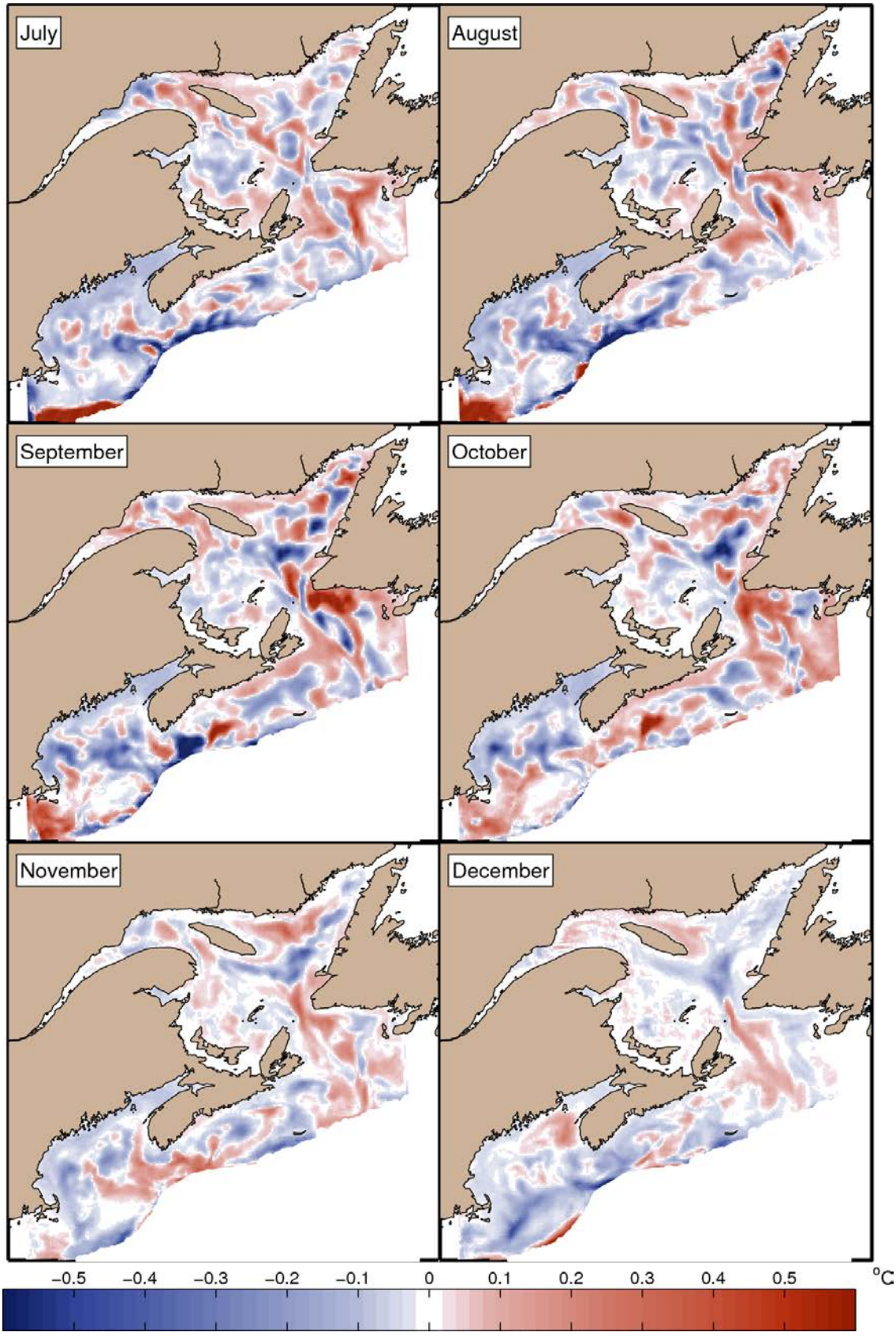

Figure 58. Differences in monthly mean 0–50 m temperatures over the six-year period between the Romaine and Little Mecatina rivers (ROMLM) and the base simulation for July to December.

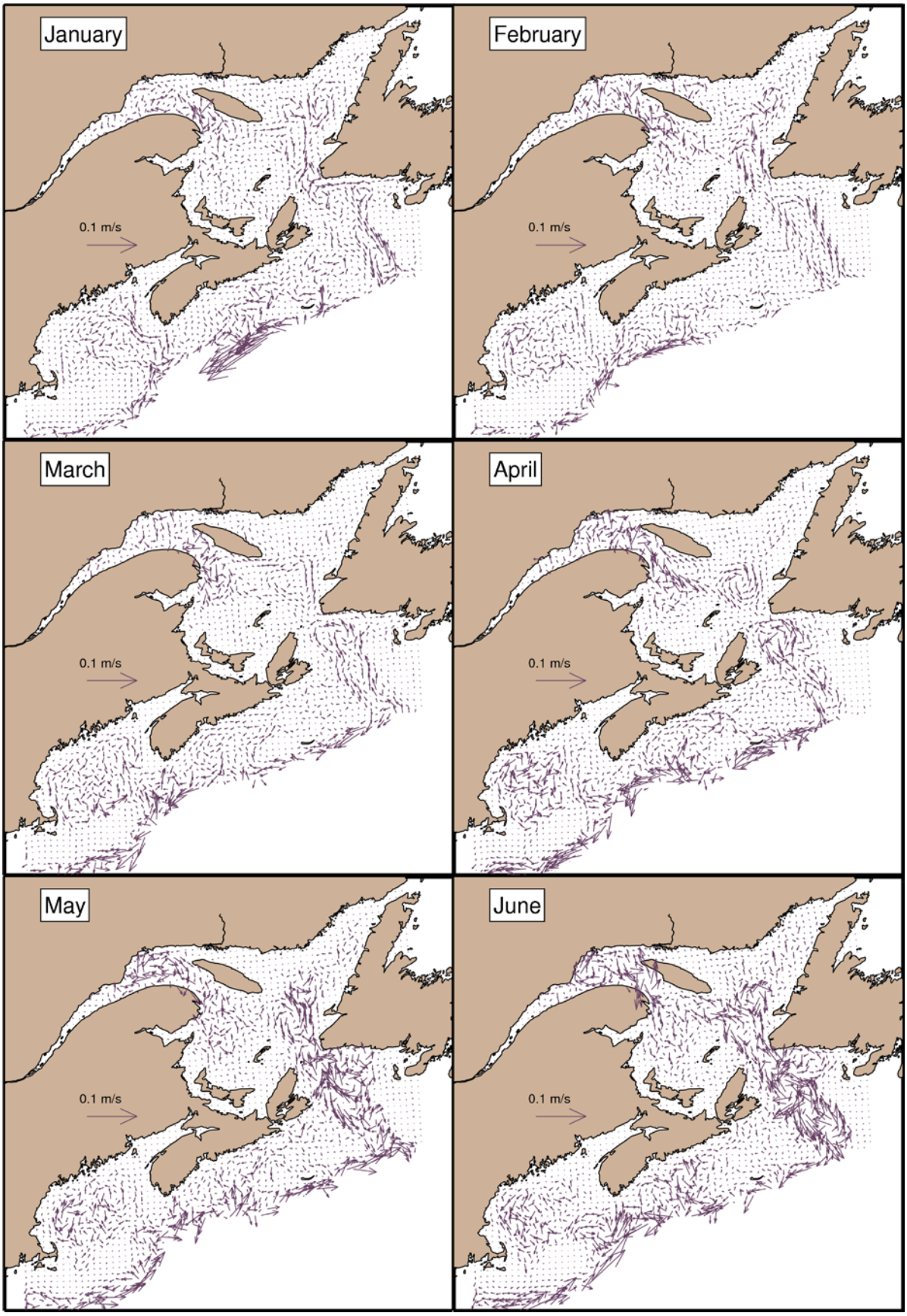

Figure 59. Differences in monthly mean 0–50 m currents over the six-year period between the Romaine River scenario (ROM) and the base simulation for January to June.

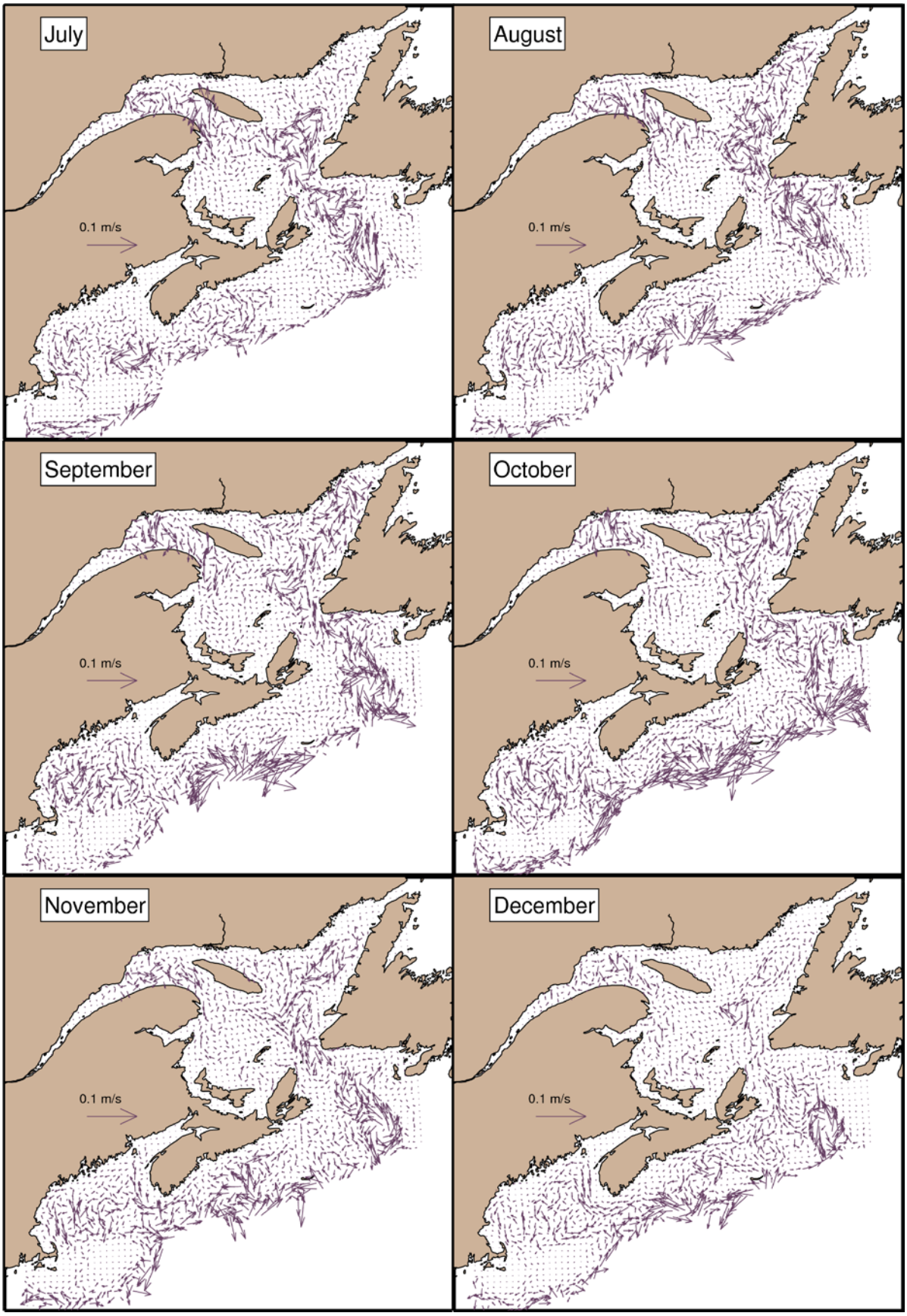

Figure 60. Differences in monthly mean 0–50 m currents over the six-year period between the Romaine River scenario (ROM) and the base simulation for July to December.

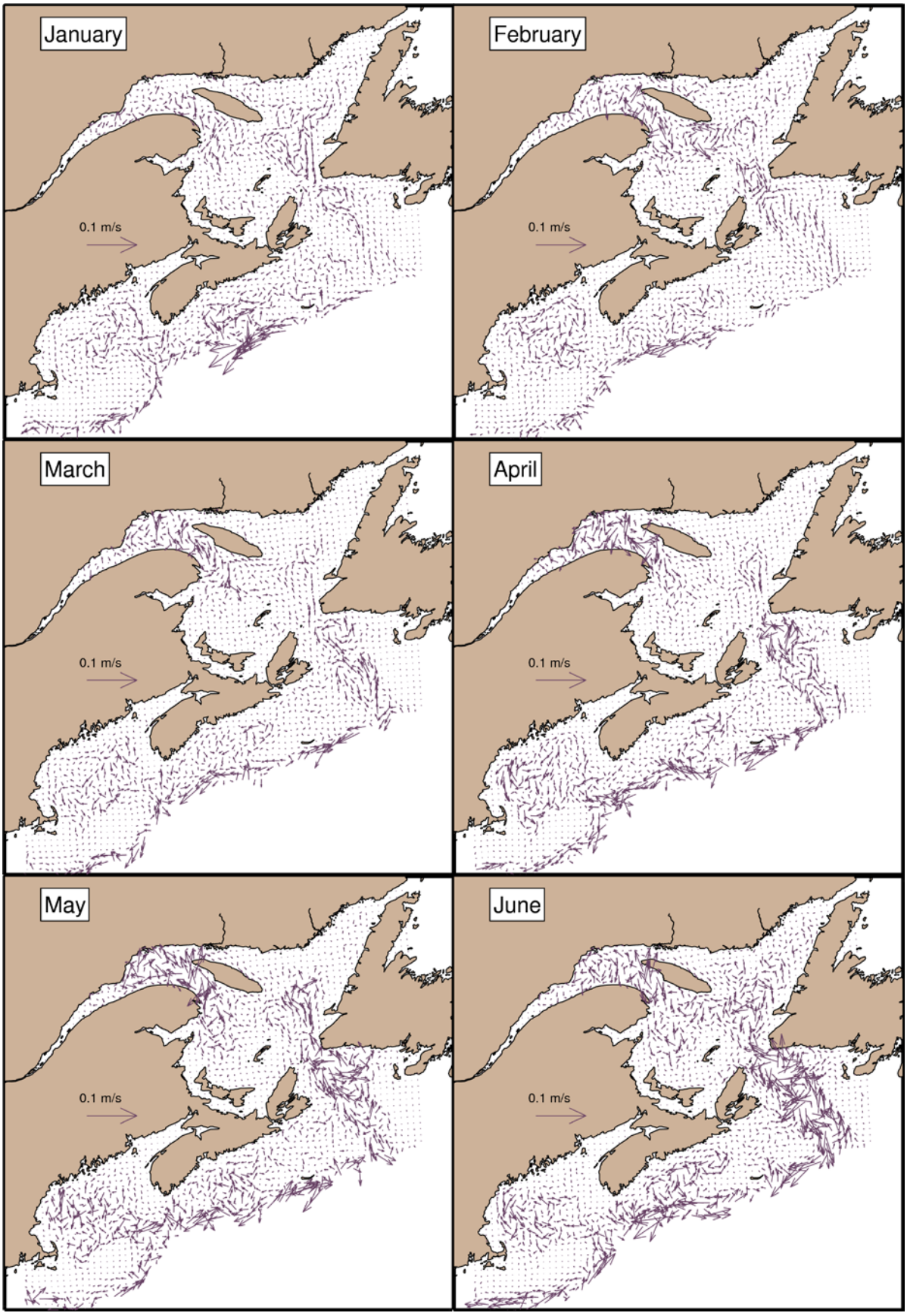

Figure 61. Differences in monthly mean 0–50 m currents over the six-year period between the Romaine and Little Mecatina rivers (ROMLM) and the base simulation for January to June.

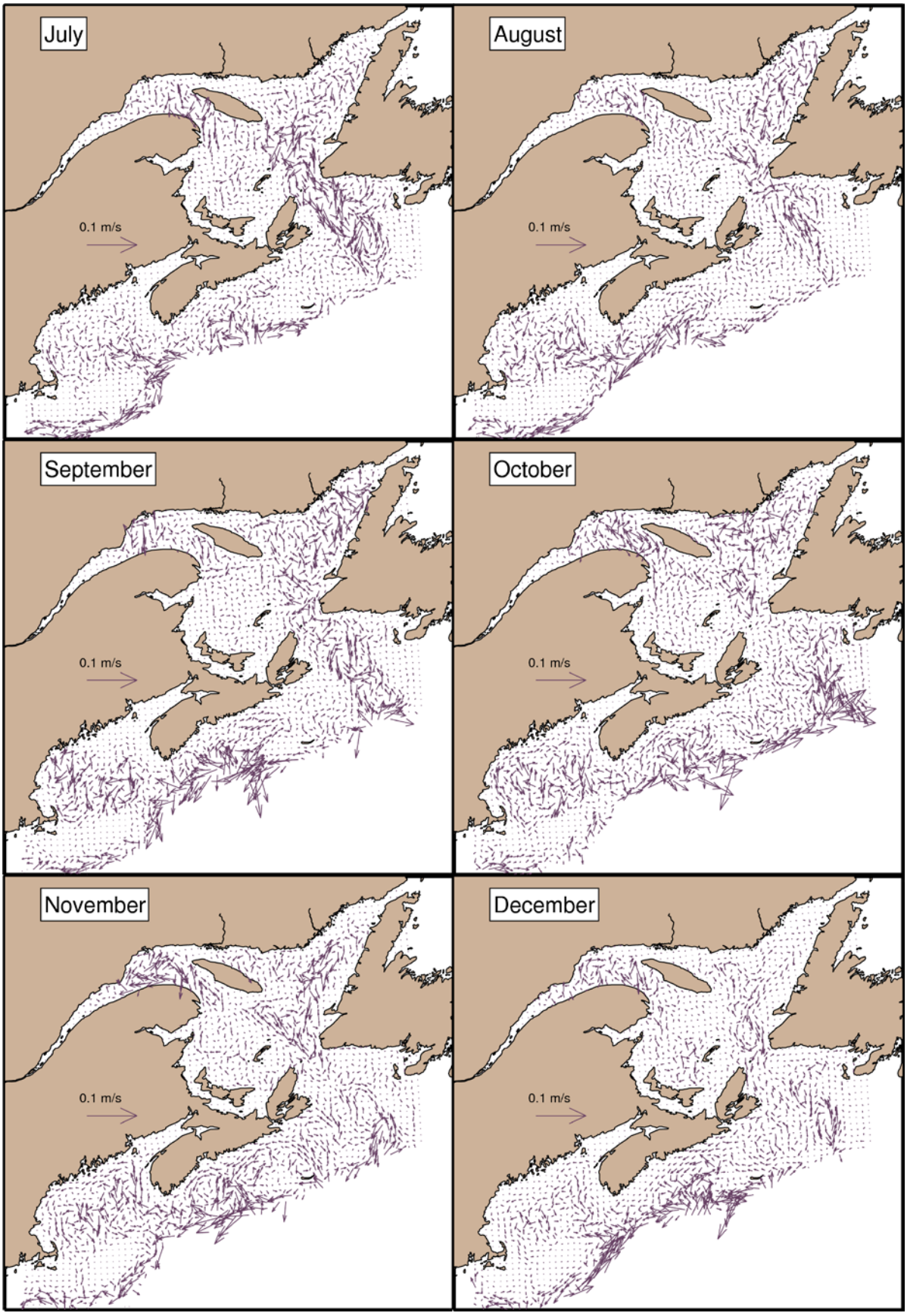

Figure 62. Differences in monthly mean 0–50 m currents over the six-year period between the Romaine and Little Mecatina rivers (ROMLM) and the base simulation for July to December.

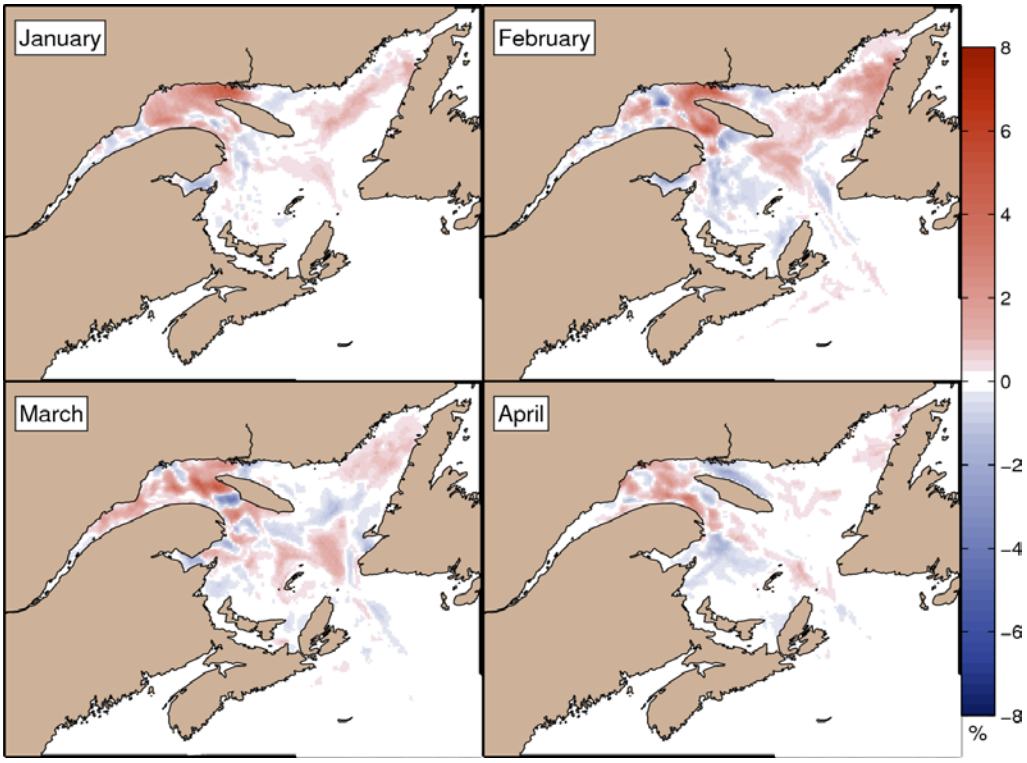

Figure 63. Differences in monthly mean sea-ice concentration over the six-year period between the Romaine River scenario (ROM) and the base simulation for January to April.

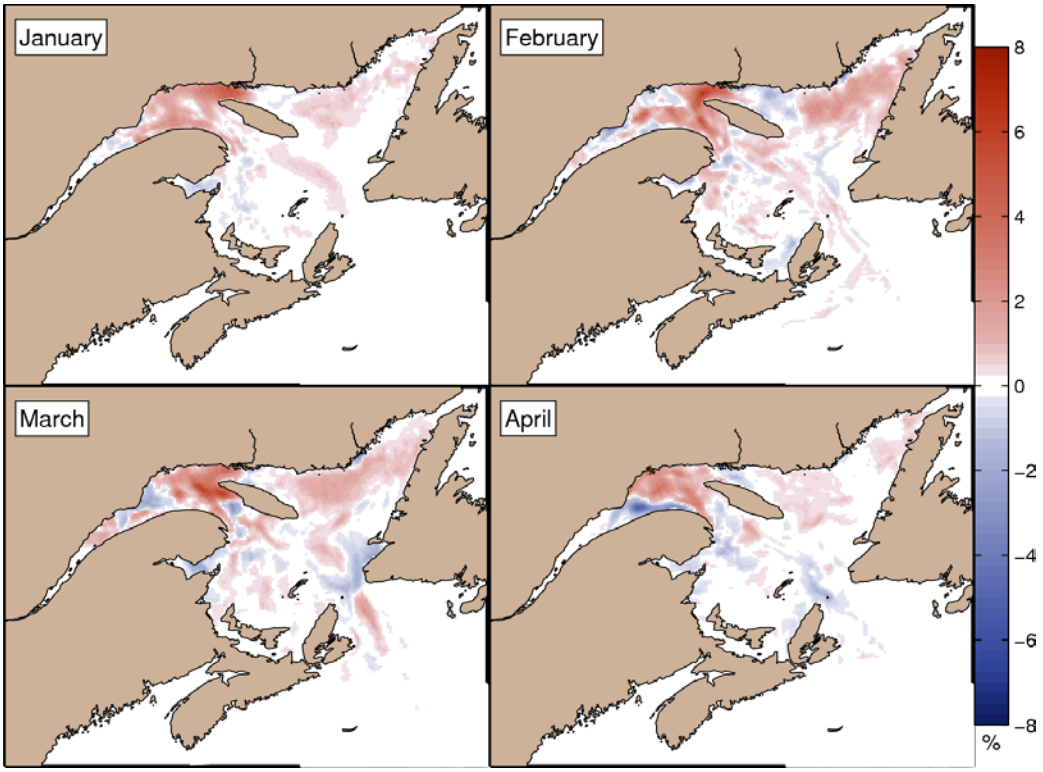

Figure 64. Differences in monthly mean sea-ice concentration over the six-year period between the Romaine and the Little Mecatina rivers (ROMLM) and the base simulation for January to April.

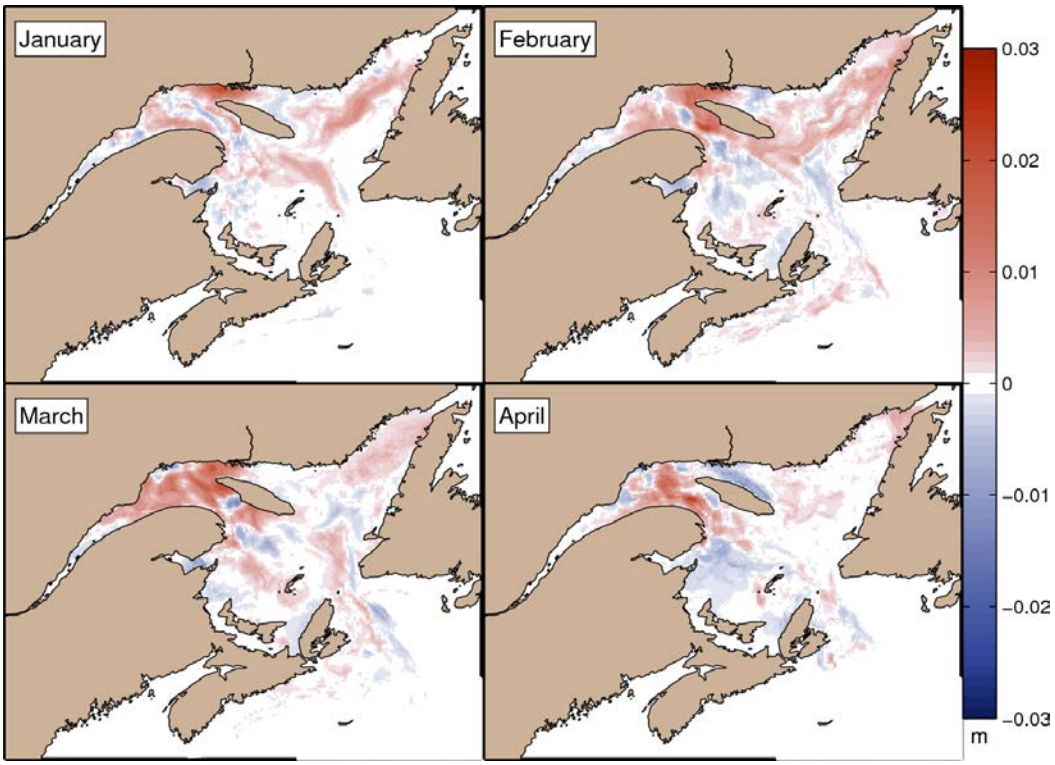

Figure 65. Differences in monthly mean sea-ice thickness over the six-year period between the Romaine River scenario (ROM) and the base simulation for January to April.

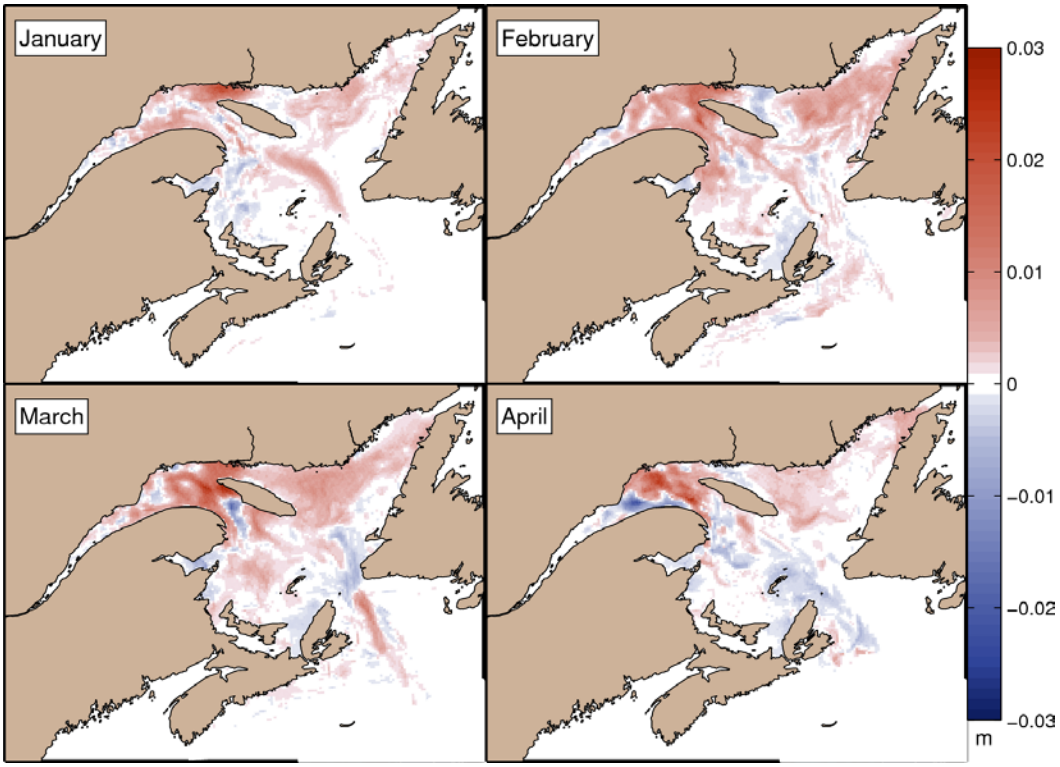

Figure 66. Differences in monthly mean sea-ice thickness over the six-year period between the Romaine and Little Mecatina rivers (ROMLM) and the base simulation for January to April.

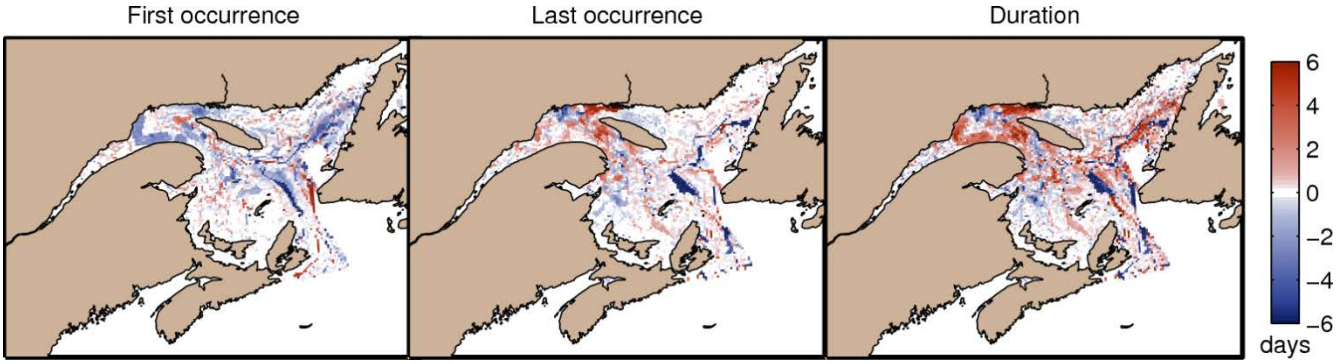

Figure 67. Differences in the 2006–2011 mean of start, end, and length of the sea-ice period (concentration > 5%) between the Romaine River scenario (ROM) and the base simulation.

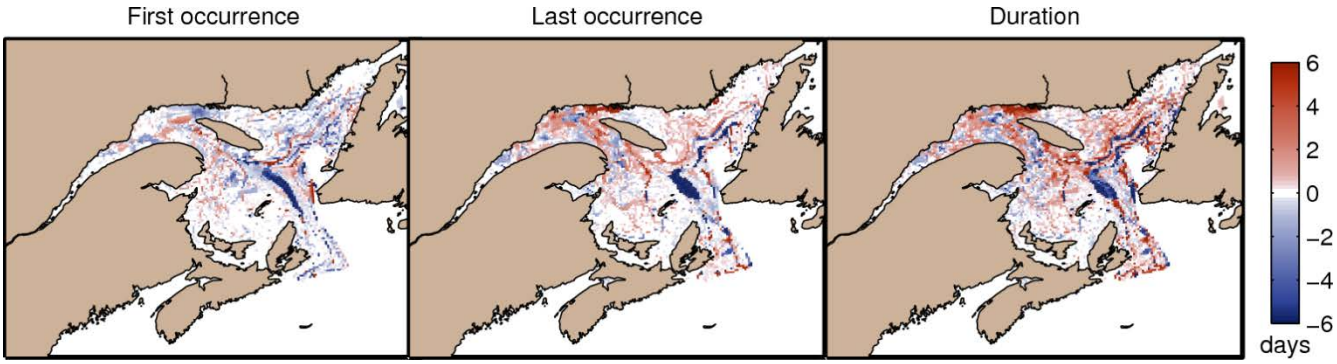

Figure 68. Differences in the 2006–2011 mean of start, end, and length of the sea-ice period (concentration > 5%) between the Romaine and Little Mecatina rivers (ROMLM) and the base simulation.

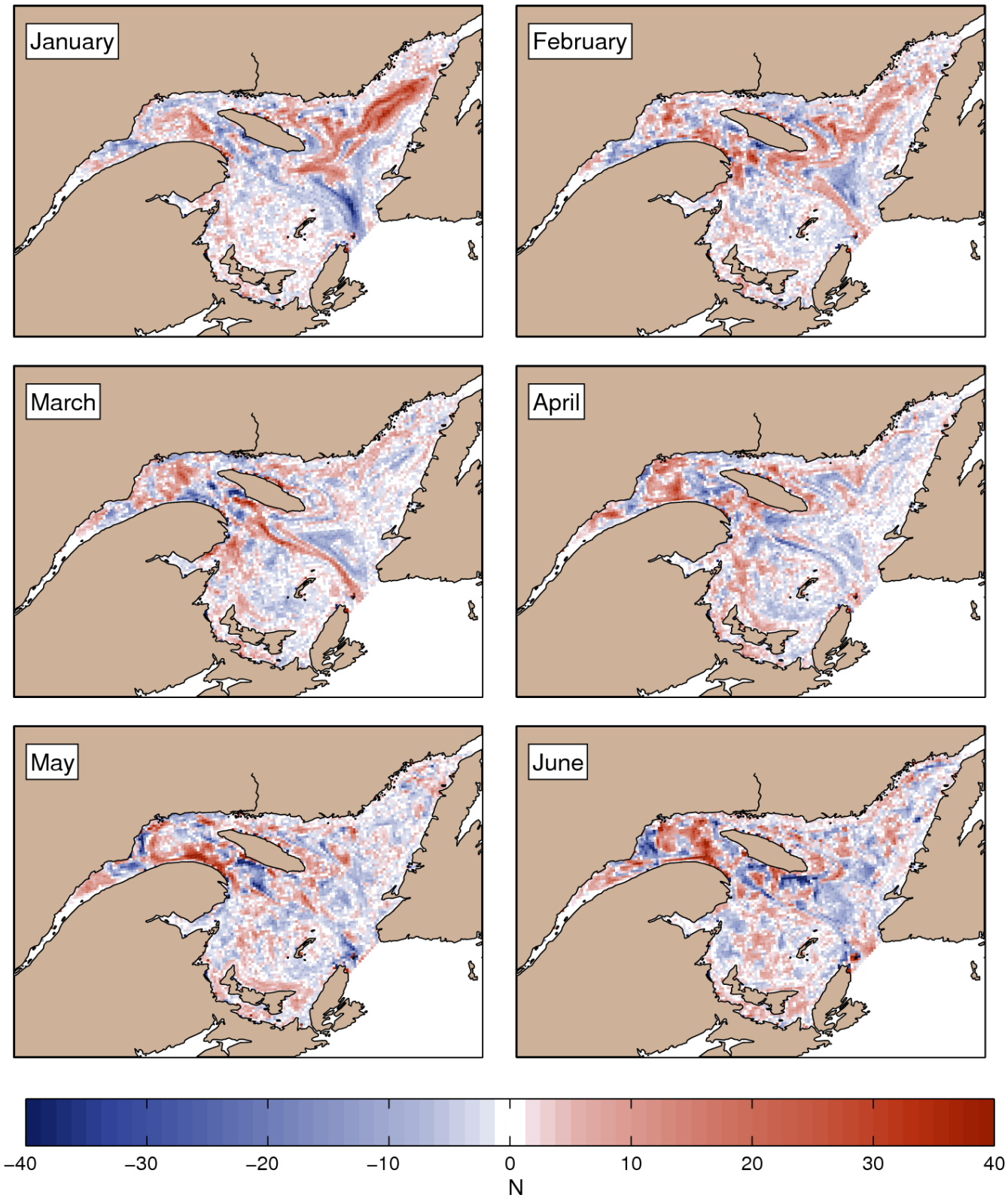

Figure 69. Differences in monthly mean krill density (number of particles per grid cell) with the LD vertical distribution over the five-year period (2007–2011) between the Romaine River scenario (ROM) and the base simulation for January to June.

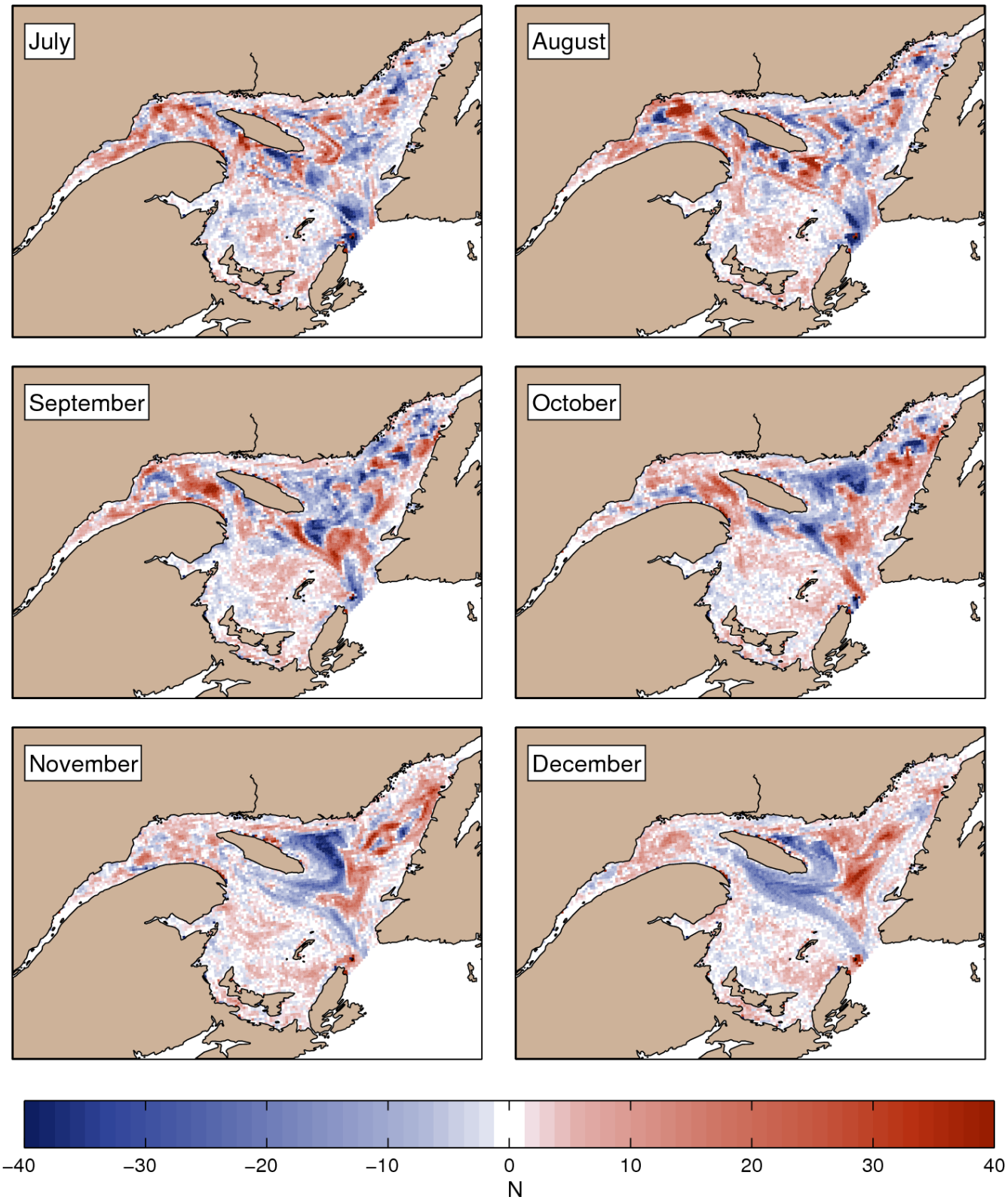

Figure 70. Differences in monthly mean krill density (number of particles per grid cell) with the LD vertical distribution over the five-year period (2007–2011) between the Romaine River scenario (ROM) and the base simulation for July to December.

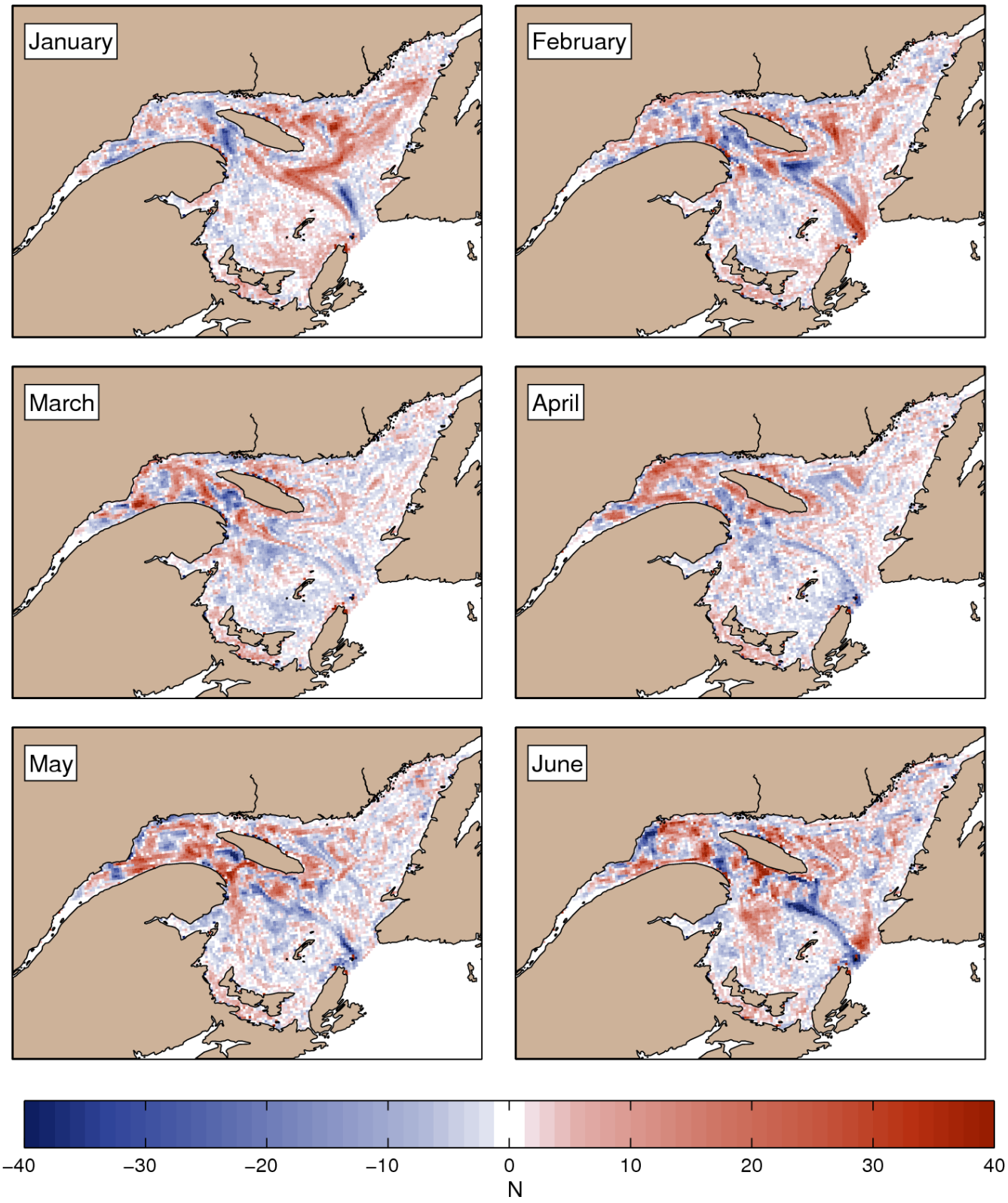

Figure 71. Differences in monthly mean krill density (number of particles per grid cell) with the LD vertical distribution over the five-year period (2007–2011) between the Romaine and Little Mecatina rivers (ROMLM) and the base simulation for January to June.

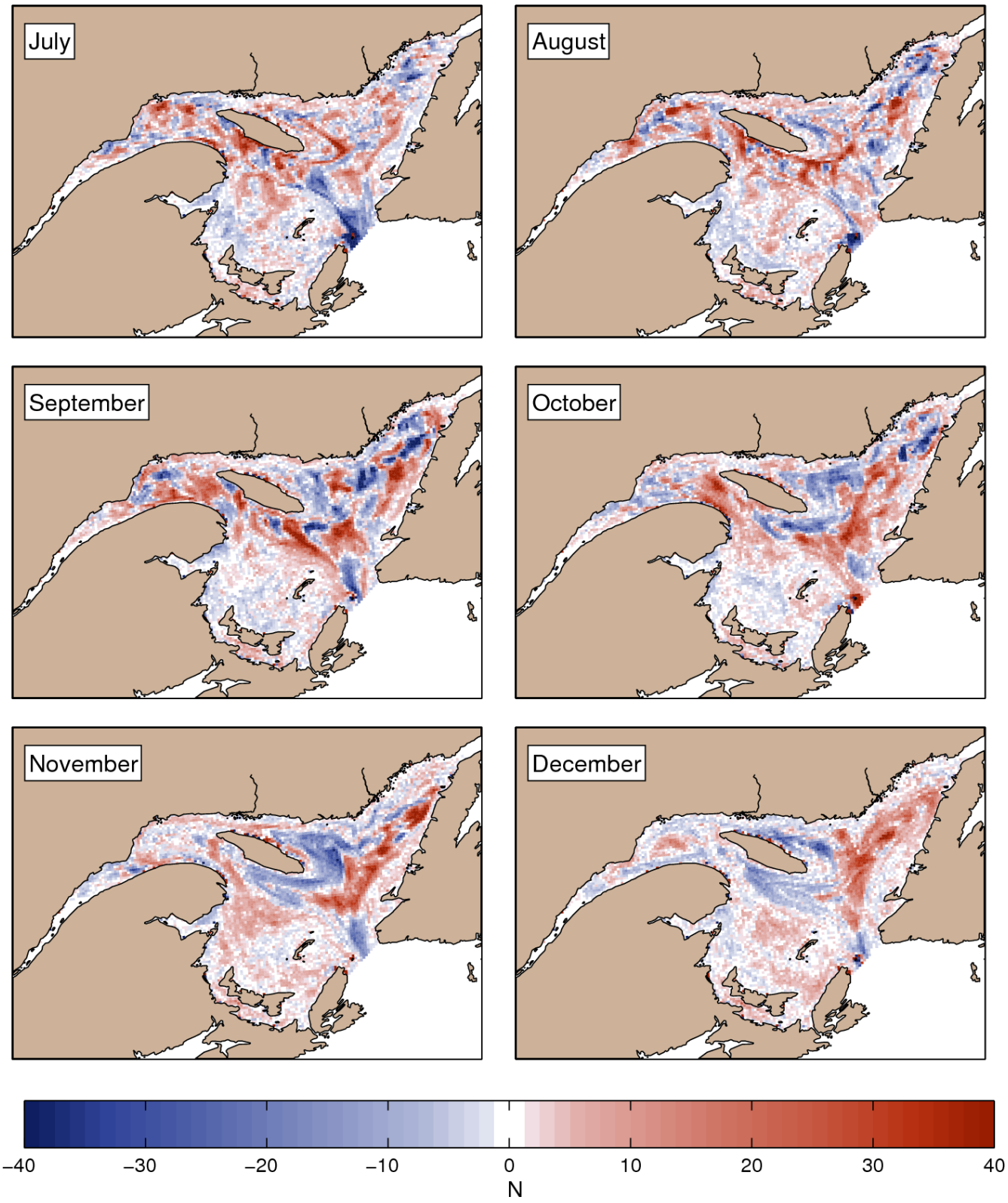

Figure 72. Differences in monthly mean krill density (number of particles per grid cell) with the LD vertical distribution over the five-year period (2007–2011) between the Romaine and Little Mecatina rivers (ROMLM) and the base simulation for July to December.

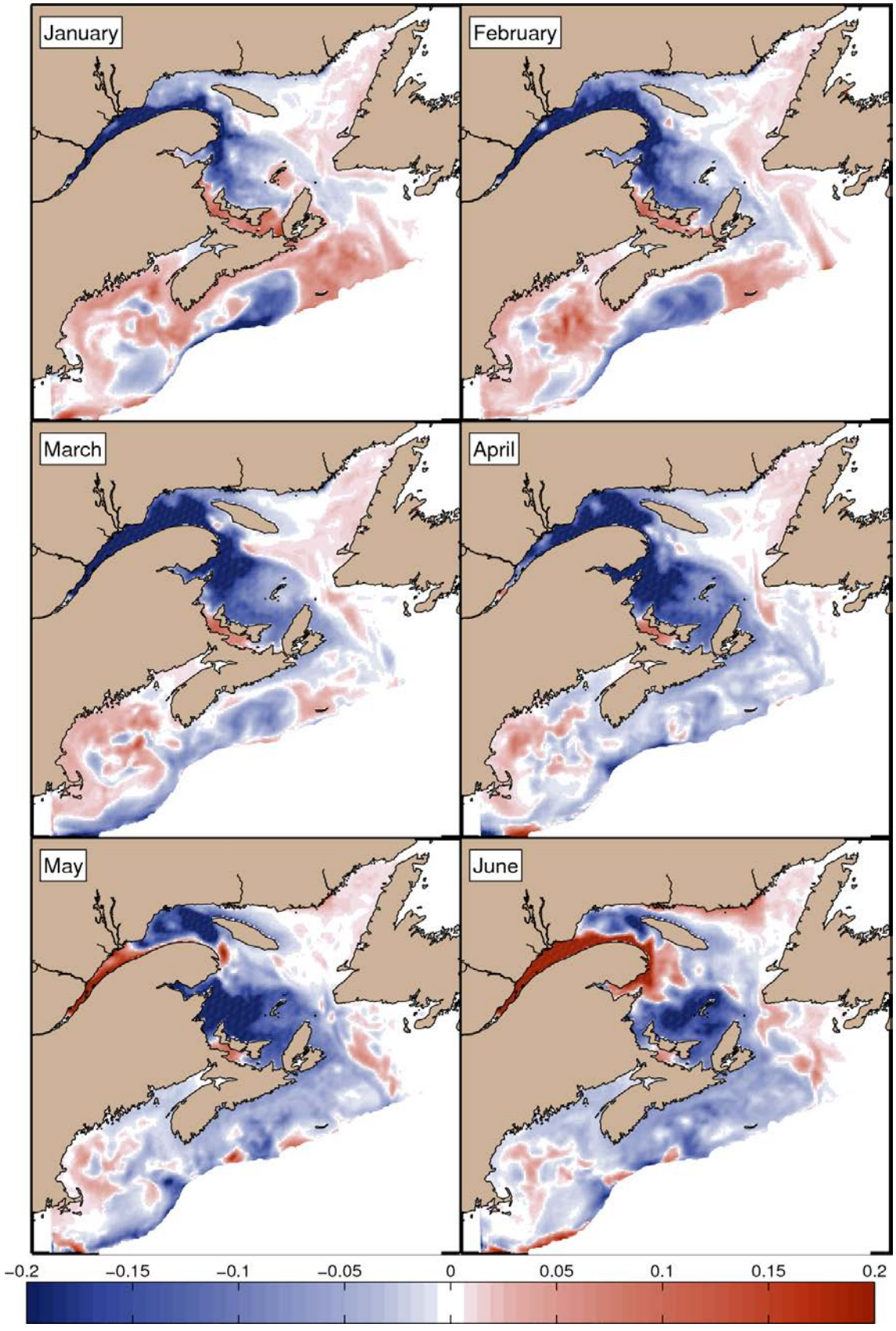

Figure 73. Differences in monthly mean 0–50 m salinities over the six-year period between the simulation with all the rivers harnessed (ALL scenario) and the base simulation for January to June.

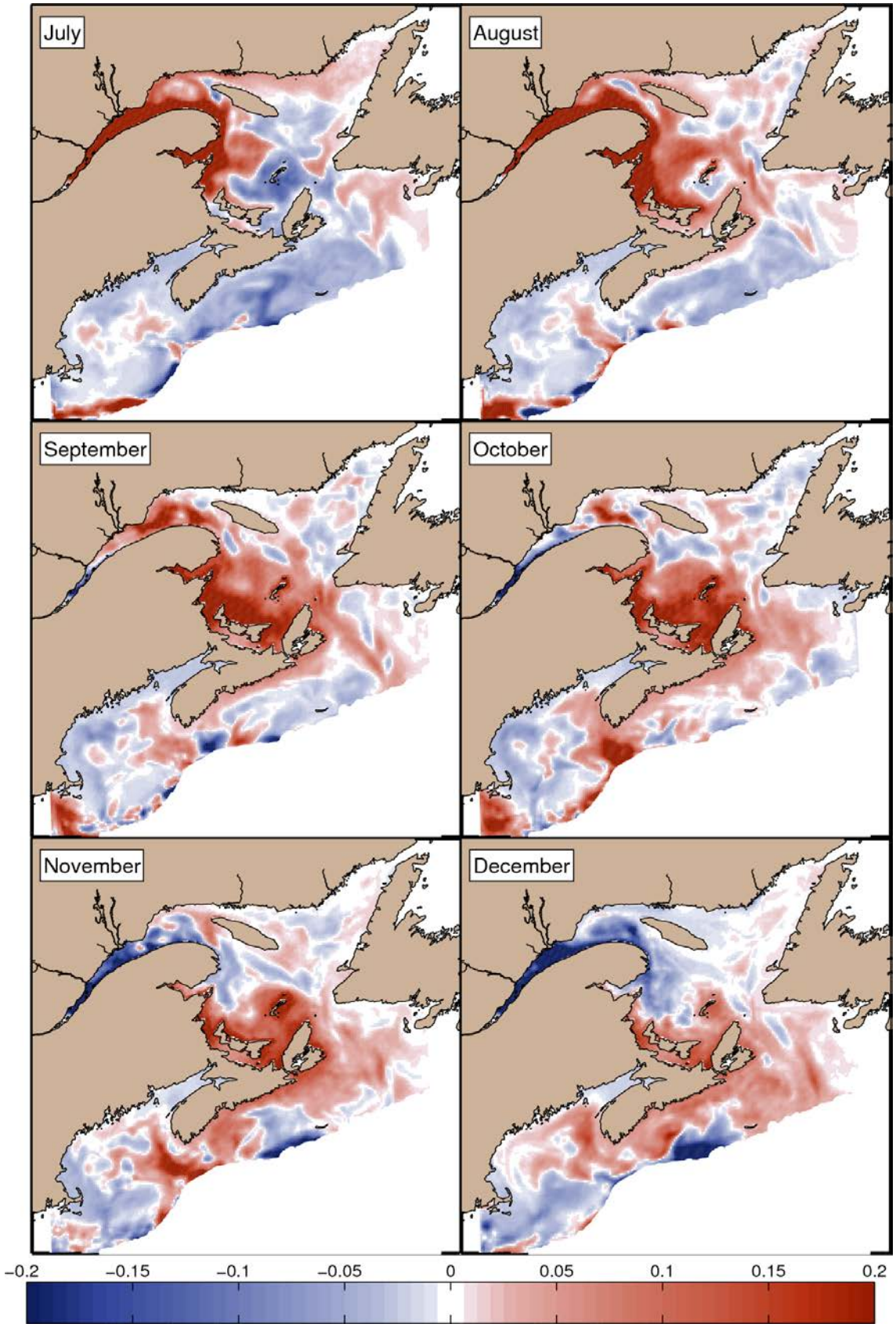

Figure 74. Differences in monthly mean 0–50 m salinities over the six-year period between the simulation with all the rivers harnessed (ALL scenario) and the base simulation for July and December.

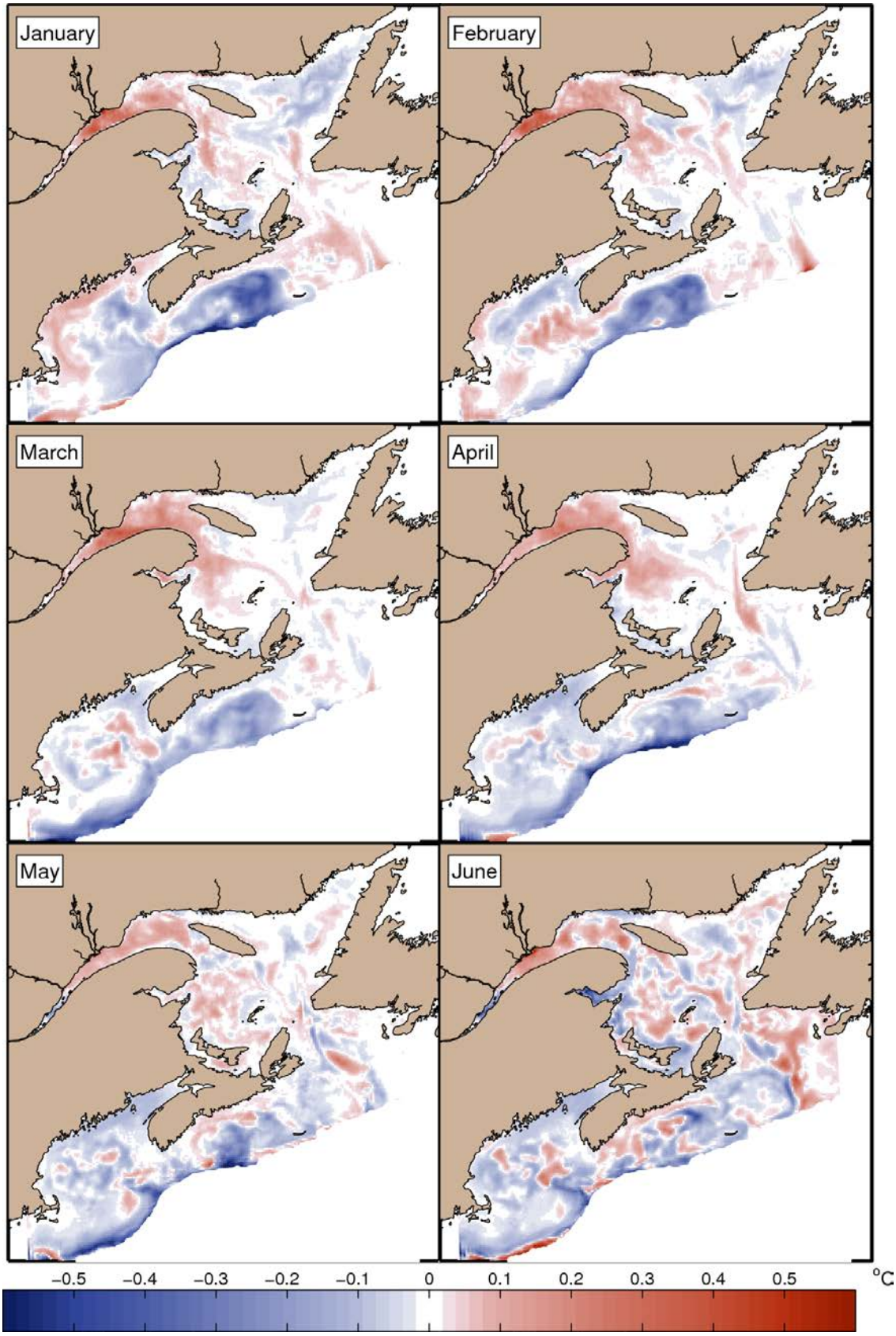

Figure 75. Differences in monthly mean 0–50 m temperatures over the six-year period between the simulation with all the rivers harnessed (ALL scenario) and the base simulation for January to June.

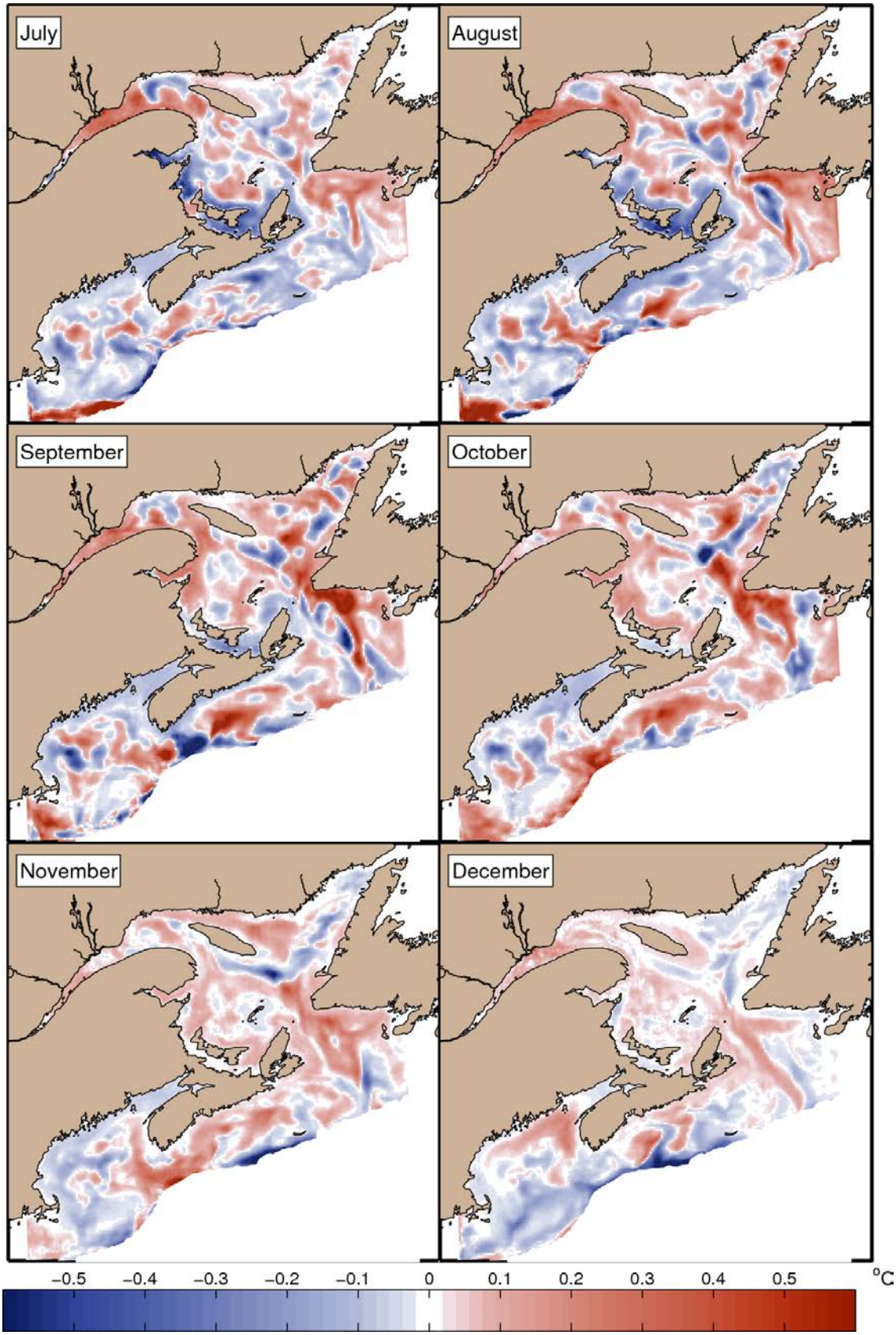

Figure 76. Differences in monthly mean 0–50 m temperatures over the six-year period between the simulation with all the rivers harnessed (ALL scenario) and the base simulation for July to December.

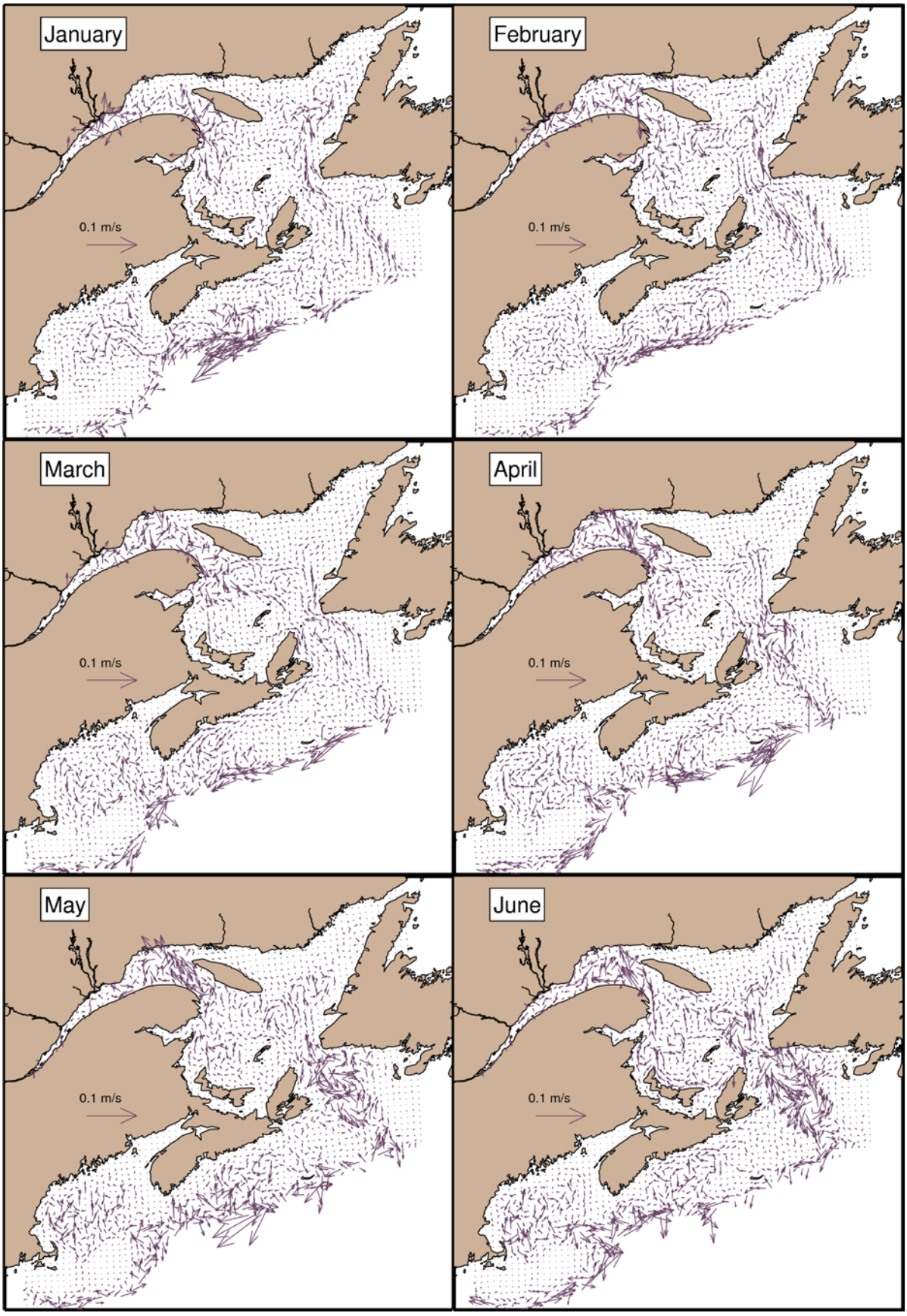

Figure 77. Differences in monthly mean 0–50 m currents over the six-year period between the simulation with all the rivers harnessed (ALL scenario) and the base simulation for January to June.

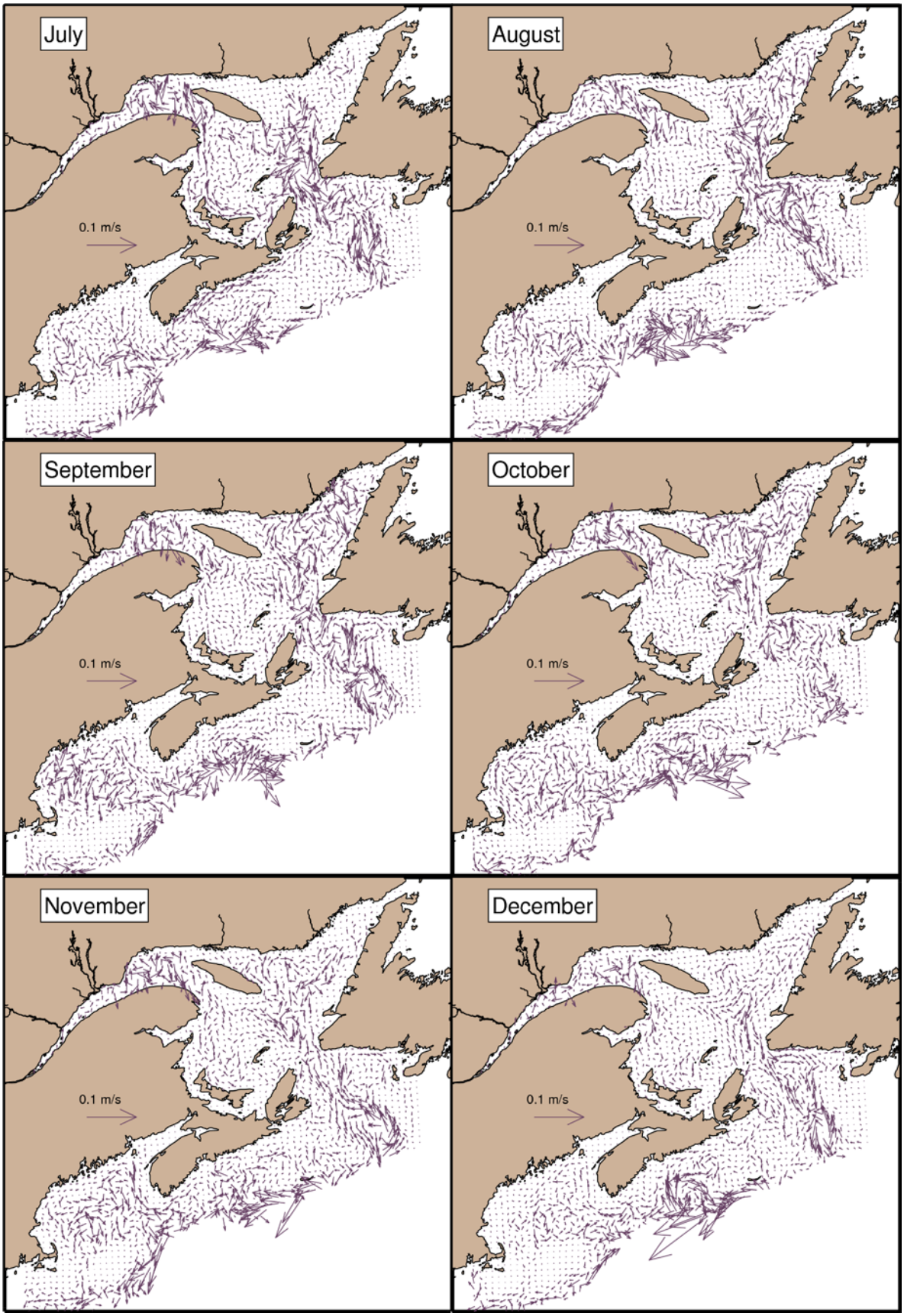

Figure 78. Differences in monthly mean 0–50 m currents over the six-year period between the simulation with all the rivers harnessed (ALL scenario) and the base simulation for July to December.

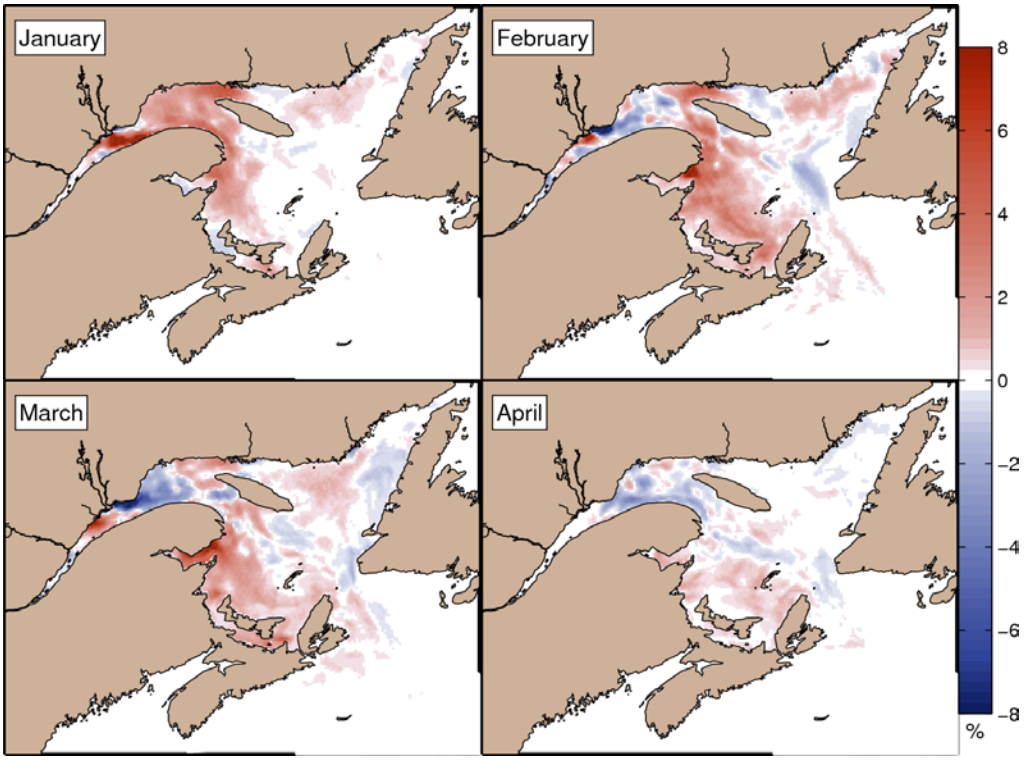

Figure 79. Differences in monthly mean sea-ice concentration over the six-year period between the simulation with all the rivers harnessed (ALL scenario) and the base simulation for January to April.

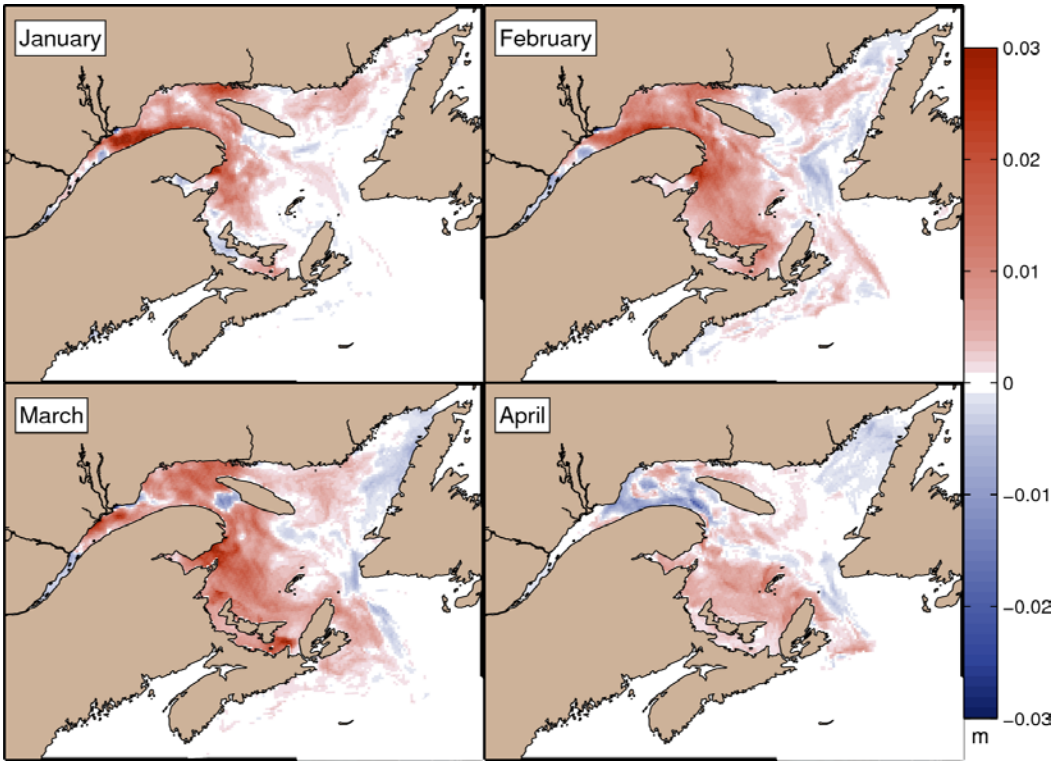

Figure 80. Differences in monthly mean sea-ice thickness over the six-year period between the simulation with all the rivers harnessed (ALL scenario) and the base simulation for January to April.

.

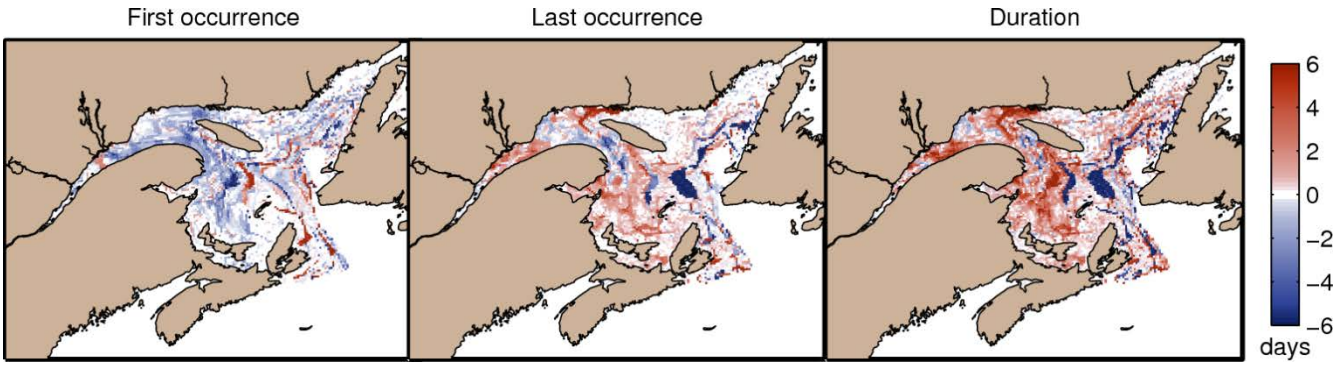

Figure 81. Differences in the 2006–2011 mean of start, end, and length of the sea-ice period (concentration > 5%) between the simulation with all the rivers harnessed (ALL scenario) and the base simulation.

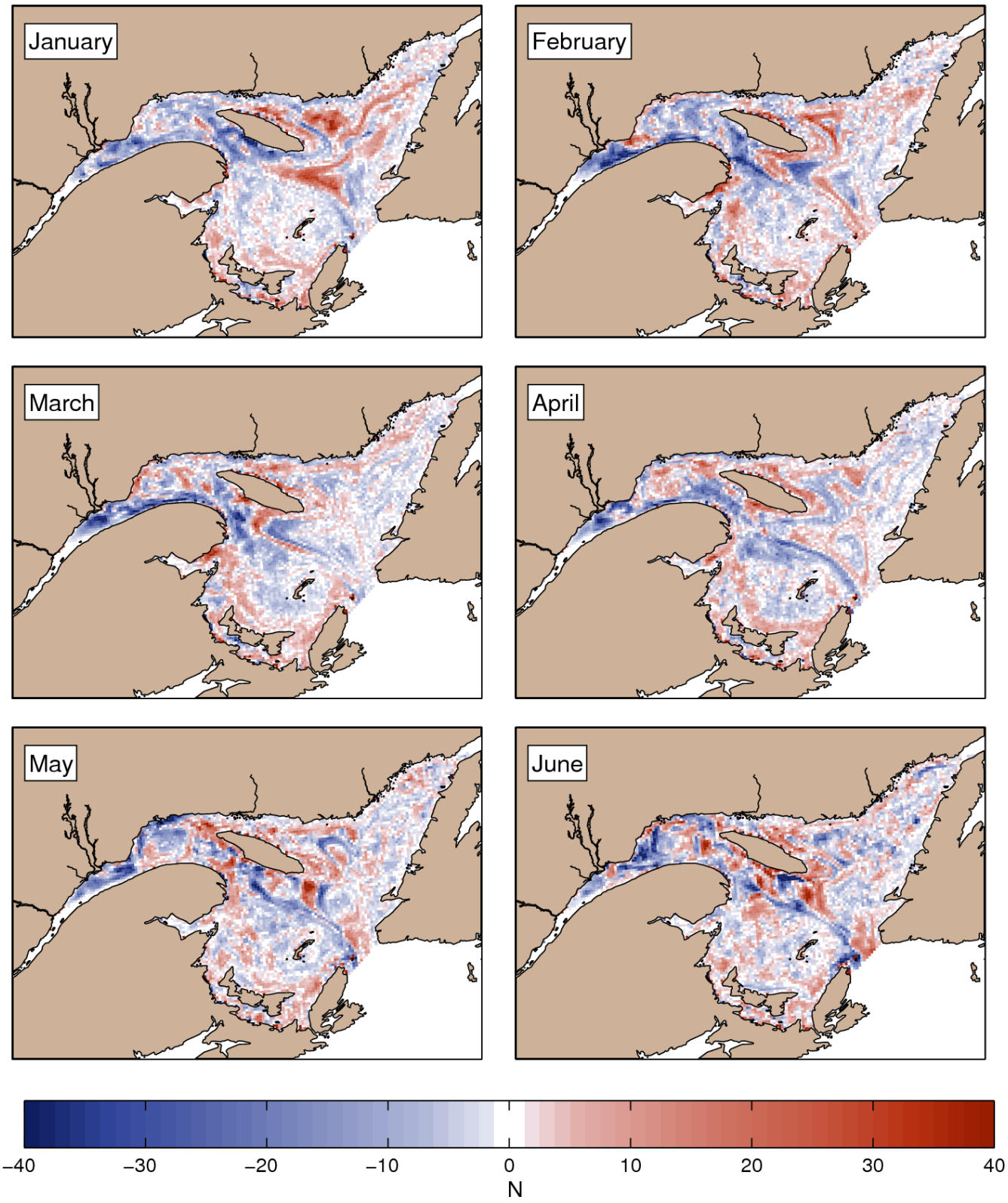

Figure 82. Differences in monthly mean krill density (number of particles per grid cell) with the LD vertical distribution over the five-year period (2007–2011) between the simulation with all the rivers harnessed (ALL scenario) and the base simulation for January to June.

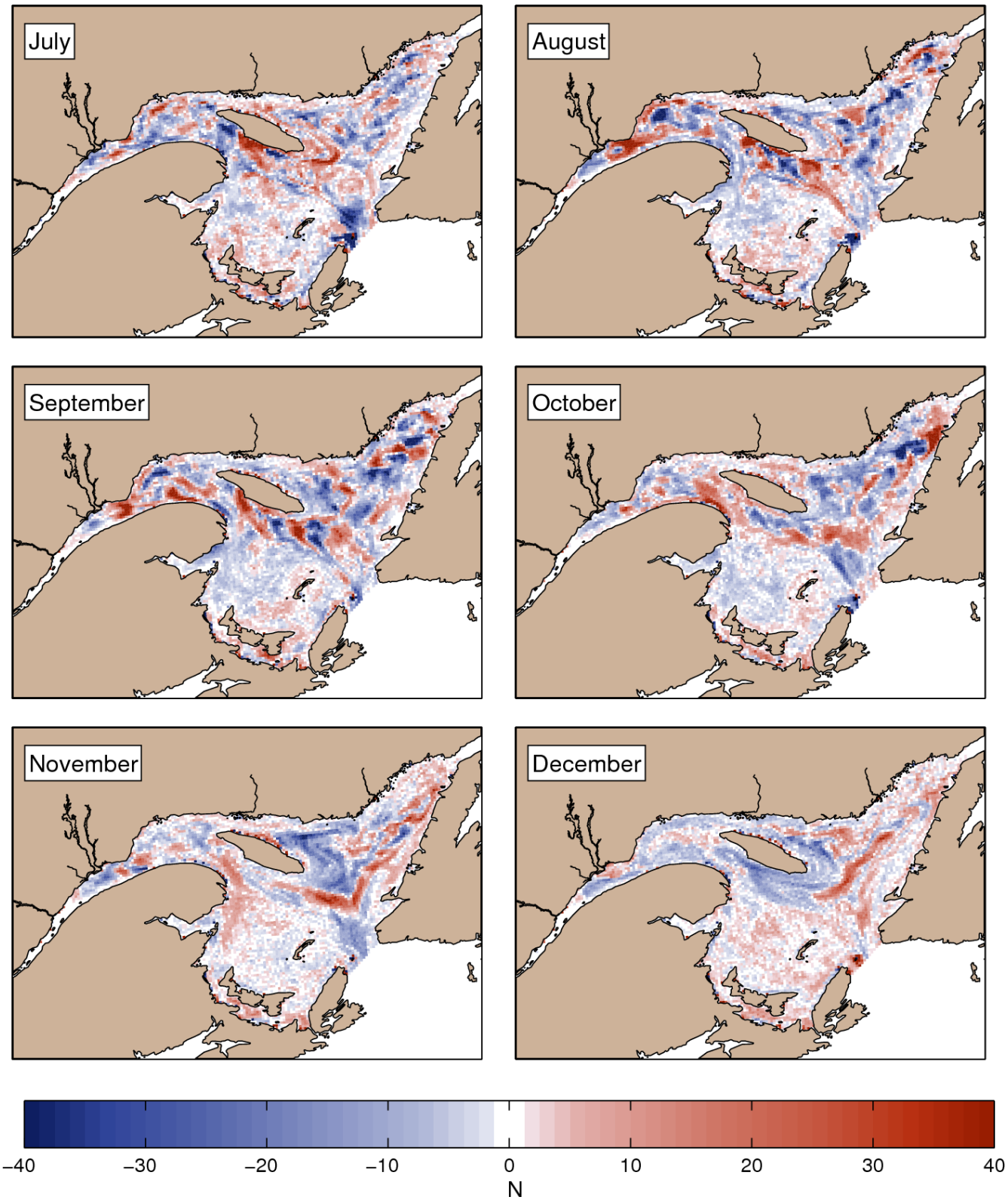

Figure 83. Differences in monthly mean krill density (number of particles per grid cell) with the LD vertical distribution over the five-year period (2007–2011) between the simulation with all the rivers harnessed (ALL scenario) and the base simulation for July to December.